Occultation Studies of Neptune

by

Pamela A. Melroy

B. A., Physics and Astronomy
Wellesley College
(1983)

Submitted to the Department of
Earth, Atmospheric, and Planetary Sciences
in Partial Fulfillment of the
Requirements of the Degree of

Master of Science

at the

Massachusetts Institute of Technology

May, 1984

Signature of Author_____
Department of Earth, Atmospheric, and Planetary Science
11 May 1984

Certified By_____
Professor James L. Elliot, Thesis Supervisor

Certified By_____
Dr. Richard G. French, Thesis Supervisor

Accepted By_____
Chairman, Department Graduate Committee

OCCULTATION STUDIES OF NEPTUNE

by

Pamela A. Melroy

Submitted to the Department of
Earth, Atmospheric, and Planetary Sciences
on 11 May 1984 in Partial Fulfillment of the
Requirements of the Degree of Master of Science

ABSTRACT

Stellar occultations can provide information about the radius and oblateness of planets, provided there are enough chords observed across the planet. Numerical inversion of the light curves will give number density, pressure, and temperature profiles as a function of height in the atmosphere. Neptune occulted Hyd$-22^{\circ}58794$ on June 15, 1983. Five chords were observed from four locations. The previous best observed occultation was on April 4, 1968, when BD$-17^{\circ}4388$ was occulted by the planet. This occultation was observed with four telescopes from three different locations. Using half-light times from the light curves of the 1983 data to define the limb of the planet, a total of 8 usable points were found. The radius and oblateness were found using a non-linear least squares fit to the data. The 1983 results were compared to the 1968 results. The best fit to the 1983 data gave R $= 25263 \pm 9$ km and $\epsilon = 0.0160 \pm 0.0015$. This is within the error bars of the 1968 results. A fit was also done to the 1983 data using a constant density or pressure level to define the limb edge instead of a half-light time. The results agreed well with the result using the half-light times. A fit for the right ascension and declination of the pole was also performed.

Thesis Supervisor: Professor James L. Elliot

Title: Professor of Physics
Professor of Earth, Atmospheric, and Planetary Science

ACKNOWLEDGMENTS

I would like to acknowledge the observers listed in Table 2-1 for the use of their unpublished observations.

I am particularly grateful for the guidance of Drs. R. French and J. L. Elliot, and for the time and assistance given by D. Mink, K. Meech, R. Baron, and E. Dunham, especially in sorting out timing problems.

Dave Braunegg and the AI Laboratory deserve special thanks for the access to the computer used to write this thesis. Dave also has provided many hours solving text problems and generally making everything look good.

The support and encouragement of several people has been tremendously appreciated, including Dave Braunegg, Dick French, Wendy Hagen, Karen Meech, Jeff Myers, my parents, and Bob Stachnik; however, the person who has put out the undeniably most heroic effort on my behalf has been my roommate, Sissileh Fridovich. For lasagna noodles, horrible phone calls and good talks, and putting up with the strange noises I make, thank you!

This thesis is appropriately dedicated to a person who has my deepest respect, admiration, and gratitude. Thanks for the hundreds of hours, tons of paper, and gallons of ink spent answering my questions over the last five years.

To Dick French

TABLE OF CONTENTS

Chapter 1.

INTRODUCTION

The use of stellar occultations as a probe of planetary structure was first recognized by Pannekoek (1904). An occultation occurs when a planet passes in front of a star. The light from the star is refracted as it passes through the planet's atmosphere along the line of sight to the observer. In the upper atmosphere, number density and pressure are so low that extinction effects are negligible. As the ray from the star passes through deeper and deeper levels in the atmosphere, the change in refractivity at each level is enough to cause a differential in the bending angle of the ray. Since the ray is successively more delayed as it probes deeper into the atmosphere, there is a decrease in stellar flux measured from Earth. The disappearance of the star behind the planet is called immersion, and the reverse process is the emersion.

The plot of stellar flux as a function of time is the light curve of the occultation. The stellar flux is normalized to full stellar flux, so that flux values range between 0 and 1. The drop in flux is proportional to the change in refractivity through the atmosphere. If the atmosphere is perfectly isothermal, the number density varies exponentially. The refractivity is directly proportional to the number density, so

the flux will drop in a smooth, continuous way (see Fig. 1-1). In fact, there are non-isothermal features in the atmosphere which cause regions of varying refractivity. These regions may cause higher photon fluxes than otherwise expected over a given time interval, forming short duration intensity peaks, or spikes, in the light curve (Elliot, 1979). Spikes can be used to probe the spatial scale of the non-isothermal features along the limb of the planet.

The radius and oblateness of the planet can also be found. Each immersion and emersion time defines a point on the limb of the planet. Different locations on Earth observe the planet occult the star at different chords across the planet. Assuming that the pole position is perfectly known, there will be four free parameters: the north and east offsets of the center of the planet from the predicted position; R_e, the equatorial radius; and ϵ, the oblateness. The oblateness, or flattening of the planet, is defined as

$$\epsilon = 1 - \frac{R_p}{R_e}. \tag{1.1}$$

R_p represents the polar radius. Ideally, as many chords as possible should be included in the fit. If two occultations are observed, information about the tilt of the pole toward or away from Earth can be obtained; this may make it possible to also fit for the pole position.

The importance of the oblateness of a planet is its direct relationship with the moment of inertia of the planet, the rotation rate, and J_2, the coefficient of the second order gravitational harmonic. The rotation rate was determined by Terrile and Smith (1983) to be approximately 18 hours based on imaging data. The value for J_2 was calculated by Harris from the regression rate of the orbit of Triton. The

moment of inertia is a direct probe of the internal structure of the planet.

In addition to the analysis described above, a numerical inversion can be performed on the light curve to obtain the number density, the pressure, and the temperature as a function of height in the atmosphere. Comparison of different temperature profiles at different locations along the planet's limb can provide information about the planet's large scale atmospheric structure. Occultations may also be observed in order to search for rings.

Neptune is a good planet for occultation studies because it is so distant (about 30 AU) and so faint that there are very few other ways of gaining information about it. It has only been possible to observe occultations since the development high-speed photometry; and, unfortunately, observable occultations of bright stars with large coverage across the planet are rare. The first occultation of Neptune with enough coverage to find the oblateness was on April 7, 1968. The star occulted was BD-17°4388, a 7.8 magnitude star. The occultation was observed with four telescopes at three different geographical locations, giving four independent chords. The analysis was done by Kovalevsky and Link (1969). The values they found for the equatorial radius and the oblateness were

$$R_e = 25225 \pm 30\,\mathrm{km},$$

$$\epsilon = 0.021 \pm 0.004\,.$$

The pole position used was computed by Gill and Gault (1968). Observations after this were primarily motivated by a search for rings, which gave negative results (Elliot et al., 1981; Elliot et. al., 1984). The next Neptune occultations observed

were in 1981 on May 10 and May 24. Unfortunately, each provided only one or two chords, not enough data to do a fit. Only atmospheric information could be obtained from the light curves.

The most recent occultation of Neptune was observed on June 15, 1983. Neptune occulted Hyd-22 58794, a 10.2 magnitude star. It was observed with six different telescopes from four locations. Chapter 2 discusses the observations. The accuracies of the ephemeris, pole position, and time determination are significantly improved from the 1968 data. This should lead to a better determination of the radius and oblateness. The time defining the limb of the planet was determined in two ways for the 1983 data. The first method, which was used for the 1968 data, was to find the time of half stellar flux; this time has been used in the past because it is a value that may be found in a repeatable way. The method used to find the time of half-light is described in Chapter 3. The results of the fit for the radius and oblateness of Neptune are also discussed. Since two occultations were used, it was also possible to fit for the pole position.

The time of half light does not correspond to a physically meaningful parameter in the atmosphere of the planet. Chapter 4 reviews how a method of numerical inversion of a light curve can give physical parameters such as number density and pressure as a function of height in the atmosphere. Constant number density and pressure levels were selected and the times associated with those levels were found for the 1983 data sets. These times were used to define the limb of the planet instead of the half-light times, and a new fit for the radius and oblateness from the 1983 data was performed.

Chapter 2.

OBSERVATIONS

The data from two different occultations were used to find the radius and oblateness of Neptune. In order to find these parameters, there must be a sufficient number of chords with wide coverage observed across the planet. The timing of the data is of great importance. Table 2-1 gives a summary of the observations. This chapter describes the data used from the two occultations in more detail.

The occultation of BD$-17^{\circ}4388$ by Neptune on April 7, 1968 was successfully observed from three different geographical locations in Japan and Australia using four telescopes. A total of eight points were obtained, with excellent separation across Neptune (see Fig. 2-1).

The occultation of Hyd$-22^{\circ}58794$ by Neptune on June 15, 1983 was observed from four separate geographical locations, using six telescopes, with varying degrees of success. The locations on Earth spanned from Hawaii to southern Australia (see Fig. 2-2). The separation of the four locations was excellent, but poor seeing conditions and noise resulted in the use of only three of the locations; a total of eight points were used.

Three of the 1983 data sets had photometric problems. At Hawaii, the condi-

tions were fine for immersion, but emersion took place during the dawn. This caused a non-linear increase in the background level throughout the emersion, making stellar flux measurements unreliable. At Siding Spring, in Australia, there were transient clouds during immersion and emersion. The data from the Anglo-Austrlaian Telescope (AAT), also at Siding Spring, were taken in the IR so the clouds did not affect those data. At the Mt. Stromlo location the immersion was very cloudy; the emersion was entirely clouded out.

Several of the data sets were taken using two channels. One channel is centered at a wavelength where the signal is depressed from Neptune, but is strong from the star. An additional channel may be used as the so-called "sky channel". There is signal from the planet but not the star in the wavelength of the sky channel; any changes other than noise in the signal are due to changes in the sky alone, such as clouds or other seeing variations.

When using occultation data for the purpose of oblateness determination, each data set must be referenced to the other data sets in order to put them in one coordinate system. Therefore, the absolute time of each data set must be as precise as possible in order to translate them correctly into one plane of reference. The 1983 Kuiper Airborne Observatory (KAO), Mt. Stromlo, and AAT observations initially had problems with the absolute timing; these were eventually tracked down to errors in the reduction programs.

The analysis of the data requires an accurate measure of the stellar flux as a function of time. Even transient clouds in the data will cause a problem. For the two 1983 data sets with cloud problems, Mt. Stromlo and the Siding Spring 1

meter, a color correction technique was used. This provides a way of removing the effect of the clouds in the occultation channel using the information about the depth of the clouds from the sky channel. The intensity for each channel is modelled as

$$I_1 = [n_{b_1} + n_{*_1}\phi(t)]e^{-\tau_1} + C_1 \tag{2.1}$$

$$I_2 = [n_{b_2} + n_{*_2}\phi(t)]e^{-\tau_2} + C_2 \tag{2.2}$$

where n_{b_1} and n_{b_2} are the background counts for each channel, n_{*_1} and n_{*_2} are the full star counts, and $\phi(t)$ is the normalized flux level. That is, it is the level of star counts normalized to full star counts, ranging between 0 and 1.0. C_1 and C_2 are the background intensities in each channel; defining

$$I_1' = I_1 - C_1 \text{ and } I_2' = I_2 - C_2\,,$$

one channel can be divided by the other. It is assumed that the cloud is a grey absorber, so that $\tau_1 \approx \tau_2$.

$$\frac{I_1'}{I_2'} = \frac{n_{b_1} + n_{*_1}\phi(t)}{n_{b_2} + n_{*_2}\phi(t)} \tag{2.3}$$

This relation provides no information unless the data sets are at different wavelengths. Solving this equation for $\phi(t)$,

$$\phi(t) = \frac{n_{b_2}(\frac{I_1'}{I_2'}) - n_{b_1}}{n_{*_1} - n_{*_2}(\frac{I_1'}{I_2'})}\,. \tag{2.4}$$

The flux as a function of time is retrieved, with the effects of the cloud essentially divided out.

The lower baselines n_{b_1} and n_{b_2} and the upper baselines $n_{*_1} + n_{b_1}$ and $n_{*_2} + n_{b_2}$ must be known to use this technique. The baselines were found by averaging the

values at full stellar flux and zero stellar flux for unclouded sections in the light curve near the event. In the case of Siding Spring, there were sufficient amounts of upper and lower baseline because the clouds were very transient. They were also not very deep. The color correction worked very well on the Siding Spring data (see Fig. 2-3). There was a problem for the Mt. Stromlo data (see Fig. 2-4) because there was very little baseline that was not clouded out. If the baseline is underestimated, then the resulting light curve from the color correction will not have the cloud fully divided out. If the baseline is overestimated, then the resulting light curve must compensate by reflecting the cloud upward, creating an artificial intensity peak.

The color correction method has another drawback in that it introduces the noise of both data sets into the resulting light curve:

$$\sigma_{eff}^2 = (\sigma_1^2 + \sigma_2^2) \ , \tag{2.5}$$

where σ is the rms deviation for a given data set, and σ_{eff} is the noise of the resulting curve. The Mt. Stromlo data was very noisy initially, making the resulting curves extremely unreliable. The clouds were so deep, and covered so much of the immersion and emersion, that there was little true information to be obtained. The emersion curve was especially bad; it was impossible to discern when the emersion even began. The Siding Spring data were good enough that this was not a problem.

Chapter 3.

OBLATENESS — HALF-LIGHT DETERMINATION

The biggest problem in the determination of a planet's oblateness is where on the light curve to define the limb of the planet. If the light curve were a perfect step function this would be easy. For bodies with a solid surface and no atmosphere, such as the moon, the light curve is very nearly a step function when the diffraction effects from the star are removed. For a planet with an atmosphere, however, the limb is not distinct. This is particularly true for the giant planets, which are presumed to be gaseous to at least a very deep level. How can the beginning of the atmosphere be defined? Ideally, a surface in the atmosphere corresponding to a physical parameter, such as a constant number density or pressure level, should be used. The reliability of different inversion methods used to obtain those parameters has been debated (Jokipii and Hubbard, 1977; French, Elliot, and Gierasch, 1978). The parameter that has been used is the half-light time, or the time at which the stellar flux has dropped to half its full value. The half-light level does not correspond to any physically meaningful parameter in the atmosphere. The usefulness of the half-light time is that it can be found in a consistently repeatable way for a given

light curve. Baum and Code (1953) developed a model for predicting the light curve resulting from the occultation of a perfect isothermal atmosphere. The equation they developed contains the half-light time as a reference point. The equation defining the curve for an isothermal atmosphere is

$$\frac{v\ (t - t_{\frac{1}{2}})}{H} = \left[\left(\frac{1}{\phi} - 2\right) + \ln\left(\frac{1}{\phi} - 1\right)\right] \tag{3.1}$$

where $v_{\perp}$ is velocity of the star perpendicular to the limb of the planet, t is time, $t_{\frac{1}{2}}$ is the time of half light, and ϕ is the observed stellar flux normalized to full stellar flux. H is the scale height, defined as

$$H = \frac{kT}{\overline{\mu} m_{H} g} \tag{3.2}$$

where k is the Boltzmann constant, T is temperature, $\overline{\mu}$ is mean molecular weight, m_{H} is the mass of the hydrogen atom, and g is the acceleration due to gravity. For an isothermal atmosphere, this will be the vertical distance over which the number density drops by e^{-1}. The scale height in Neptune's atmosphere is about 50 km (Rages et al.,1974; Veverka et al.,1974; Wallace, 1975). The isothermal light curve is a continuous, decreasing function (see Fig. 3-1). It is possible to fit any given light curve to a model isothermal curve, and solve for $v_{\perp}$, H, and $t_{\frac{1}{2}}$. It is immediately obvious that the atmosphere is not isothermal because spikes are observed in the data (see Fig. 3-2, a-j). Wasserman and Veverka (1973) have shown that the scale height found from an isothermal fit to a real light curve has a large uncertainty if the true atmosphere has a temperature gradient. That is, an isothermal light curve can actually be fit to a non-isothermal atmosphere with a constant temperature gradient, and the fit will give a value for the scale height which

is unreliable. However, the half-light time depends primarily on the determination of the full and zero stellar flux levels, and is only weakly correlated to the scale height (French and Taylor, 1981); the half-light time should correspond to the same level in the atmosphere for any occultation.

The half-light times for the 1983 data were found by fitting the data to the model equation for an isothermal atmosphere using a non-linear least squares fit. The half-light times are listed in Table 3-1.

It was shown by French, Elliot, and Gierasch (1978) that the error expected in the half-light time found from an isothermal curve with random white noise is

$$\sigma(t_{\frac{1}{2}}) = 3.55\left[\frac{H}{v_{\perp}}\right]^{\frac{1}{2}}\epsilon(\phi) \tag{3.3}$$

where

$$\epsilon(\phi) = \frac{(n_b + n_*\phi)^{\frac{1}{2}}}{n_*}; \tag{3.4}$$

$\sigma(t_{\frac{1}{2}})$ is typically less than 0.1 second (see Table 3-2) for the 1983 data. The true error from random noise can be measured by the discrepancy in the half-light times found for the data sets taken with different telescopes at the same location. The spikes and half-light time should be identical, since the same location in Neptune's atmosphere is being probed; however, the random noise will be different. The data taken from the two telescopes at Siding Spring showed a discrepancy of 0.3 second for both immersion and emersion. At Hawaii there were two telescopes taking data independently. In addition, at the IRTF, two data systems were used to take data from the same telescope. Data System 1 had a small time constant, of order 0.025 second. The data from System 2 passed through an amplifier with a high, unknown

time constant, of order 1 second. The response to signal variations was then much slower in System 2. The noise and spikes in the curve are therefore somewhat suppressed compared to the data from System 1. The discrepancies between the half-light times for the immersion data for these two data sets and the UH 2.2 meter data set was less than 0.4 second. The 2.2 meter emersion data were so noisy that they could not even be fit, and hence were discarded. The IRTF data were less noisy because the data were taken in the IR. However, the discrepancy between the two IRTF emersion data sets was 2 seconds. Several sources of error were checked; the most probable were the effect of the uncertainty in the baseline, and the shifting effect from the time constant. The baseline uncertainty should cause an error of under 0.6 seconds (see discussion below). The spikes were very precisely matched to find an absolute shift due to the time constant of under 0.25 second. These sources of error are not sufficient to account for the observed discrepancy. Since the data from System 2 passed through an amplifier of unknown properties, it is probable that some effect in the electronics other than the time constant changed that data. For this reason, the data from System 1 were used. The overall uncertainty from random noise is about 0.4 second.

Another error expected in the half-light time is due to the uncertainty in the baselines. This was found to be the most important source of error in the half-light determination for these data. Since the isothermal fit program also solves for the star and background counting rates, the uncertainty in the baselines can be found in an empirical way for each data set. Two isothermal fits were performed on each data set, with different amounts of baseline used in each fit. The discrepancy in the counting rates found from the two fits is considered to be the approximate

uncertainty. The first fit used 100 seconds of data at 0.01 second resolution. The other used 200 seconds at 0.02 second resolution, effectively including more baseline. Table 3-3 shows the variation in the upper and lower baselines when different amounts of baseline are used in the fit. The background flux was normalized to the full stellar flux, so the uncertainties for the two baselines are normalized and can be compared. It was found that both the upper and lower baselines are known to better than 3% for most of the data sets, corresponding to an uncertainty in the half-light time of about 0.4 second. The IRTF emersion data had an uncertainty of 6% in the upper baseline and 4% in the lower baseline, giving a discrepancy in the half-light time of 0.5 to 0.6 second. The Mt. Stromlo data and one of the KAO channels had uncertainties of 5 to 6% in both baselines. This produced an uncertainty in the half-light time of the order of 0.8 second. The IRTF emersion and Mt. Stromlo data were eliminated from the fit as a consequence. The KAO set was retrieved by summing it with the other channel used, bringing the overall baseline uncertainty down to about 3% for both upper and lower baselines. The half-light times used in the fit for the oblateness were those found using 200 seconds of data because they included more baseline; the overall error is estimated at 0.4 second. This is only true if the baselines are stable over the whole section used; for the data used here, the baselines were sufficiently stable.

The half-light times from the 1968 data set were taken from the analysis done by Kovalevsky and Link (1969). The half-light times for the Japan data sets were those given by Hirose (1968); these differ by up to 3 seconds for the values given by Osawa et al. (1968) and Takenouchi et al. (1968). The half light times for the Australia data set were given by Miller (1969). Freeman and Lyngå (1970)

quote a standard deviation of 2 seconds for the that data. The Japan light curves were published in Kovalevsky and Link; in an attempt to find a definitive half-light time, they were digitized and the half-light times found from a least squares fit to an isothermal light curve. The values found (see Table 3-4) differ from the values quoted by Hirose by up to 1.5 second. The digitization was done from a copy of the light curve; distortions due to the copying, and smoothing from the digitization can account for a formal error in the time of up to 2 seconds. The uncertainty in radius and oblateness for the 1983 data is predicted then to be a factor of 3 to 4 lower than the uncertainty for the 1968 data.

Once a half-light time for each location is found, the times must be changed into coordinates on some reference plane. The routine RINGPREP, written by D. Mink, was used. The coordinates used are based on Smart (1965). Smart defines the fundamental plane as the plane through Earth perpendicular to the line of sight from the occulting planet to the star (see Fig. 3-3). The origin of the fundamental plane is at the center of Earth, with the η axis pointing north and the ξ axis pointing east. The coordinates (ξ_1, η_1) of the observer as projected on the fundamental plane will be

$$\xi_1 = \rho \cos\phi' \sin h\,, \tag{3.5}$$

and

$$\eta_1 = \rho[\cos\delta_* \sin\phi' - \sin\delta_* \cos\phi' \cos h]\,. \tag{3.6}$$

In this case ρ is distance of the observatory from the center of Earth, ϕ' is geocentric latitude, and h is hour angle. The geocentric latitude is the latitude determined from the center of Earth, rather than from the astronomical zenith. The hour angle

is the difference between the local apparent sidereal time and the right ascension of the occulted star; δ_* is the declination of the occulted star.

The location of the center of Neptune on the fundamental plane is defined by the coordinates (ξ_2, η_2) as follows:

$$\xi_2 = \mathrm{D} \cos \delta_* (\Delta\alpha) , \tag{3.7}$$

and

$$\eta_2 = \mathrm{D}\Delta\delta . \tag{3.8}$$

Here D is Earth-Neptune distance, and $\Delta\alpha$ and $\Delta\delta$ are the differences in right ascension and declination between the star and the center of Neptune.

It should be noted that the above coordinates are time dependent. The coordinates of the observer relative to the center of Neptune on the fundamental plane will then be evaluated at the half-light time:

$$\Delta\xi = \xi_1 - \xi_2 , \tag{3.9}$$

and

$$\Delta\eta = \eta_1 - \eta_2 . \tag{3.10}$$

The assumption is that the half-light times correspond to points on the surface of an oblate spheroid in the atmosphere, coaxial to the planet. A rotation of the coordinates with respect to the projected pole of the planet must be done. The position angle, P, is defined as the angle of the pole projected on the fundamental plane as measured east from north (see Fig. 3-5). The coordinates corresponding to the location of the star on the plane at the half-light times will be (u, v) as follows:

$$u = -\Delta\xi \cos P + \Delta\eta \sin P, \tag{3.11}$$

and

$$v = \Delta\xi \sin P + \Delta\eta \cos P\,. \tag{3.12}$$

The final step is to change the coordinates from the fundamental plane to the sky plane. The sky plane is defined as the plane passing through the occulting planet, parallel to the fundamental plane. The sky plane is expanded relative to the fundamental plane; that is, the size of the occulting planet appears smaller at the fundamental plane than it actually is, due to the effects of general relativity and refraction. The gravitational field of the planet bends the starlight, as does the refraction through the atmosphere of the planet, making the planet appear smaller. The transformation to the sky plane corrects for the effects of general relativity and refraction. The bending angle θ_{GR} of the rays from the star due to general relativity is

$$\theta_{GR} = \frac{4GM_N}{c^2 r} \tag{3.13}$$

so the change in u will be

$$\Delta u = \frac{Du}{r}\theta_{GR}\,, \tag{3.14}$$

and in v will be

$$\Delta v = \frac{Dv}{r}\theta_{GR}\,, \tag{3.15}$$

where G is the gravitational constant, M_N is the mass of Neptune, c is the speed of light, and $r^2 = u^2 + v^2$. D is the Earth-Neptune distance. The change in v is exactly analogous. The bending angle θ_{ref} of the ray at half-light time due to refraction from the atmosphere will be

$$\theta_{ref} = \frac{H}{D}\,, \tag{3.16}$$

and the change in u will be

$$\Delta u = \frac{Du}{r}\theta_{ref}\,, \tag{3.17}$$

$$\Delta v = \frac{Dv}{r}\theta_{ref}\,. \tag{3.18}$$

Once the sky plane coordinates are calculated, the radius and oblateness of the spheroid can be found. A non-linear least squares method is used to find the best fit for the parameters. The obvious method is to fit the data to an ellipse on the sky plane, of the form

$$\frac{u^2}{R_e^2} + \frac{v^2}{s^2} = 1, \tag{3.19}$$

where R_e is the semimajor axis and s is the semiminor axis of the ellipse. The semi-major axis is the equatorial radius. The semiminor axis will depend on the equatorial radius, the polar radius, and B, the declination of Earth:

$$s^2 = R_e^2 \sin^2 B + R_p^2 \cos^2 B\,. \tag{3.20}$$

However, flux is measured as a function of time, not radius. It would be preferable to find the residuals of the parameters in terms of time, the true independent variable. Equation 3.19 must then be solved as a function of time. The minimum residuals in the fit will be found from the change in the predicted half-light time as a function of the change in parameters. Table 3-3 shows the differences in fit values, errors, and residuals for a fit in time and a fit in radius. The change in the solutions to the fit is much less than the error bars. For this event, it does not make a significant difference if the residuals are calculated in radius or in time.

The planet will have some offset from the predicted ephemeris position, f_0 to the east and g_0 to the north. The parameters being fit are then f_0, g_0, R_e, and ϵ.

The fitting routine was tested by putting in data sets which have known solutions to the parameters. The data sets were fit, and the convergence values compared to the known solutions. The first set was ideal data; the parameters converged perfectly to the correct values with zero residuals. Data from the ϵ Geminorum occultation by Mars were tested to show the same convergence values found by French and Taylor (1981). Data from the Uranus occultation of SAO 158687 analyzed by Elliot et al. (1980) were also tested with the same satisfactory results.

The 1968 half-light times as given by Kovalevsky and Link (1969) were fit. Their results were reproduced using the pole position found by Gill and Gault (1968), the ephemeris given, and their corrections for refractivity and general relativity. The next fit was done using their half-light times, but using the ephemeris calculated by Standish et al. (1976), and the pole position found by Harris (1984). The corrections for refractivity and relativity were also slightly different because a different value for the mass of Neptune was used. The results of this fit (see Table 3-5) gave values of $R_e = 25243 \pm 30$km and$\epsilon = 0.0198 \pm 0.003$. This is within the error bars quoted by Kovalevsky and Link. The known uncertainty in the half-light time was 2 seconds; the data were changed at random by that uncertainty to find the formal error. Their error for the oblateness is larger than that found in this fit because they did not actually do a fit for the oblateness; they stepped the oblateness by 0.001 and found the minimum of the sum of the squared residuals when fitting for the radius. The minimum value was at 0.021; however, since the radius is correlated with the oblateness, the error in the oblateness was not 0.001, but much higher. In this analysis, the oblateness was actually fit for, which eliminates that problem.

The 1968 data were also fit using the half-light times found from digitizing the Japan light curves and using the least squares fit to an isothermal curve. The results give $R_e = 25202 \pm 30$km and $\epsilon = 0.0188 \pm 0.0030$. The error bars were found in the same way as discussed above. These results are compatible with those found by Kovalevsky and Link.

The 1983 data were then fit; the results give

$$R_e = 25263 \pm 9 \text{ km and}$$

$$\epsilon = 0.0160 \pm 0.0015 .$$

This value is lower than but still within the error of the value obtained with the 1968 half-light times. The errors in the parameters from the fit using the 1983 data were found by changing each data set by the uncertainty in the half-light time, 0.4 second.

When a joint fit of the 1983 and 1968 data was done, the formal result of the fit gave $R_e = 25248 \pm 9$ km and $\epsilon = 0.0195 \pm 0.0012$. It can be seen from Figure 3-6 that the value given by the joint fit is closer to the 1968 data because the sum of the squared residuals from the 1983 data is an order of magnitude lower than from the 1968 data. This suggests that improvements in observing methods have had a significant effect on the quality of data. However, it also means that the 1983 data have little leverage on the sum of squared residuals from the combined data sets. The fit cannot be considered useful because the quality of the two data sets is so different; for a joint fit to be truly effective, the minimum of the sum of the squared residuals for both sets would have to be comparable. If using a non-linear

least squares method, the proper step to take is to weight the 1983 data by the comparative uncertainty in time; however, the residuals from the 1983 data are a factor of four lower than the residuals from the 1968 data. Weighting the 1983 data by $\frac{1}{\sigma^2}$ would cause the reverse problem; the 1968 data would have no leverage in the fit. Since the data sets are so small, systematic errors may have a significant effect, so neither data set can be entirely dismissed.

The results from the 1983 and 1968 data are compatible, but there is still a significant discrepancy. There are too few data points in either data set to make a definitive determination of the oblateness; another occultation of Neptune with good coverage across the planet should be observed to confirm the 1983 results. Because of the large uncertainty in the half-light times for the 1968 data, the values from the 1983 data are the most reliable.

It was suggested by Dermott (1984) that the uncertainties in Harris' pole position might significantly change the values from the fit. Harris used the orbit of Triton in his analysis. Dermott shows that the most significant uncertainty in Harris' calculation was in the moment of inertia. A new pole position was calculated for twice the maximum uncertainty in the moment of inertia, and the new position was used in the fit for the 1983 data. The results gave $R_e = 25259$ km, and $\epsilon = 0.0159$, still within the error bars of the formal fit. Table 3-5 gives a summary of all the fits done using the half-light times.

The position angle of the pole, P, can be found using data from one occultation. However, the fit did not converge in a stable way for either the 1968 or the 1983 data sets alone. Using both data sets, it becomes possible to fit for the true variables

of the pole position, the right ascension and declination of the pole. Since B, the declination of Earth (see Fig. 3-5), and P are the variables used in the calculation of the model equation, the transformation of right ascension and declination to B and P must be known. The transformation as described by Harris (1984) was used.

The fitting routine for a non-linear least squares fit requires the function of the change in predicted half-light time with the change in a given parameter. The derivatives of time with respect to right ascension and declination proved to be extremely complex in the analytical form, so the derivatives were calculated numerically. The fit successfully converged, giving

$$\alpha_p(1950.0) = 291.5^\circ \pm 7.6\,,$$

$$\delta_p(1950.0) = 34.6^\circ \pm 5.1\,.$$

Figure 3-7 shows the error ellipse. The results were within the error bars of the right ascension and declination of the pole as calculated by Harris (1984). The error bars are much larger than Harris', but the fact that the fit was successful indicates that fitting more data sets might bring down the error bars to a comparable level. This provides an independent means of locating the pole position.

Chapter 4.

OBLATENESS — N, P LEVEL DETERMINATION

In the first part of this analysis, the time in the light curves used to define the limb of the planet for the purpose of finding the radius and oblateness was the time of half stellar flux, the half-light time. Since the atmosphere is not isothermal, this does not correspond to a physical parameter in the atmosphere of Neptune. A better way to define the limb of a planet with an atmosphere is to use a surface corresponding to some physical level in the atmosphere, such as a constant number density or pressure level. Numerical inversion of light curves allows us to obtain reliable n, p, and T profiles as a function of height in the atmosphere. French and Lovelace (1983) determined that inversion profiles reflect the large scale structure of an atmosphere. However, each data set must be tested for the accuracy of the profiles found in the inversion method; noise and uncertainties in the data may affect the alignment of the number density, pressure, or temperature with a given height. For the purpose of finding a radius and oblateness, it must be known how well a number density, pressure, or temperature found in the inversion corresponds to the time assigned to it. The error in the half-light time determination from an

isothermal fit for the data sets of interest is about 0.4 second. If the time associated with a given number density or pressure level in the atmosphere can be found more accurately than this in each light curve, then a better fit for radius and oblateness can be obtained.

The method used to do the inversion of the light curve is the method described by Wasserman and Veverka (1973) and French, Elliot, and Gierasch (1978). The inversion routine was QINV2, written by R. French. The first step is to determine the bending of the light ray as it passes through material of varying refractivity. This can be derived from Huygen's principle. The bending angle, θ, is defined as

$$\theta = \int_{-\infty}^{+\infty} \frac{d[\ln(n)]}{dr} dx \tag{4.1}$$

where dr is depth in the atmosphere and dx is along the line of sight (see Fig. 4-1). The assumptions are that

1. light rays do not cross,
2. $n \approx 1$, so $\frac{1}{n}\frac{dn}{dr} \approx \frac{dn}{dr}$, and
3. the depth in the atmosphere probed by an occultation is much less than the radius of the planet.

The approximate inversion solution to Equation (4.1) is

$$\nu(r) = \frac{1}{(2\pi \mathrm{R}_p)^{\frac{1}{2}}} \int_{\infty}^{r} \frac{\theta(r')dr'}{(r'-r)^{\frac{1}{2}}}, \tag{4.2}$$

where R_p here is the planetary radius; θ, r', and dr' must be calculated from the change in flux. If ϕ is normalized stellar flux at a given time, and D is distance to the planet,

$$\frac{1}{\phi} = \frac{dr + \mathrm{D}d\theta}{dr} = 1 + \mathrm{D}\frac{d\theta}{dr}. \tag{4.3}$$

It is also true, from occultation geometry, that

$$\Delta r + \mathrm{D}\Delta\theta = -v\Delta t\,. \tag{4.4}$$

These equations can be solved for Δr and $\Delta\theta$:

$$\Delta r = -v\Delta t\phi \tag{4.5}$$

$$\Delta\theta = -(1-\phi)\frac{v\Delta t}{\mathrm{D}} \tag{4.6}$$

Then θ and r can be calculated from the light curve by

$$\theta_i = \sum_{i=1}^{N}\Delta\theta_i \quad \text{and} \quad r_i = \sum_{i=1}^{N}\Delta r_i\,. \tag{4.7}$$

Once $\nu(r)$ is obtained, number density can be solved for:

$$\mathrm{n}(r) = \frac{\mathrm{n}_{STP}}{\nu_{STP}}\nu(r) \tag{4.8}$$

The refractivity at STP is evaluated for solar fractions by number of H and He, 0.9 and 0.1 respectively. The hydrostatic equation

$$\frac{d\mathrm{p}}{dr} = -\overline{\mu}m_H\mathrm{n}(r)g \tag{4.9}$$

is integrated to find pressure, p; $\overline{\mu}$ is the mean molecular weight, m_H is the mass of the hydrogen atom, and g is the gravitational acceleration. The gravitational acceleration is assumed to be constant for a given inversion because the depth of the region probed by the inversion is much less than the radius of the planet. Once pressure and number density are obtained, the temperature profile is found using the perfect gas law,

$$\mathrm{p}(r) = \mathrm{n}(r)k\mathrm{T}(r) \tag{4.10}$$

where k is Boltzmann's constant.

There are some inherent limitations in this method. One limitation is that no information on scales shorter than the Fresnel zone can be obtained. The Fresnel zone is defined as the scale perpendicular to the line of sight across which there will be constructive interference. Across an area proportional to λ, interference occurs and the image is "smeared out" over this scale. This is the resolution limit of an occultation. The Fresnel scale is defined as

$$R_F = \sqrt{\lambda D}\,. \tag{4.11}$$

Empirically, Elliot et al. (1981) have found that the scale over which information can obtained is more nearly

$$R_F = 1.7\sqrt{\lambda D}\,. \tag{4.12}$$

For Neptune, this value is about 3.4 km for $\lambda = 0.78\mu$ and about 5.1 km for $\lambda = 2.2\mu$. This is one-tenth of a scale height or less.

In addition, an assumption made in the inversion analysis is that severe ray-crossing does not occur. The light from the star can be considered as a wavefront passing through the planet's atmosphere. The wavefront will be successively more delayed deeper in the atmosphere. However, large fractional temperature variations over a short scale can produce variations in number density and hence refractivity. Ripples will form in the wavefront (see Fig. 4-2). If the length of the ripple is defined as L, then it is easy to see that the shorter L is, the more likely it is that rays from the rippled wavefront will converge on each other and form crossed rays. French and Lovelace (1983) showed that the limit on fractional temperature variations $\Delta T/T$

necessary to assume no ray crossing is

$$\frac{\Delta T}{T} > \left(\frac{2\pi H}{L}\right)^{\frac{3}{2}}. \tag{4.13}$$

They show that the inversion process essentially ignores the information when severe ray crossing occurs and the temperature variations do not show up in the retireved temperature profile. This means that the corresponding number density and pressure variations are also suppressed. Therefore it must be assumed that severe ray crossing does not occur for the inversion to be believed.

There are other limitations to the method which will depend to some extent on the data. One source of error is the assumption that g, the gravitational acceleration of the planet, is a constant. In fact, g will depend on latitude, and the rotation of the planet adds an additional acceleration:

$$g_{eff} = \frac{GM_N}{R^2(\epsilon,\phi)} - \Omega^2 R(\epsilon,\phi)\cos\phi \tag{4.14}$$

where Ω is the rotation rate, M_N is the mass of Neptune and ϕ is latitude on the planet. Approximating g as a constant will not affect the number density determination, because g is used in the hydrostatic equation. The hydrostatic equation is only used when finding p and T. Table 4-2 shows g_{eff} for each data set. The value varies about 2% across the whole latitude range. This corresponds to an error of 2% in the scale height in the atmosphere. Since the scale height of Neptune is about 50 km, and the perpendicular velocity of the event is about 22 km s^{-1}, the error from g_{eff} would cause a misalignment in the time of only 0.01 second.

A more important source of error comes from the fact that the inversion must be started at an arbitrary point in the light curve. The initial conditions, where

$\theta = 0$ and $r = 0$, are decided by the value at this arbitrary point. This point will be subject to the noise in the light curve. In the upper atmosphere, the number density is very low; fluctuations due to noise in the upper part of the light curve are interpreted by the inversion process as huge variations in the temperature. Wasserman and Veverka (1973) showed that, although this error propagates through the entire inversion, the contribution is fractionally most important high in the light curve. The first three to four scale heights in the inversion should be ignored altogether. The resulting error that is propagated through the profile can be checked by changing the initial conditions (starting at some other equally arbitrary point) and checking how the well the resulting profiles converge to the same profile (French, Elliot and Gierasch, 1978). This may produce a significant error in the time associated with a specific n, p, or T level before the level where the profiles will converge. This was tested by inverting light curves at four different points, ranging from 5 to 8 back scale heights in the light curve from the half-light time (see Table 4-3). The profiles from the light curve were compared. Figure 4-3 shows how well the profiles for a sample light curve converged. It was found that the profiles obtained from inversions starting from between 6.8 and 8.0 scale heights back converged most completely. The first few scale heights of the profiles did not converge at all, which was predicted. At levels deeper than $n \sim 3 \times 10^{13} cm^{-3}$, and $p \sim 8 \times 10^{-4}$mbars the profiles converged with a discrepancy in time of less than 0.2 seconds for a given number density or pressure level. This is better than the uncertainty in the half-light time found by the isothermal fit. The Hawaii emersion sets and the Mt. Stromlo data set were not used because the baselines were so poorly known. All profiles used in the following tests and results were inverted

starting from 7.5 scale heights back in the light curve.

Another source of error in the inversion, as for the half-light time, is the uncertainty in the baselines. To carry out the inversion, the upper and lower baselines are assumed to be perfectly known. An error in the baseline means that the calculated change in stellar flux as a function of time will be incorrect. The fractional error due to an uncertainty in the upper basseline will be largest at the top of the light curve; for an uncertainty in the lower baseline, it will be largest at the bottom of the light curve (French, Elliot and Gierasch, 1978). Table 4-1 shows how well the baselines are known, from the isothermal fit. It is clearly critical to select the correct number density and pressure levels for the fit. They must be far enough down in the fit to avoid errors due to the initial conditions and the uncertainty in the upper baseline, and high enough to avoid the error due to uncertainty in the lower baseline.

The error due to uncertainties in the baseline is an important one in the inversion. Tests were run to predict the uncertainty in time from the inversion. An isothermal light curve with a scale height of 50 km and a perpendicular velocity of 22.5 km s^{-1} was tested first. The upper and lower baselines were varied by 1, 2, and 3%; the lower baseline was normalized to the full stellar counts so that changes in one baseline are comparable to changes in the other. Figure 4-4 shows the resulting profiles. An error in the upper baseline causes a divergence from the expected curve high in the profile; below the $n = 9 \times 10^{13}$ cm^{-3} and $p = 9 \times 10^{-4}$ mbar levels, the profiles converge to better than 0.01 second for a given number density or pressure. An error in the lower baseline causes the profile to diverge at levels

lower than n = 2×10^{14} cm ^{3} and p = 10 ^{3} mbar; there is a minimum, then, when the error from the upper baseline is becoming less important and the error from the lower baseline is just starting to become important. Based on an isothermal light curve, this minimum occurs at n = 10^{14} cm ^{3} and p = 10 ^{3} mbar. The half-light time for an isothermal atmosphere, at a planet of the size and distance of Neptune and a scale height of 50 km, occurs at approximately n = 4.3×10^{13} cm ^{3}, so this corresponds to about 0.85 scale heights in the atmosphere after half-light time.

Other tests were run on the true data, varying the baselines by 1, 2, and 3%. The resulting profiles agreed qualitatively with the results from the isothermal tests. However, the true convergence for the profiles was not as good as those predicted from the isothermal tests. This was expected, partly because the true data have noise, and partly because the atmosphere is not really isothermal. The number density has an uncertainty in time of about 0.25 second, for the n = 10^{14}cm^{-3} level; the p = 10^{-3} mbar level has an uncertainty of 0.4 second, comparable to the isothermal fit. The results of the isothermal tests had indicated that the pressure may not be as good a parameter as the number density, and this result was also confirmed by the profiles. The error from the upper baseline overlaps with the error from the lower baseline so that the minimum of the two effects still produces an error of 1 second or more. This agrees with the theoretical result of French, Elliot and Gierasch (1978); the pressure is integrated from the number density, so the effects from the initial conditions are weighted more farther down in the light curve for pressure. This weighting brings the error due to the initial condition farther down into the profile than for number density. The error from the upper baseline does not begin to drop off until the error due to the lower baseline begins to be

important.

The number density levels selected for the fit were 5×10^{13}, 8×10^{13}, 10^{14}, and 2×10^{14}cm ^{3}. The times associated with these levels for each data set and the results from fitting each level for radius and oblateness are summarized in Table 4-3. The best result was found using the n = 10^{14}cm ^{3} level:

$$R_e = 25171 \pm 7 \text{ km and}$$

$$\epsilon = 0.0150 \pm 0.0011 .$$

This agrees well with the results from the half-light time fits, and the best fit is just at the level predicted from the tests of the isothermal curve and the true data. The fit at this level was significantly better than the fit using the half-light times. Actually, the change in the radius and oblateness found at each level shows that the true error bars are much higher than the formal ones quoted. This method is still useful and could give good results with more data sets.

The pressure levels selected were 8×10^{-4}, 10^{-3}, 2×10^{-3}, and 7×10^{-3}mbar. The times for these levels are listed in Table 4-4. All of the results were worse than using the half-light times. The best fit was for the at 10^{-3}, as predicted from the tests:

$$R_e = 25288 \pm 9 \text{ km and}$$

$$\epsilon = 0.0172 \pm 0.0015 ,$$

agreeing well with the half-light time fit and the best number density fit. The fit was a factor of three worse than using the best number density level. For this data set, number density is a better physical parameter than pressure to define the limb of the planet.

Chapter 5.

IMPLICATIONS AND CONCLUSIONS

The light curves from the 1983 occultation of Neptune were used to find the radius and oblateness of Neptune, using the time of half-light to define the limb of the planet. These data have much lower uncertainties in time than the 1968 occultation used by Kovalevsky and Link (1969), leading to a more accurate determination of the radius and oblateness. The 1968 data were re-analyzed using the half-light times used by Kovalevsky and Link, but with an improved ephemeris and pole position (Harris, 1984). The oblateness found using the 1983 data is marginally consistent with the values found by Kovalevsky and Link. It is somewhat more consistent with the re-analyzed 1968 data. The 1968 data had such large uncertainties in timing that the 1983 results are more trustworthy.

The importance of the oblateness is that it is, to first order, directly related to the rotation rate of the planet, Ω, and the coefficient of the second order zonal harmonic, J_2:

$$\epsilon = \frac{3}{2} J_2 + \frac{3\Omega^2}{8\pi G \overline{\rho}} \tag{5.1}$$

where G is the gravitational constant and $\overline{\rho}$ is the mean density of the planet. The unknowns in the above equation are Ω, J_2, and ϵ; each may be independently

determined. The uncertainty in the mean density can be ignored in this approximation because it depends only on the mass, which is well known, and the radius to the third power. The latest value for the rotation rate is 17.8 $\pm$ 0.1 hours (Terrile et al., 1984). This value was obtained from observations of markings on the planet with time (Smith et al., 1979). Neptune's J_2 was found by Harris (1984) to be 0.0043 $\pm$ 0.0003, assuming the mass ratio of Triton to Neptune is 0.00128. If Triton is actually much less massive, then the J_2 is 0.0037 $\pm$ 0.0002. The previous best value for the oblateness was 0.021. These three values are not very consistent (see Figure 5-1), but it was uncertain why. It has been shown in this analysis that the uncertainty in time in the 1968 data is so great that the oblateness from that data is not very reliable. Dermott (1984) has shown that a rotation rate of 17.8 hours, a J_2 of 0.0041, and an oblateness of 0.017 lead to a self-consistent model of Neptune. This is in very good agreement with the result found using the 1983 data (see Figure 5-1).

The oblateness, combined with J_2 and the rotation rate, can provide information about the internal structure of the planet. The Darwin-Radau relation gives the moment of inertia around the polar axis, C, for a given oblateness and J_2, provided those values are small and C is large:

$$\left[1 - \frac{3}{2}\frac{C}{MR^2}\right]^2 = \left(\frac{4}{25}\right)\left(\frac{5m}{2\epsilon} - 1\right) \tag{5.2}$$

where

$$m = \frac{\Omega^2 \mathrm{R}^3}{\mathrm{GM}}. \tag{5.3}$$

For a solid, homogeneous sphere, the moment of inertia is 0.4. Zharkov and Trubitsyn's (1978) two-layer model, with a homogeneous core and homogeneous mantle,

predicts a moment of inertia of 0.25. Figure 5-1 shows that this model agrees with Kovalevsky and Link's oblateness, but not with the observed J_2 and rotation rate. The value for the oblateness found from the 1983 data is quite consistent with the rotation rate and J_2, but the two layer model no longer explains the data. Hubbard and MacFarlane (1980) have calculated a more condensed, three-layer model which is marginally consistent (Hubbard, 1984) with the preliminary value for the oblateness found by Hubbard et al.(in preparation); however, it requires that the rotation rate be 13.7 hours, which is not supported by data.

The oblateness found from this analysis of the 1983 data are the most consistent with other data. The results indicate that Neptune is less centrally condensed than the previous best model, the Zharkov and Trubitsyn model, predicts. A new interior model is needed. It is interesting that the moment of inertia for Neptune, about 0.28, is significantly different from that deduced by Dermott (1984) for Uranus, 0.20. This suggests that the interiors of Neptune and Uranus are very dissimilar.

A numerical inversion of the 1983 light curves was performed to obtain the number density, pressure, and temperature as a function of height in the atmosphere. Tests were run using isothermal light curves to determine how well a given time in the light curve corresponds to the number density or pressure level assigned to it by the inversion process. The uncertainties in the baselines were found to be the largest source of error in the inversion process for this data set. An error in the upper baseline will cause a large initial uncertainty in the number density, pressure and temperature profiles; an error in the lower baseline causes a large uncertainty deep in the profile. The location in the profiles which correspond to a minimum

in the uncertainty from combined errors in the upper and lower baselines is about 0.85 scale heights in the atmosphere deeper than the level at the half-light time. This result, found in the isothermal test curves, was confirmed in the true data. Several fits for radius and oblateness were done, using a variety of number density and pressure levels to define the limb rather than the half-light time. The levels were selected to scan across the region of the predicted minimum uncertainty in time; the lowest residuals for the fit were found at the levels predicted by the tests. These levels are the $n = 10^{14} cm^{-3}$ and $p = 10^{-3} mbar$ levels. The values for the oblateness found using these fits agree well with the value found using the half-light times from the 1983 data. The residuals from these fits indicate that using the appropriately chosen number density level to define the limb is a more accurate way of finding the oblateness than using the half-light time; the constant pressure level method is comparable to the half-light method.

The pole position was also found using the data from both the 1968 and 1983 occultations. The error ellipse is not consistent with the value for the pole found by Harris (1984) from the regression rate of Triton's orbit; however, the uncertainties in the parameters found from the fit using the occultation data are probably greater than the formal errors found from the fit, because of the large uncertainty in time of the 1968 data. At this time Harris' value is certainly the most accurate.

Another step that may be taken with the 1983 data is to check the correlation of spikes found from light curves probing different locations along the limb of Neptune. A correlation would indicate that the spikes are being formed from some large scale horizontal feature in the atmosphere, such as a layer. Preliminary analysis indicates

no correlation of spikes, in contrast to the results of French et al. (1983), which indicate possible global atmospheric layering. The lack of correlation suggests that the spikes may be formed by turbulence or some other non-isothermal process. A thorough analysis would be useful.

The values found for the radius and oblateness of Neptune from the 1983 data are a significant improvement from the 1968 data. It is unfortunate that the uncertainty in time for the 1968 data is so high so that a joint fit of both data sets was not useful. Another occultation observation with good timing accuracy and wide coverage (at least three chords) across Neptune would further improve the oblateness, and constrain the interior models to a greater extent.

In addition, new data could be combined with the 1983 data to obtain a good pole position. Data from several occultations, with widely different aspects of the planet, would give a good enough determination to provide an independent check of the dynamical determination of the pole position.

REFERENCES

Baum, W. A. and Code, A. D. 1953 *A. J.*, 58, 108–112

Born, M. and Wolf, E. 1970 *Principles of Optics*, Pergamon Press, New York

Dermott, S. F. 1984 *Phil. Trans. Roy. Soc. Lond. A.*, in press

Elliot, J. L. 1979 *Ann. Rev. Astron. Astrophys.*, 17, 445–475

Elliot, J. L., Dunham, E., Mink, D. J., and Churms, J. 1980 *Ap. J.*, 236, 1026–1030

Elliot et al., 1981 *Nature*, 294, No. 5841, 526

Elliot et al. 1984 in preparation

French, R.G.. Elliot, J. L., and Gierasch, P. J. 1978 *Icarus*, 33, 186–202

French, R. G., Elias, J. H., Mink, D. J., and Elliot, J. L. 1983 *Icarus*, 55, 332-336

French, R. G., and Lovelace, R. V. E. 1983 *Icarus*, 56, 122–146

French, R. G., and Taylor, G. 1981 *Icarus*, 45, 577–585

Gill, J. R. and Gault, B. L. 1968 *A. J.*, 73, 595

Harris, A. 1984 proceedings from conference

Hirose, H. 1968 *IAU circ.* No. 2068, 22 April 1968

Hubbard, W. B. 1984 proceedings from conference

Hubbard et al., (in preparation)

Jokipii, J. R. and Hubbard, W. B. 1977 *Icarus*, 30, 537–550

Kovalevsky, J. and Link, F. 1969 *Astron. Astrophys.*, 2, 398–412

Miller, M. J. 1968 *IAU circ.* No.2067, 18 April 1968

Mink, D. J., Klemola, A. R., and Elliot, J. L. 1981 *A. J.*, 86, 135–137

Osawa, K., Ichimura, K., and Shimuzu, M. 1968 *Tokyo Astron. Bull.*, Second Series, No. 184

Pannekoek, A. 1904 *Astron. Nachr.*, 164, 5–10

Rages, K., Veverka, J., and Wasserman, L. 1974 *Icarus*, 23, 59–65

Smith, B. A.,Reitsema, H. J., and Larson, S. M. 1979 *Bull. AAS*, 11, 570

Standish, E. M., Keesey, M. S. W., and Newhall, X. X. 1976 JPL Technical Report 32-1603

Takenouchi, T., Tomita, K., and Hirayama, T. 1968 *Tokyo Astron. Bull.*, Second Series, No. 183

Taylor, G. 1970 *Mon. Not. R. Astr. Soc.*, 147, 27–33

Terrile, R. J. and Smith, B. A. (in preparation)

Veverka, J. Wasserman, L., and Sagan, C. 1974 *Ap.J.*, 189, 569-575

Wallace, L. 1975 *Ap. J.*, 197, 257-261

Wasserman, L. H. and Veverka, J. 1973 *Icarus*, 20, 322–345

Zharkov, V. N., and Trubitsyn, V. P. 1978 *Physics of Planetary Interiors*, Pachart Publ. House

Appendix A.

DERIVATION OF ISOTHERMAL LIGHT CURVE

First define the scale height, H, such that

$$H \equiv \frac{k\mathrm{T}}{\bar{\mu} m_H g} \qquad (A.1)$$

where k is Boltzmann's constant, T is temperature, $\bar{\mu}$ is mean molecular weight, m_H is the mass of the H atom, a g is the gravitational acceleration. The refractivity ν for an isothermal atmosphere is

$$\nu = \nu_0 \exp\left[\frac{-(r - r_0)}{H}\right] \qquad (A.2)$$

where ν_0 is the refractivity at the top of the atmosphere, r_0 is the height in the atmosphere, and r is the distance from the center of the planet to a given point along the ray (see Figure A-1). See Appendix C for the derivation of the bending angle due to refraction in the atmosphere; it will be assumed that it is known that

$$\theta = \int_{-\infty}^{+\infty} \frac{d\nu}{dr}\, dx\,. \qquad (A.3)$$

Now,

$$\frac{d\nu}{dr} = \frac{-\nu}{H} \exp\left[\frac{-(r - r_0)}{H}\right] dx\,; \qquad (A.4)$$

see Figure 4-1 for the inversion geometry.

$$x^2 = r^2 - r_1^2 \text{ and} \tag{A.5}$$

$$(r - r_0) = (r - r_1) + (r_1 - r_0)\,. \tag{A.6}$$

Since $r \approx r_0 \approx r_1$,

$$x^2 = (r - r_1)(r + r_1) \approx (r - r_1)2r_1 \tag{A.7}$$

and so

$$(r - r_1) \approx \frac{x^2}{2r_0}\,. \tag{A.8}$$

It follows that

$$(r - r_0) = \frac{x^2}{2r_0} + (r_1 - r_0)\,, \tag{A.9}$$

and the bending angle equation becomes

$$\theta = \frac{-2\nu_0}{H}\ \exp\left[\frac{(r_1 - r_0)}{H}\right] \int_0^{+\infty}\ \exp\left[\frac{-x^2}{2r_0 H}\right] dx\,. \tag{A.10}$$

Integrating this gives

$$\theta = \frac{-2\nu}{H}\left[\frac{\pi r_0 H}{2}\right]^2\ \exp\left[\frac{-(r_1 - r_0)}{H}\right]. \tag{A.11}$$

Now, we will define

$$\tilde{\phi} = \frac{\phi^*}{\phi} = \frac{1}{\phi} \tag{A.12}$$

where ϕ^* is full stellar flux, normalized to be 1, and ϕ is the flux at time t. From geometry it can be seen that

$$\tilde{\phi} = 1 - D\frac{d\theta}{dr_1} \text{ and} \tag{A.13}$$

$$\frac{d\theta}{dr_{\perp}} = \frac{-\theta}{D}, \text{ so} \tag{A.14}$$

$$\tilde{\phi} = 1 + \frac{D\theta}{H}. \tag{A.15}$$

Also from the geometry,

$$\frac{d\theta}{dt} = \left[1 - \frac{1}{\tilde{\phi}}\right]\frac{v_{\perp}}{D}. \tag{A.16}$$

D is the Earth-Neptune distance, and $v_{\perp}$ is the perpendicular velocity of the event.

$$\frac{d\tilde{\phi}}{dt} = \frac{D}{H}\frac{d\theta}{dt} \text{ and} \tag{A.17}$$

$$\frac{d\tilde{\phi}}{dt} = \frac{v_{\perp}}{H}\left[\frac{\tilde{\phi} - 1}{\tilde{\phi}}\right]. \tag{A.18}$$

This can be separated into two integrals over $\tilde{\phi}$ and t, and integrated from the time of half stellar flux, where $\tilde{\phi}$ will be 2, to any $\tilde{\phi}$:

$$\int_2^{\tilde{\phi}} \frac{\tilde{\phi}}{\tilde{\phi} - 1} d\tilde{\phi} = \frac{v_{\perp}}{H}\int_{t_{\frac{1}{2}}}^{t} dt. \tag{A.19}$$

Integrating gives

$$(\tilde{\phi} - 1) - (2 - 1) + \ln(\tilde{\phi} - 1) - \ln(2 - 1) = \frac{v_{\perp}}{H}(t - t_{\frac{1}{2}}) \tag{A.20}$$

and so, substituting ϕ back in,

$$(\frac{1}{\phi} - 2) + \ln(\frac{1}{\phi} - 1) = \frac{v_{\perp}}{H}(t - t_{\frac{1}{2}}). \tag{A.21}$$

Appendix B.

OBLATENESS FITTING PROGRAM

```
 10 ! REFIT9 8/6/83 JLE, KJM MOD
    IFIED BY PAM 9/1;12 10:2/8,2
    /21
 20 ! I/O IN DEG, INTERNAL CALC
    IN RAD
 30 !
 40 CLEAR
 50 COM F1,G1,F2,G2,D1,A
 60 OPTION BASE 1
 70 RAD
 80 DIM B(6),P0(6),B1(6),B2(6)
 90 A=297.813 @ D1=41.185
100 CALL "FITPOL" ( A,D1,B(),P0(
    ) )
110 GOSUB 2920
120 R=25225 @ E= 021 @ G9=7.6475
    1459833E-5 @ H=50 ! G9=GM(ne
    p)/C^2
130 !
140 DIM F1(20),G1(20),F2(20),G2(
    20),T0(20),Z1(20),Z2(20),Z3(
    20),Z4(20),Z5(20),Z6(20)
150 DIM I(10),J(10),P(10),Y(10),
    D1(20,10),A(10,10),X(10),Y1(
    10),E(10),R1(20),R0(20),F(10
    )
160 DIM T(20),T1(20),T2(20)
170 DIM D(2),F0(2),G0(2)
180 F0(1)=-5000 @ G0(1)=-4900 @
    F0(2)=-17000 @ G0(2)=300
190 D(1)=4376387000 @ D(2)=44178
    37600
200 DIM C$[10],D$[4],M$[5],C1$[1
    7],P8$[60],P9$[40],P$[100],Z
    1$[77],Z2$[63],Z$[140]
210 C$="COMPLETE" @ D$="DATA" @
    M$="MODEL" @ C1$="----COMPUT
    ING----"
220 P8$[1,60]="F0-α ERRORF1-α ER
    RORG0-δ ERRORG1-δ ERRORP-POS
     ANG P8-POS ANG"
230 P9$[1,40]="αPOL ERRORδPOL ER
    ROREQ RADIUS OBLATENESS"
240 P$[1,100]=P8$&P9$
250 Z1$[1,77]="MKOBSIMIRTF1IMIRT
    F1EMSS040IMSS040EMAAT3MIMAAT
    3MEMKA034IMKA034EMKA0#4IMKA0
    #4EM"
260 Z2$[1,63]="MTS74IM00D68IM00D
    68EM0KA68IM0KA68EMM6874IMM68
    74EMM6830IMM6830EM"
270 Z$[1,140]=Z1$&Z2$
280 !
290 DATA -27552.2475,-27542.601,
    17752.947,-29172.316,19274.0
    79,-29179.3175,19279.8505
300 DATA -27204.938,17293.925,-2
    7227.407,17286.762,-29233.02
    84
310 DATA -41323.3048,5800.2855
```

54's

```
320 DATA -41305.7693,5693.1532,-
    40416.7411,1759.954,-40416.7
    411,1759.954
330 MAT READ Z1
340 DATA 24.07,24.07,24.018,24.2
    241,24 21925,24.2241,24.2192
    5
350 DATA 24.272,24.267,24.272,24
     267,24.206
360 DATA 17.422,17.45,17.415,17.
    45,17.442,17.457,17.442,17.4
    57
370 MAT READ Z2
380 DATA 6467.7662,6467.594,5647
    .479,2185.505,1572.403,2185.
    123,1571.834
390 DATA 7139.871,6643.092,7140.
    151,6643.09,1745.7907
400 DATA 1184.4497,-11273.5652
410 DATA 889.0679,-11509.1887,-5
    801.2434,-16986.2153,-5801.2
    434,-16986.2153
420 MAT READ Z3
430 DATA -.4296,-.4296,-.44065,-
    .2959,-.31742,-.2959,-.31742
440 DATA -.305,-.317,-.305,-.317
    ,- 295
450 DATA -4.598,-4.622,-4.587,-4
    .611,-4.617,-4.639,-4.617,-4
    .639
460 MAT READ Z4
470 DATA 50.71163,51.1124,1934.9
    626,186.92945,2187.00478,186
    .6247,2187.21801
480 DATA 255.753314,2103.89344,2
    54.82,2103.586,184.86277
490 DATA 85.5,2788,115.5,2811.5,
    89,2506,89,2506
500 MAT READ Z5
510 ON KEY# 1,"DATA" GOSUB 600
520 ON KEY# 2,"ST FIT" GOSUB 930
530 ON KEY# 3,"END FIT" GOSUB 28
    80
540 ON KEY# 4,"RST PRM" GOSUB 29
    00
550 ON KEY# 5,"PUNT" GOTO 2950
560 CLEAR @ KEY LABEL
570 GOTO 570
580 !
590 !
600 CLEAR @ DISP "WHICH DATA SET
    S TO USE?"
610 FOR J=1 TO 20 STEP 2
620 DISP USING 630 ; J,Z$[J*7-6,
    J*7],J+1,Z$[(J+1)*7-6,(J+1)*
    7]
630 IMAGE 2D,2X,8A,3X,2D,2X,8A
640 NEXT J
710 DISP "NUMBER SETS INCLUDE";@
     INPUT I5
```

F's

$\dot{F}$'s

g's

$\dot{g}$'s

t½'s

```
720 REDIM Z6(I5)
730 O1=0
740 DISP "INPUT DATA SETS TO INC
    LUDE"
750 FOR K=1 TO I5
760 INPUT Z6(K)@ IF Z6(K)<12 THE
    N O1=O1+1
770 NEXT K
780 REDIM F1(I5),G1(I5),F2(I5),G
    2(I5),T0(I5)
790 !
800 K1=0
810 FOR J=1 TO 20
820 FOR K=1 TO I5
830 IF J=Z6(K) THEN SFLAG 10
840 NEXT K
850 IF NOT FLAG(10) THEN GOTO 89
    0
860 K1=K1+1
870 F1(K1)=Z1(J) @ F2(K1)=Z2(J)
    @ G1(K1)=Z3(J) @ G2(K1)=Z4(J
    ) @ T0(K1)=Z5(J)
880 CFLAG 10
890 NEXT J
900 CLEAR @ DISP D$&" "&C$ @ KEY
     LABEL @ RETURN
910 !
920 !
930 CLEAR @ DISP "PARM TO FIT"
940 DISP "F01,F02,G01,G02,P01,P0
    2,α,δ,R,E"
950 MAT INPUT I
960 DISP "# OF ITNS" @ INPUT N5
970 M=1
980 FOR J=1 TO 10
990 IF I(J)#0 THEN REDIM J(M)@ J
    (M)=J @ M=M+1
1000 NEXT J
1010 !
1020 N3=M-1 @ S9=SQR(I5-N3)
1030 !
1040 REDIM D1(I5,N3),A(N3,N3),Y1
     (N3),J(N3),R1(I5),R0(I5),T(
     I5),T1(I5),T2(I5)
1050 GOSUB 2670
1060 MAT Y=P
1070 !
1080 !
1090 PRINT ,,TAB(12);"NEPTUNE" @
      PRINT TAB(4);"RADIUS-OBLAT
     ENESS JOINT FIT"
1100 PRINT TAB(12);"REFIT9"
1110 PRINT ,,DATE$&"  "&TIME$ @
     PRINT VAL$(I5)&" PTS"
1120 PRINT "INPUT DATA F,G"
1130 FOR J=1 TO I5
1140 PRINT USING 1150 ; F1(J),G1
     (J)
1150 IMAGE 7D.3D,4X,7D.3D
1160 NEXT J
```

```
1170 PRINT @ PRINT "VALUES OF CO
     NSTANTS" @ PRINT
1180 X6=RTD(B(1)) @ X7=RTD(P0(1)
     )
1190 X8=RTD(B(2)) @ X9=RTD(P0(2)
     )
1200 PRINT "B=    ";VAL$(X6)&" DE
     G" @ PRINT "P=    ";VAL$(X7)
     &" DEG"
1210 PRINT "B8=    ";VAL$(X8)&" D
     EG" @ PRINT "P8=    ";VAL$(X
     9)&" DEG"
1220 PRINT @ PRINT "ORIG PARAM"
     @ K=10 @ REDIM F(K)@ MAT F=
     Y@ GOSUB 2810 @ PRINT
1230 !
1240 !
1250 DISP TIME$;C1$ @ R0=INF
1260 FOR N2=1 TO N5
1270 !
1280 FOR J=1 TO I5
1290 Q=1
1300 IF J>01 THEN Q=2
1310 B1=B1(Q) @ B2=B2(Q) @ B3=B1
     (Q+2) @ B4=B2(Q+2) @ B5=B1(
     Q+4) @ B6=B2(Q+4)
1320 P=P0(Q) @ P2=P0(Q+2) @ P3=P
     0(Q+4)
1330 D=D(Q) @ F=F0(Q) @ G=G0(Q)
1340 U=G1(J)-G @ V=F1(J)-F
1350 R6=U*U+V*V @ X,R7=SQR(R6)
1360 !
1370 FOR K=1 TO 3 @ Z=1+4*D*G9/R
     6+H/R7 @ R7=Z*X @ R6=R7*R7
     @ NEXT K
1380 !
1390 A1=SIN(P) @ A2=COS(P) @ X1=
     SIN(P2) @ X2=COS(P2) @ W1=S
     IN(P3) @ W2=COS(P3)
1400 U=Z*U @ V=Z*V @ U1=Z*G2(J)
     @ V1=Z*F2(J)
1410 U2=U*A1-V*A2 @ V2=U*A2+V*A1
      @ U3=U1*A1-V1*A2 @ V3=U1*A
     2+V1*A1
1420 L=B1+(1-E)*(1-E)*B2
1430 C1=U3^2*L+V3^2 @ C2=U3*U2*L
     +V3*V2 @ C3=(U2+R)*(U2-R)*L
     +V2^2 @ A3=C2^2 @ A4=C3^2
1440 T(J)=T0(J)-C3/(2*C2)-C1*A4/
     (8*A3*C2)
1450 IF I(7)=0 THEN GOTO 1500
1460 U4=U*X1-V*X2 @ V4=U*X2+V*X1
      @ U5=U1*X1-V1*X2 @ V5=U1*X
     2+V1*X1
1470 L1=B3+(1-E)*(1-E)*B4
1480 Y1=U5^2*L1+V5^2 @ Y2=U5*U4*
     L1+V5*V4 @ Y3=(U4+R)*(U4-R)
     *L1+V4^2 @ X3=Y2^2 @ X4=Y3^
     2
1490 T1(J)=T0(J)-Y3/(2*Y2)-Y1*X4
     /(8*X3*Y2)
```

MODEL

```
1500 IF I(8)=0 THEN GOTO 1550
1510 U6=U*W1-V*W2 @ V6=U*W2+V*W1
      @ U7=U1*W1-V1*W2 @ V7=U1*W
     2+V1*W1
1520 L2=B5+(1-E)*(1-E)*B6
1530 Z1=U7^2*L2+V7^2 @ Z2=U7*U6*
     L2+V7*V6 @ Z3=(U6+R)*(U6-R)
     *L2+V6^2 @ W3=Z2^2 @ W4=Z3^
     2
1540 T2(J)=T0(J)-Z3/(2*Z2)-Z1*W4
     /(8*W3*Z2)
1550 A5=(2*A3+C1*C3)/(2*C2*A3) @
      A6=(4*C3*A3+3*A4*C1)/(8*A3
     ^2) @ A7=A4/(4*C2*A3)
1560 !
1570 IF FLAG(2) THEN GOTO 1950
1580 !
1590 M=1 ! F01
1600 IF I(1)=0 THEN GOTO 1640
1610 IF Q=2 THEN D1(J,M)=0 @ GOT
     O 1630
1620 D1(J,M)=Z*(-(A5*(L*U2*A2-V2
     *A1))+A6*(L*U3*A2-V3*A1))
1630 M=M+1 ! F02
1640 IF I(2)=0 THEN GOTO 1680
1650 IF Q=1 THEN D1(J,M)=0 @ GOT
     O 1670
1660 D1(J,M)=Z*(-(A5*(L*U2*A2-V2
     *A1))+A6*(L*U3*A2-V3*A1))
1670 M=M+1 ! G01
1680 IF I(3)=0 THEN GOTO 1720
1690 IF Q=2 THEN D1(J,M)=0 @ GOT
     O 1710
1700 D1(J,M)=Z*(A5*(L*U2*A1+V2*A
     2)-A6*(L*U3*A1+V3*A2))
1710 M=M+1 ! G02
1720 IF I(4)=0 THEN GOTO 1760
1730 IF Q=1 THEN D1(J,M)=0 @ GOT
     O 1750
1740 D1(J,M)=Z*(A5*(L*U2*A1+V2*A
     2)-A6*(L*U3*A1+V3*A2))
1750 M=M+1 ! P01
1760 IF I(5)=0 THEN GOTO 1800
1770 IF Q=2 THEN D1(J,M)=0 @ GOT
     O 1790
1780 D1(J,M)=(L-1)*(-(A5*U2*V2)+
     A6*(U3*V2+U2*V3)-A7*U3*V3)
1790 M=M+1 ! P02
1800 IF I(6)=0 THEN GOTO 1840
1810 IF Q=1 THEN D1(J,M)=0 @ GOT
     O 1830
1820 D1(J,M)=(L-1)*(-(A5*U2*V2)+
     A6*(U3*V2+U2*V3)-A7*U3*V3)
1830 M=M+1 ! α
1840 IF I(7)=0 THEN GOTO 1870
1850 D1(J,M)=(T(J)-T1(J))/DTR(-.
     5)
1860 M=M+1 ! δ
1870 IF I(8)=0 THEN GOTO 1900
1880 D1(J,M)=(T(J)-T2(J))/DTR(-.
     5)
```

MODEL

DERIVATIVES

```
1890 M=M+1 ! R
1900 IF I(9)=0 THEN GOTO 1930
1910 D1(J,M)=A5*R*L
1920 M=M+1 ! E
1930 IF I(10)=0 THEN GOTO 1950
1940 D1(J,M)=(1-E)*B2*(A5*(U2+R)
     *(U2-R)-2*A6*U3*U2+A7*U3^2)
1950 NEXT J
1960 !
1970 IF FLAG(2) THEN CFLAG 2 @ G
     OTO 2290
1980 !
1990 MAT A=TRN(D1)*D1
2000 MAT R1=T0-T
2010 MAT X=TRN(D1)*R1
2020 MAT Y1=SYS(A,X)
2030 MAT A=INV(A)
2040 R1=FNORM(R1)
2050 !
2060 R2=R1*R1 @ IF R1<R0 THEN R0
     =R1 @ N9=N2-1 @ MAT E=P@ MA
     T R0=R1
2070 !
2080 FOR J=1 TO N3 @ P(J(J))=P(J
     (J))+Y1(J) @ NEXT J
2090 !
2100 GOSUB 2700
2110 IF N2=1 THEN R3=R2 @ R4=R3/
     (I5-N3)
2120 PRINT USING 2130 ; TIME$,N2
     -1,R2,(R2-R3)/R4 @ MAT DISP
      Y1
2130 IMAGE 8A,2D,X,D.3DE,X,D.2DE
2140 !
2150 IF FLAG(1) THEN GOTO 2260
2160 IF I(7)=0 AND I(8)=0 THEN G
     OTO 2230
2170 A=RTD(A) @ D1=RTD(D1)
2180 CALL "FITPOL" ( A,D1,B(),P0
     () )
2210 GOSUB 2920
2220 !
2230 NEXT N2
2240 !
2250 N2=N2-1
2260 CFLAG 1 @ DISP M$ @ SFLAG 2
      @ GOTO 1280
2270 !
2280 MAT R1=T0-T@ R1=FNORM(R1)
2290 IF R1<R0 THEN MAT E=P@ N9=N
     2 @ R0=R1 @ MAT R0=R1
2300 R2=R1*R1 @ PRINT USING 2130
      ; TIME$,N2,R2,(R2-R3)/R4
2310 !
2320 S1=R0/S9 @ MAT P=E@ REDIM E
     (N3)@ GOSUB 2700
2330 FOR J=1 TO N3 @ E(J)=1/SQR(
     A(J,J)) @ NEXT J
2340 FOR J=1 TO N3
2350 FOR K=J TO N3
```

RESIDUALS CALCULATED

```
2360 X=E(J)*E(K)
2370 A(J,K)=A(J,K)*X
2380 IF J=K THEN 2400
2390 A(K,J)=A(K,J)*X
2400 NEXT K
2410 E(J)=S1/E(J)
2420 NEXT J
2430 !
2440 !
2450 MAT A=(100)*A
2460 FOR J=1 TO N3 @ A(J,J)=99 @
      NEXT J
2470 !
2480 PRINT ,,TAB(5);"FIT RESULTS
       "&DATE$&"  "&TIME$
2490 PRINT "ITNS=";N2
2500 PRINT ,,"BEST PARM ON ITN="
     ;N9
2510 K=10 @ REDIM F(K)@ MAT F=P@
      GOSUB 2810
2520 PRINT ,,"σ^2";R0*R0
2530 PRINT ,,"ERRORS"
2540 K=N3 @ REDIM F(K)@ MAT F=E@
      GOSUB 2730
2550 PRINT ,,"CORRL MATRIX",,
2560 MAT PRINT USING "M2Z" ; A
2570 !
2580 PRINT @ PRINT "OBS         R
     ESID" @ PRINT
2590 FOR J=1 TO I5
2600 PRINT USING 2610 ; Z$[Z6(J)
     *7-6,Z6(J)*7],R0(J)
2610 IMAGE 8A,2X,5D.5D
2620 NEXT J
2630 !
2640 PRINT @ PRINT "SUM RESIDS="
     ;SUM(R0) @ PRINT @ PRINT "R
     MS DEVIATION=";S1
2650 CLEAR @ DISP "FIT DONE" @ K
     EY LABEL @ RETURN
2660 !
2670 P(1)=F0(1) @ P(2)=F0(2) @ P
     (3)=G0(1) @ P(4)=G0(2) @ P(
     5)=P0(1) @ P(6)=P0(2)
2680 P(7)=A @ P(8)=D1 @ P(9)=R @
      P(10)=E @ RETURN
2690 !
2700 F0(1)=P(1) @ F0(2)=P(2) @ G
     0(1)=P(3) @ G0(2)=P(4) @ P0
     (1)=P(5) @ P0(2)=P(6)
2710 A=P(7) @ D1=P(8) @ R=P(9) @
      E=P(10) @ RETURN
2720 !
2730 FOR J=1 TO K
2740 N=10*(J(J)-1)+1
2750 IF J(J)>4 AND J(J)<9 THEN X
     =RTD(F(J)) ELSE X=F(J)
2760 PRINT USING 2770 ; J+1,P$[N
     ,N+9];X
2770 IMAGE 3D,X,10A,8DZ.8D
```

CORRELATION MATRIX

```
2780 NEXT J
2790 RETURN
2800 !
2810 FOR J=1 TO K
2820 N=10*(J-1)+1
2830 IF J>4 AND J<9 THEN X=RTD(F
     (J)) ELSE X=F(J)
2840 PRINT USING 2770 ; I(J),P$[
     N,N+9];X
2850 NEXT J
2860 RETURN
2870 !
2880 SFLAG 1 @ DISP "END FLAG SE
     T" @ RETURN
2890 !
2900 MAT P=Y@ GOSUB 2700 @ RESTO
     RE @ CLEAR @ DISP "PARAM RE
     SET" @ RETURN
2910 !
2920 FOR K=1 TO 6
2930 B1(K)=SIN(B(K)) @ B1(K)=B1(
     K)*B1(K) @ B2(K)=COS(B(K))
     @ B2(K)=B2(K)*B2(K)
2940 NEXT K @ RETURN
2950 CLEAR @ DISP "FINIS!" @ END
```

```
WHICH DATA SETS TO USE?
 1   MKOBSIM      2   IRTF1IM
 3   IRTF1EM      4   SS040IM
 5   SS040EM      6   AAT3MIM
 7   AAT3MEM      8   KA034IM
 9   KA034EM     10   KA0#4IM
11   KA0#4EM     12   MTS74IM
13   DOD68IM     14   DOD68EM
15   OKA68IM     16   OKA68EM
17   M6874IM     18   M6874EM
19   M6830IM     20   M6830EM
NUMBER SETS INCLUDE?
8
INPUT DATA SETS TO INCLUDE
?
1
?
2
?
4
```

SAMPLE "INPUT DATA" KEY LABEL

```
PARM TO FIT
F01,F02,G01,G02,P01,P02,α,δ,R,E
I(1)?
1,0,1,0,0,0,0,0,1,1
# OF ITNS
?
5
```

"START FIT" KEY LABEL

```
      RADIUS-OBLATENESS JOINT FIT
            REFIT9

00/00/00  00:57:47
8 PTS
INPUT DATA F,G
 -27552.248        6467.766
 -27542.601        6467.594
 -29172.316        2185.505
  19274.079        1572.403
 -29179.318        2185.123
  19279.851        1571.834
 -27204.938        7139.871
  17293.925        6643.092

VALUES OF CONSTANTS

B=    23.9467605496 DEG
P=    25.2622647306 DEG
B8=    9.46826887123 DEG
P8=    45.1724131019 DEG

ORIG PARAM
  1 F0-α ERROR     -5000.00000000
  0 F1-α ERROR    -17000.00000000
  1 G0-δ ERROR     -4900.00000000
  0 G1-δ ERROR       300.00000000
  0 P-POS ANG         25.26226473
  0 P8-POS ANG        45.17241310
  0 αPOL ERROR       297.81300000
  0 δPOL ERROR        41.18500000
  1 EQ RADIUS      25225.00000000
  1 OBLATENESS         0.02100000

00:58:20 0 4.217E+002 0.00E+000
00:58:35 1 3.159E-001 -.40E+001
00:58:49 2 1.469E-001 -.40E+001
00:59:04 3 1.469E-001 -.40E+001
00:59:18 4 1.469E-001 -.40E+001
00:59:28 5 1.469E-001 -.40E+001

FIT RESULT:  00 00 00  00 59:30
ITNS= 5

BEST PARM ON ITN= 4
  1 F0-α ERROR     -4964.57432795
  0 F1-α ERROR    -17000.00000000
  1 G0-δ ERROR     -4623.61055769
  0 G1-δ ERROR       300.00000000
  0 P-POS ANG         25.26226473
  0 P8-POS ANG        45.17241310
  0 αPOL ERROR       297.81300000
  0 δPOL ERROR        41.18500000
  1 EQ RADIUS      25262.50214480
  1 OBLATENESS         0.01602724

σ^2 .146897734122

ERRORS
  2 F0-α ERROR         6.50214745
  3 G0-δ ERROR        18.15329646
  4 EQ RADIUS          6.87141651
  5 OBLATENESS         0.00111528

CORRL MATRIX
 99 47 39 96
 47 99-59 43
 39-59 99 45
 96 43 45 99

OBS          RESID

MKOBSIM        -.18479
IRTF1IM         .21353
SS040IM         .13913
SS040EM        -.11545
AAT3MIM        -.14285
AAT3MEM         .11589
KA034IM        -.02513
KA034EM        -.00049

SUM RESIDS=- 0001596384

RMS DEVIATION=  191636200992
```

SAMPLE OUTPUT

Appendix C.

DERIVATION OF INVERSION METHOD

Huygen's principle can be described mathematically (Born and Wolf, 1970) by stating that the distance traveled by a light ray is always in a direction perpendicular to the plane wave front (see Figure C-1):

$$n\frac{d\vec{r}}{ds} = \nabla \cdot \beta . \qquad (C.1)$$

β defines the plane wave front and the derivative of $\vec{r}$ with respect to s is the direction of propagation, $\vec{s}$. n is the index of refraction, which is defined as the ratio of the speed of light in a vacuum, c, to the velocity which the ray has in the medium, v. Differentiating Equation C.1,

$$\frac{d}{ds}\left[n\frac{d\vec{r}}{ds}\right] = \nabla \cdot n \qquad (C.2)$$

or

$$\frac{d}{ds}\left[n\vec{s}\right] = \nabla \cdot n . \qquad (C.3)$$

Now, the curvature vector of a ray can be defined

$$\vec{K} = \frac{d\vec{s}}{ds} = \frac{1}{\kappa}\vec{\nu} \qquad (C.4)$$

where κ is the radius of curvature (to be further defined later), $\vec{\nu}$ is the unit normal vector (see Figure C-2), and $\vec{s}$ is the local tangent to the ray. From Equation C.2,

$$\frac{dn}{ds}\vec{s} + n\frac{d\vec{s}}{ds} = \bigtriangledown \cdot n; \tag{C.5}$$

from Equation C.3,

$$n\vec{K} = \bigtriangledown \cdot n - \frac{dn}{ds}\vec{s}. \tag{C.6}$$

Dividing through by n and multiplying through by $\vec{K}$,

$$\vec{K} \cdot \vec{K} = \frac{1}{n} \bigtriangledown \cdot n \cdot \vec{K} - \frac{1}{n}\frac{dn}{ds}\vec{s} \cdot \vec{K}. \tag{C.7}$$

But $\vec{K}$ is perpendicular to $\vec{s}$, so the second term on the right hand side goes to zero. Substituting in for $\vec{K}$,

$$|\vec{K}|^2 = \frac{1}{n} \bigtriangledown \cdot n \cdot \frac{1}{\kappa} \cdot \vec{\nu}. \tag{C.8}$$

Since

$$|\vec{K}|^2 = \frac{1}{\kappa^2}, \tag{C.9}$$

then

$$\frac{1}{\kappa} = \frac{1}{n} \bigtriangledown \cdot n \cdot \vec{\nu}. \tag{C.10}$$

The one-dimensional analogy for this equation is

$$\frac{1}{\kappa} = \frac{1}{n}\frac{dn}{ds}. \tag{C.11}$$

Now, let us change the variable called s to r for occultation geometry, and return to the radius of curvature. Rektorys (1969) defines the radius of curvature to be

$$\frac{1}{\kappa} = \frac{r''}{[1 + (r')^2]^{\frac{3}{2}}}. \tag{C.12}$$

For an occultation, r' is defined as the change in r with respect to x. The ray curve may be approximated as a right triangle, as θ, the bending angle, is small, and so

$$\frac{dr}{dx} = \tan\theta\,, \text{ so} \tag{C.13}$$

$$r'' = \sec^2\theta \frac{d\theta}{dx} = (1 + \tan^2\theta)\ \frac{d\theta}{dx}\,. \tag{C.14}$$

Using the definition for the radius of curvature,

$$\frac{1}{\kappa} = \frac{(\sec^2\theta)\frac{d\theta}{dx}}{(1+\tan^2\theta)^{\frac{3}{2}}} = \cos\theta\frac{d\theta}{dx}\,. \tag{C.15}$$

Equating this result for the radius of curvature to the previous one,

$$\frac{1}{n}\frac{dn}{dr} = \cos\theta\frac{d\theta}{dx}\,. \tag{C.16}$$

The bending angle is very small, so that $\cos\theta \approx 1$.

$$\frac{d\theta}{dx} = \frac{1}{n}\frac{dn}{dr} = \frac{d[\ln(n)]}{dr}\,. \tag{C.17}$$

Solving for θ gives

$$\theta = \int_{-\infty}^{+\infty} \frac{d[\ln(n)]}{dr} dx\,. \tag{C.18}$$

Now, for convenience, let us define $\ln(n) = Q$. A change of variables from dx to dr must be done. By the geometry of the occultation,

$$x = (r^2 - r_1^2)^{\frac{1}{2}} \text{ and } dx = \frac{r\ dr}{(r^2 - r_1^2)^{\frac{1}{2}}}\,. \tag{C.19}$$

Using another change of variables, let us define

$$r^2 = \frac{1}{w} \text{ and } r_1^2 = \frac{1}{s}\,. \tag{C.20}$$

Then

$$dr = \frac{-dw}{2rw^2}. \tag{C.21}$$

Returning to the bending angle equation,

$$\theta(s) = 2\int_{r_1}^{\infty} \frac{dQ}{dr} \frac{r\ dr}{\left(\frac{1}{w} - \frac{1}{s}\right)^{\frac{1}{2}}}, \tag{C.22}$$

and

$$\theta(s) = 2\int_{s}^{0} \frac{dQ}{dw}(-2rw^2) \frac{dw}{-2w^2} \frac{(sw)^{\frac{1}{2}}}{(s-w)^{\frac{1}{2}}}, \tag{C.23}$$

$$= -2\int_{0}^{s} \frac{dQ}{dw} r\ dw\ \frac{(sw)^{\frac{1}{2}}}{(s-w)^{\frac{1}{2}}} \tag{C.24}$$

$$= -2\int_{0}^{s} \frac{dQ}{dw} \left(\frac{sw}{w}\right)^{\frac{1}{2}} \frac{dw}{(s-w)^{\frac{1}{2}}}. \tag{C.25}$$

If the scale height H is much smaller than r_1, the radius of the planet, then $r \approx r_1$ and so the square root of the ratio of s to w is approximately unity. Thus,

$$\theta(s) = 2\int_{0}^{s} w^{\frac{1}{2}} \frac{dQ}{dw} \frac{dw}{(s-w)^{\frac{1}{2}}}. \tag{C.26}$$

We can define $\Psi(w)$ as the kernel function such that

$$\Psi(w) = w^{\frac{1}{2}\frac{dQ}{dw}}.$$

This gives

$$\theta(s) = 2\int_{0}^{s} \frac{\Psi(w)dw}{(s-w)^{\frac{1}{2}}}. \tag{C.27}$$

This is an Abel integral. The solution for this is derived at the end of this appendix. The solution is found to be

$$\Psi(w) = \frac{2}{2\pi} \frac{d}{dw} \int_{0}^{w} \frac{\theta ds}{(w-s)^{\frac{1}{2}}}. \tag{C.28}$$

Equating the two equations for Ψ,

$$(w)^{\frac{1}{2}} \frac{d[\ln(n)]}{dr} = \frac{1}{\pi} \frac{d}{dw} \int_0^w \frac{\theta ds}{(w-s)^{\frac{1}{2}}}. \qquad (C.29)$$

Solving for the change in $\ln(n)$ with dr,

$$\frac{d[\ln(n)]}{dr} = \frac{1}{r^2 \pi} \frac{d}{2w^2 r dr} \int_0^w \frac{\theta ds}{(w-s)^{\frac{1}{2}}}. \qquad (C.30)$$

Changing the variables back to to original variables,

$$\frac{d[\ln(n)]}{dr} = \frac{r}{2\pi} \frac{d}{dr} \int_0^w \frac{\theta(r r_1) ds}{(r_1^2 - r^2)^{\frac{1}{2}}}, \qquad (C.31)$$

and finally

$$\frac{d[\ln(n)]}{dr} = \frac{r}{\pi} \frac{d}{dr} \int_r^\infty \frac{-r_1 \theta dr_1}{r_1^2 (r_1^2 - r^2)^{\frac{1}{2}}}. \qquad (C.32)$$

Approximating $r \approx r_1$, then

$$\frac{d[\ln(n)]}{dr} = \frac{-1}{\pi} \frac{d}{dr} \int_r^\infty \frac{\theta dr_1}{(r_1^2 - r^2)^{\frac{1}{2}}}. \qquad (C.33)$$

Here three assumptions are made:

- severe ray crossing does not occur,
- $n \approx 1$, and
- $(r + r_1) \approx 2R_p$ where R_p is the planetary radius.

With these assumptions, the preceding equation becomes

$$\frac{dn}{dr} = \frac{-1}{\pi} \frac{d}{dr} \int_r^\infty \frac{\theta dr_1}{(r + r_1)^{\frac{1}{2}} (r_1 - r)^{\frac{1}{2}}} \qquad (C.34)$$

and so

$$\frac{dn}{dr} = \frac{-1}{\pi} \frac{1}{(2R_p)^{\frac{1}{2}}} \frac{d}{dr} \int_r^\infty \frac{\theta dr_1}{(r_1 - r)^{\frac{1}{2}}}. \qquad (C.35)$$

Now, the refractivity $\nu = n - 1$ so the change in refractivity with height is the same as the change in n with height:

$$\frac{d\nu}{dr} = \frac{-1}{\pi} \frac{1}{(2R_p)^{\frac{1}{2}}} \frac{d}{dr} \int_r^\infty \frac{\theta dr_1}{(r_1 - r)^{\frac{1}{2}}} . \qquad (C.36)$$

Integrating this equation,

$$d\nu = \frac{-1}{\pi} \frac{1}{(2R_p)^{\frac{1}{2}}} d\left[\int_r^\infty \frac{\theta dr_1}{(r_1 - r)^{\frac{1}{2}}}\right] \qquad (C.37)$$

and

$$\nu(r) = \frac{1}{\pi} \frac{1}{(2R_p)^{\frac{1}{2}}} \int_\infty^r \frac{\theta dr_1}{(r_1 - r)^{\frac{1}{2}}} . \qquad (C.38)$$

This is the formal inversion solution.

SOLUTION TO ABEL INTEGRAL

From Bocher, we know that

$$\frac{\pi}{\sin \mu\pi} = \int_\xi^z \frac{dz}{(z - x)^{\frac{1}{2}} (x - \xi)^{\frac{1}{2}}} \qquad (C.39)$$

where $(0 < \mu < 1)$. Let there be some function $\Phi(\xi)$ that is continuous, and has a continuous derivative. Multiply the above equation through by $\Phi'(\xi)d\xi$ and integrate over a to z:

$$\int_a^z \frac{\pi}{\sin \mu\pi} \Phi'(\xi) d\xi = \int_a^z \int_\xi^z \frac{\Phi'(\xi) dx d\xi}{(z - x)^{1-\mu} (x - \xi)^\mu} . \qquad (C.40)$$

Dirichlet's Generalized Formula states that

$$\int_a^b \int_a^x \frac{\Phi(x, y) dy dx}{(x - y)^\lambda (b - x)^\mu (y - a)^\nu} = \int_a^b \int_y^b \Big[(\text{same integrand})\Big] dx dy . \qquad (C.41)$$

It follows that

$$\frac{\pi}{\sin \mu\pi}\Big[\Phi(z) - \Phi(a)\Big] = \int_a^z \frac{1}{(z-x)^{1-\mu}} \int_a^x \frac{\Phi'(\xi)d\xi dx}{(x-\xi)^{\mu}}. \qquad (C.42)$$

Now, the equation of interest has the following form:

$$f(x) = \int_a^x \frac{\mu(\xi)d\xi}{(x-\xi)^{\lambda}}, \qquad (C.43)$$

again for $(0 < \lambda < 1)$. The unknown in this equation is the function $\mu(x)$; if $f(x)$ is continuous, and $f(a) = 0$, then divide through by $(z-x)^{1-\lambda}dx$, and integrate from a to z:

$$\int_a^z \frac{f(x)dx}{(z-x)^{1-\lambda}} = \int_a^z \frac{1}{(z-x)^{1-\lambda}} \int_a^x \frac{\mu(\xi)d\xi dx}{(x-\xi)^{\lambda}}. \qquad (C.44)$$

The right hand side of the equation above corresponds to the right hand side of the previously shown relation, so that

$$\int_a^z \frac{f(x)dx}{(z-x)^{1-\lambda}} = \frac{\pi}{\sin \lambda\pi}\Big[\int_a^z \mu(\xi)d\xi\Big]; \qquad (C.45)$$

now, taking the derivative of each side,

$$\frac{d}{dz}\int_a^z \frac{f(x)dx}{(z-x)^{1-\lambda}} = \frac{\pi}{\sin \lambda\pi}\Big[\mu(z) - \mu(a)\Big]. \qquad (C.46)$$

Solving for $\lambda = \frac{1}{2}$,

$$\mu(z) = \frac{1}{\pi}\frac{d}{dz}\int_a^z \frac{f(x)dx}{(z-x)^{\frac{1}{2}}}. \qquad (C.47)$$

DATE	LOCATION	APERTURE (m)	$\lambda(\mu)$	$\Delta\lambda(\mu)$	CONDITIONS	DATA INTERVAL (s)	OBSERVERS
7 Apr 1968	Mt. Stromlo, Austr.	1.27	V*		good		K.C. Freeman
		0.76	V*				G. Lynga
	Mt. Dodaira Japan	0.91	B*		good		
	Mt. Okayama Japan	0.91	B*		good		
15 June 1983	IRTF, Hawaii	3.0	2.2	0.4	immersion good, emersion during dawn	0.01	K. Meech
	Univ. Hawaii	2.2	0.855	0.08		0.01	J. Goguen, H. Hammel
	KAO (near Guam)	0.9	2.27	0.4	good	0.01	J. Elliot, E. Dunham, D. Mink
			0.83	0.066			
			0.78	0.2			
			0.73	0.09			
			0.50	0.07			
	AAT (Sid. Spr.)	3.9	2.2	0.4	good	0.01	D. Allen
	Siding Spring, (Austr.)	1.0	0.85	0.1	transient clouds	0.02	K.C. Freeman, M. Ashley
			0.55	0.1			
	Mt. Stromlo (Austr.)	1.9	0.85	0.1	cloudy immersion, no emersion	0.01	R. Baron
			0.55	0.1			

Table 2-1. Observations

* - standard UBV system

DATA	IM LATITUDE ON NEPTUNE	D* (km)	EM LATITUDE ON NEPTUNE	D* (km)
1968 Mt. Dodaira	-40.1	-	+13.8	-
Mt. Okayama	-40.5	300	+13.2	260
1983 KAO	+42.4	-	-3.2	-
IRTF/UH	+40.5	760	-	-
AAT/Sid. Spring	+32.6	5365	-7.4	5515

Table 2-2. Immersion and emersion latitudes of chords; D is distance along limb from northernmost observation for given date.

DATA	t(1/2) UT 15 June 83	φ	λ	Altitude (m)
IRTF (IM)	$14^h24^m51^s.1$	$19°49'34''.0$	$-155°28'13''$	4100
UH 2.2m(IM)	$14^h24^m50^s.7$	$19°49'34''.0$	$-155°28'20''$	4215
KAO(IM)	$14^h28^m15^s.8$	$16°60'50''.0$	$-151°69'60''$	9879
KAO(EM)	$14^h59^m03^s.9$	$17°33'67''.0$	$-148°37'84''$	9978
SID. SPR. (IM)	$14^h27^m06^s.9$	$-31°16'22''.0$	$-149°03'39''.4$	1150
SID. SPR. (EM)	$15^h00^m27^s.0$			
AAT(IM)	$14^h27^m06^s.6$	$-31°16'37''.3$	$-149°03'57''.9$	1165
AAT(EM)	$15^h00^m27^s.2$			
MT. STROMLO (IM)	$14^h27^m04^s.9$	$-35°19'14''.3$	$-149°00'27''.6$	767

Table 3-1. 1983 data observatory locations and half-light times. φ - Earth latitude, λ - longitude

DATA	$\Delta n_*/n_*$	$\Delta n_b/n_*$	$\Delta t(1/2)$ (s)	$\sigma(t(1/2))^*$
IRTF (IM)	0.026	0.018	0.23	0.03
IRTF (EM)	0.057	0.035	0.51	0.08
UH 2.2m (IM)	0.015	0.011	0.12	0.03
SID. SPR.(IM)	0.024	0.021	0.33	0.32
SID. SPR.(EM)	0.025	0.012	0.06	0.32
AAT (IM)	0.016	0.029	0.12	0.01
AAT (EM)	0.021	0.010	0.03	0.01
KAO (IM)	0.031	0.027	0.42	0.08
KAO (EM)	0.007	0.003	0.01	0.21
MT. STROMLO (IM)	0.063	0.052	0.82	0.34

Table 3-2. Uncertainty in baselines and half-light times; * - predicted from Equation 3-3.

DATA	φ	λ	Alt. (m)	t(1/2) UT 7 April 1968
MT. DODAIRA (IM)	36°00'10".2	-139°11'46".8	879	$15^h56^m25^s$ (Takenouchi et al., 1968)
				$15^h56^m25^s.5$ (Hirose, 1968)
				$15^h56^m26^s.8$ (Melroy, 1984)
MT.DODAIRA (EM)				$16^h41^m31^s$ (Takenouchi et al.)
				$16^h41^m28^s$ (Hirose)
				$16^h41^m27^s$ (Melroy)
MT. OKAYAMA (IM)	34°34'22".8	-133°35'46".6	365	$15^h56^m54^s$ (Takenouchi et al.)
				$15^h56^m55^s.5$ (Hirose)
				$15^h56^m56^s.7$ (Melroy)
MT. OKAYAMA (EM)				$16^h41^m51^s$ (Takenouchi et al.)
				$16^h41^m51^s.5$ (Hirose)
				$16^h41^m50^s.5$ (Melroy)
MT. STROMLO (IM)	-35°19'14".3	-149°00'27".6	767	$15^h56^m29^s$ (Freeman and Lynga, 1970)
MT. STROMLO (EM)				$16^h36^m46^s$

Table 3-3. 1968 data observatory locations and half-light times.
φ - Earth latitude, λ - longitude

DESCRIPTION OF FIT	R (km)	ϵ	# points used	rms dev.-(sec)	$\Sigma_{(res)^2-(sec)^2}$
1968 (Kovalevsky and Link)	25225 ± 30	0.021 ± 0.004	8	-	-
1968; t(1/2) from KL, improved pole and ephemeris	25239 ± 30	0.0192 ± 0.00030	8	0.476	0.906
1968; fit in radius instead of time	25239 ± 30	0.0192 ± 0.0030	8	-	-
1968; t(1/2) for Japan found by Melroy	25199 ± 30	0.0188 ± 0.0030	8	0.643	0.826
1983; changing pole position used by 2 uncertainty in pole	25259 ± 10	0.0159 ± 0.0017	8	0.1917	0.1471
1983 + 1968; joint fit	25246 ± 10	0.0191 ± 0.0150	16	0.462	2.138
1983 (Adopted value)	25263 ± 9	0.0160 ± 0.0015	8	0.1916	0.1469

Table 3-4. t(1/2) fits.

	R (km)	ϵ	$\alpha_{p(1950)}$	$\delta_{p\ (1950)}$
Best pole fit (1983 and 1968 data)	25252 ± 51	0.0197 ± 0.0033	291°.5 ± 7.6	34°.6 ± 5.1

Table 3-5. Results of fit for right ascension and declination of pole.

Mean molecular weight	2.2 g $mole^{-1}$
Acceleration of gravity	1090 cm sec^{-2}
Atmospheric refractivity at STP	1.26×10^{-4}
Temperature/Scale height	2.88 K/km
Composition	.9 H_2, .1 He by number

Table 4-1. Atmospheric parameters assumed for inversion.

DATA	LATITUDE ON NEPTUNE	$(\Delta g/g_o)_1$	$(\Delta g/g)_2$
KAO (IM)	42.4	0.0150	0.0005
KAO (EM)	3.2	0.0001	0.0005
IRTF/UH (IM)	40.5	0.0130	0.0005
SID. SPR./ AAT (IM)	32.6	0.0090	0.0005
SID. SPR./AAT (EM)	7.4	0.0005	0.0005

Table 4-2. g_{eff}, for $\epsilon \equiv 0.0160$, and $g_o \equiv$ 1090 cm sec^{-2} calculated from the two terms in Equation 4-14

DATA	time at $n = 5 \times 10^{13}$	$n = 8 \times 10^{13}$	$n = 10^{14}$	$n = 2 \times 10^{14}$
KAO (IM)	$14^h28^m15^s.3$	$14^h28^m18^s.5$	$14^h28^m20^s.5$	$14^h28^m27^s.1$
KAO (EM)	$14^h59^m03^s.9$	$14^h59^m01^s.4$	$14^h59^m00^s.0$	$14^h58^m52^s.9$
IRTF (IM)	$14^h24^m50^s.4$	$14^h24^m53^s.8$	$14^h24^m55^s.3$	$14^h25^m01^s.1$
UH 2.2m (IM)	$14^h24^m50^s.8$	$14^h24^m54^s.0$	$14^h24^m55^s.4$	$14^h25^m01^s.5$
SID. SPR. (IM)	$14^h27^m06^s.2$	$14^h27^m09^s.3$	$14^h27^m10^s.8$	$14^h27^m16^s.9$
SID. SPR. (EM)	$15^h00^m27^s.7$	$15^h00^m25^s.0$	$15^h00^m23^s.5$	$15^h00^m17^s.3$
AAT (IM)	$14^h27^m06^s.6$	$14^h27^m09^s.6$	$14^h26^m10^s.9$	$14^h27^m17^s.5$
AAT (EM)	$15^h00^m27^s.7$	$15^h00^m24^s.9$	$15^h00^m23^s.4$	$15^h00^m17^s.1$

Table 4-3. Number density levels (n in units of cm^{-3}) at times (times in UT on 15 June 1983). $n = 10^{14}$ cm^{-3} is best fit.

DATA	time at $p = 8 \times 10^{-4}$	$p = 10^{-3}$	$p = 2 \times 10^{-3}$	$p = 7 \times 10^{-3}$
KAO (IM)	$14^h28^m14^s.3$	$14^h28^m14^s.9$	$14^h28^m20^s.0$	$14^h28^m36^s.1$
KAO (EM)	$14^h59^m04^s.4$	$14^h59^m03^s.6$	$14^h58^m59^s.9$	$14^h58^m42^s.1$
IRTF (IM)	$14^h24^m48^s.7$	$14^h24^m49^s.9$	$14^h24^m54^s.1$	$14^h25^m07^s.5$
UH 2.2m (IM)	$14^h24^m49^s.9$	$14^h24^m50^s.5$	$14^h24^m55^s.4$	$14^h25^m09^s.8$
SID. SPR. (IM)	$14^h27^m05^s.0$	$14^h27^m05^s.8$	$14^h27^m10^s.4$	$14^h27^m24^s.6$
SID. SPR. (EM)	$15^h00^m27^s.9$	$15^h00^m27^s.3$	$15^h00^m23^s.5$	$15^h00^m11^s.8$
AAT (IM)	$14^h27^m05^s.1$	$14^h27^m05^s.9$	$14^h27^m10^s.8$	$14^h27^m27^s.3$
AAT (EM)	$15^h00^m28^s.0$	$15^h00^m27^s.3$	$15^h00^m23^s.4$	$15^h00^m10^s.9$

Table 4-4. Pressure levels (p in units of mbar) at times (times in UT on 15 June 1983). $p = 10^{-3}$ mbar is best fit.

LEVEL OF FIT	R (km)	ϵ	$\sum_{(res)^2}$ $(sec)^2$	
$n = 5 \times 10^{13}$ cm^{-3}	25286	0.0180	0.154	
$n = 8 \times 10^{13}$ cm^{-3}	25209	0.0167	0.140	
$n = 10^{14}$ cm^{-3}	25171 ± 7	0.0150 ± 0.0011	0.034	*
$n = 2 \times 10^{14}$ cm^{-3}	25024	0.0194	1.190	
$p = 8 \times 10^{-4}$ mbar	25305	0.0168	0.732	
$p = 10^{-3}$ mbar	25288 ± 9	0.0172 ± 0.0015	0.186	*
$p = 2 \times 10^{-3}$ mbar	25174	0.0169	1.057	
$p = 7 \times 10^{-3}$ mbar	24940	0.0390	11.238	

Table 4-5. n, p level fit results; best $n = 10^{14}$ cm^{-3}; best $p = 10^{-3}$mbar

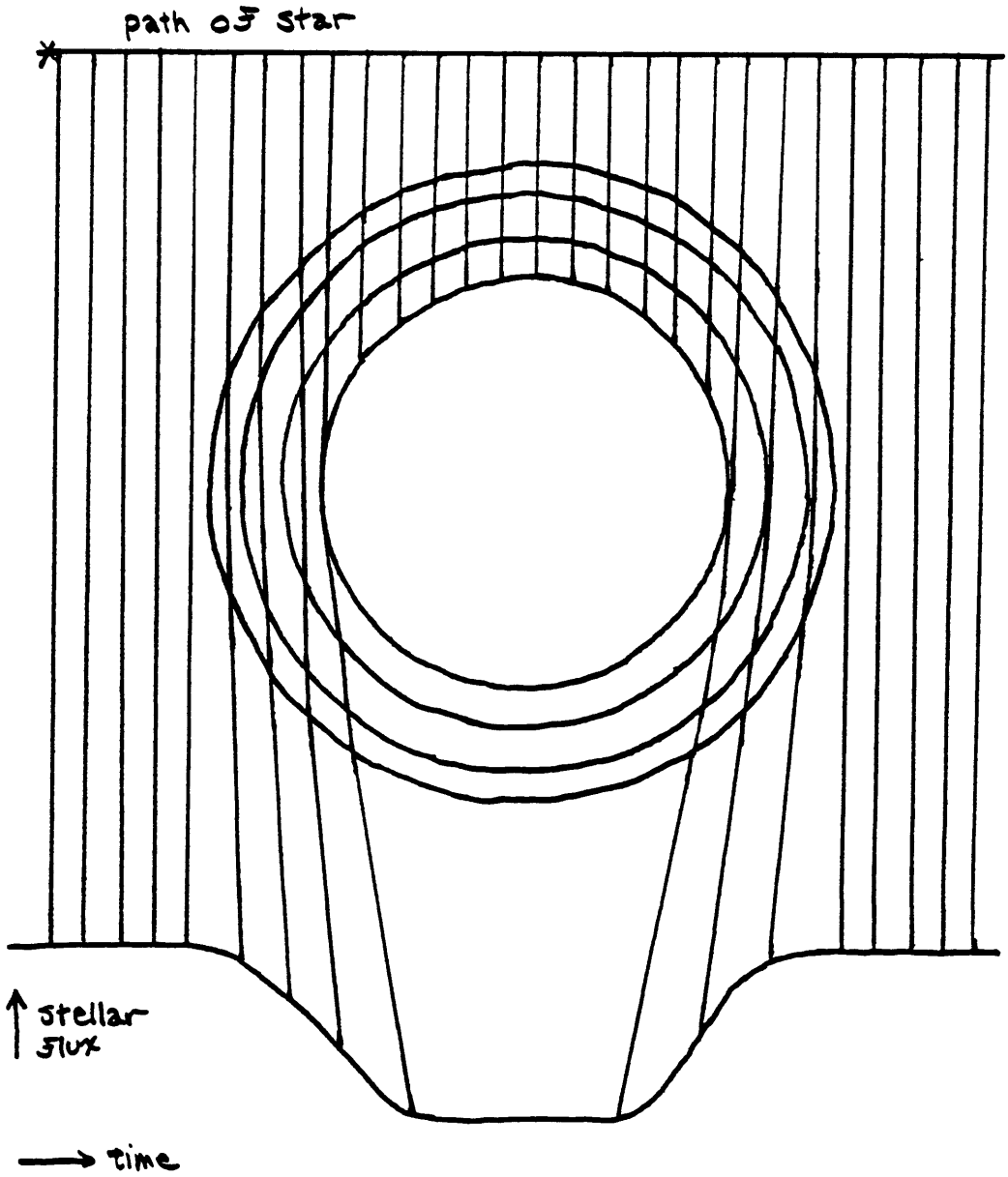

Figure 1-1. Occultation of a star by a planet.

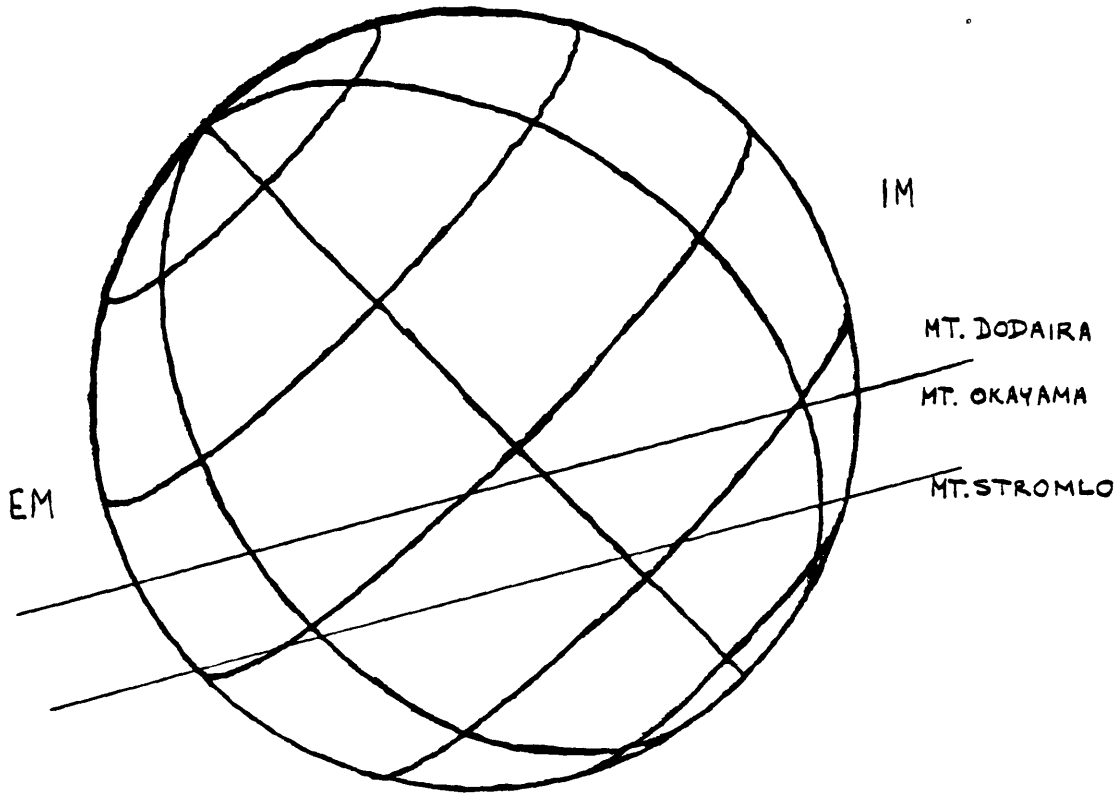

Figure 2-1. 1968 data chords; B = 9.5, P = 45.2

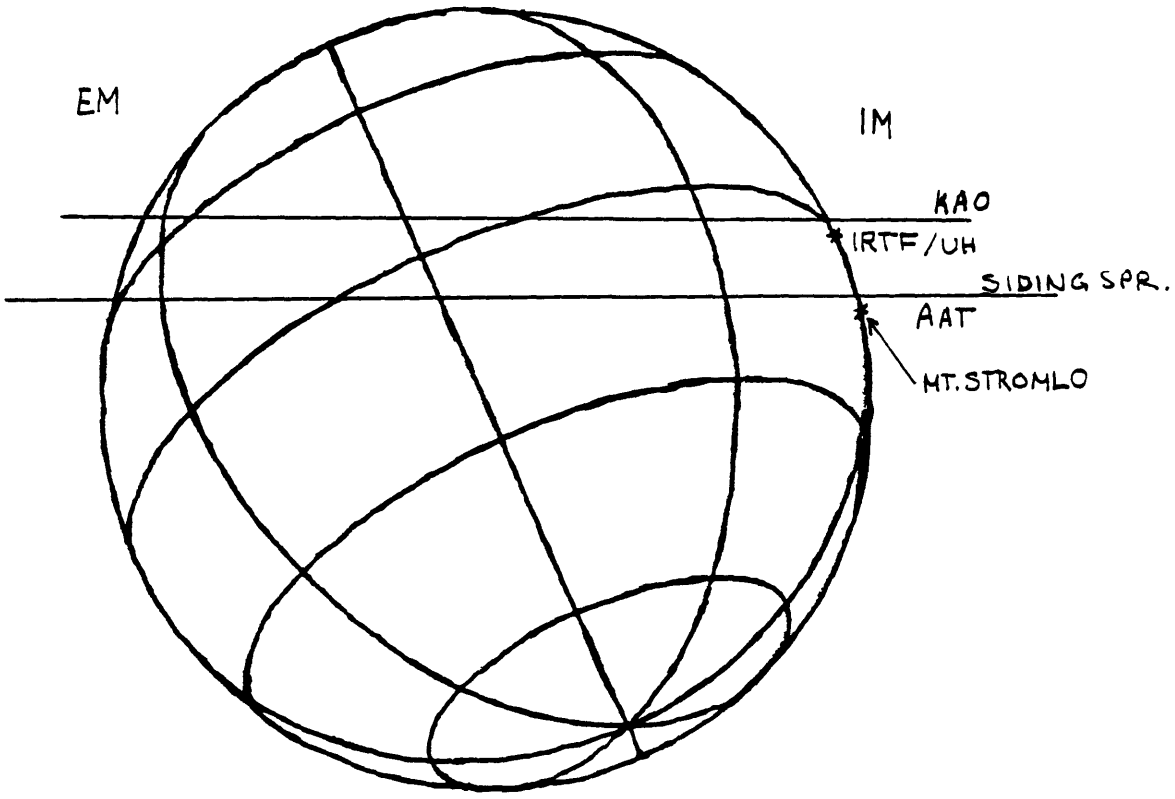

Figure 2-2. 1983 data chords; B = -23.9, P = 25.3

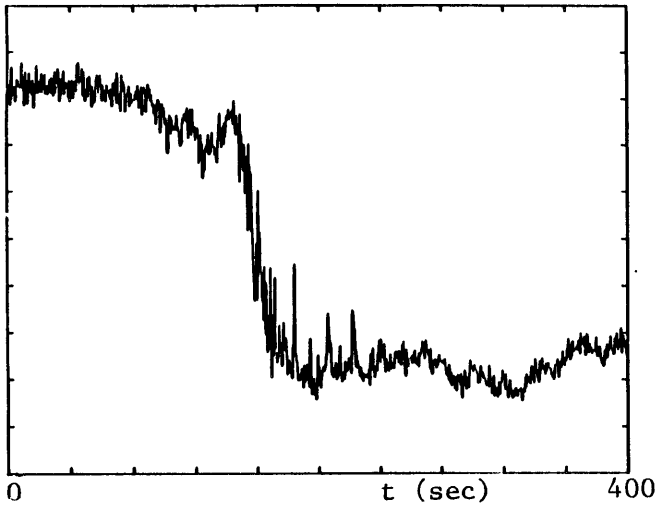

Figure 2-3,a. Pre-color corrected Siding Spring immersion light curve.
Start time = $14^h24^m30^s$ UT 15 June 1983

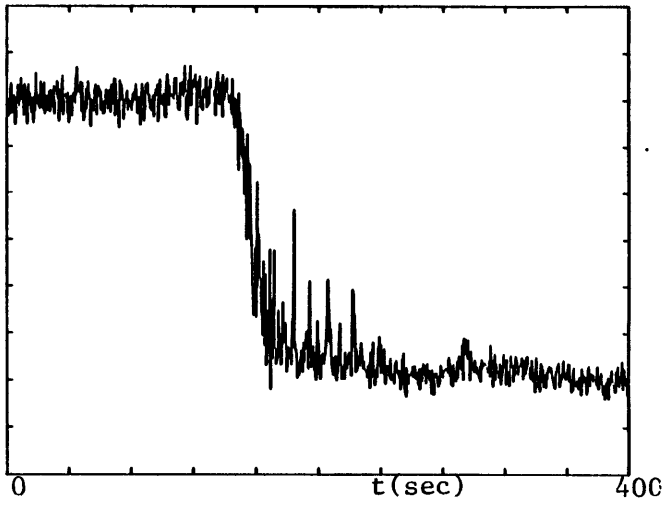

Figure 2-3,b. Color corrected Siding Spring immersion light curve.
Start time = $14^h24^m30^s$ UT 15 June 1983

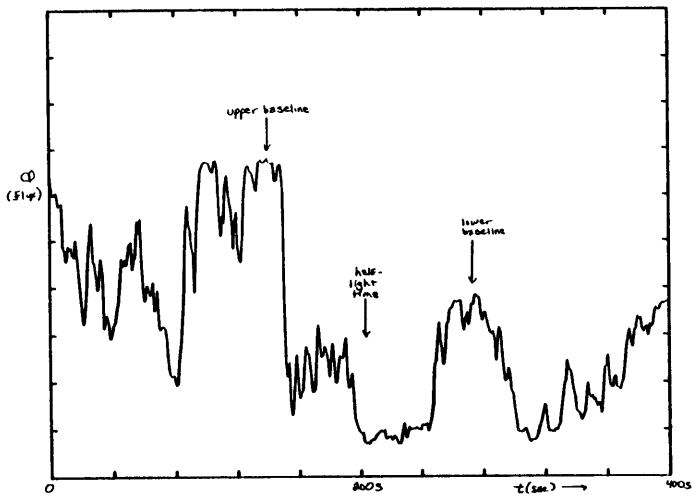

Figure 2-4,a. Pre-color corrected Mt. Stromlo immersion curve.
Start time = $14^h23^m41^s$ UT 15 June 1983

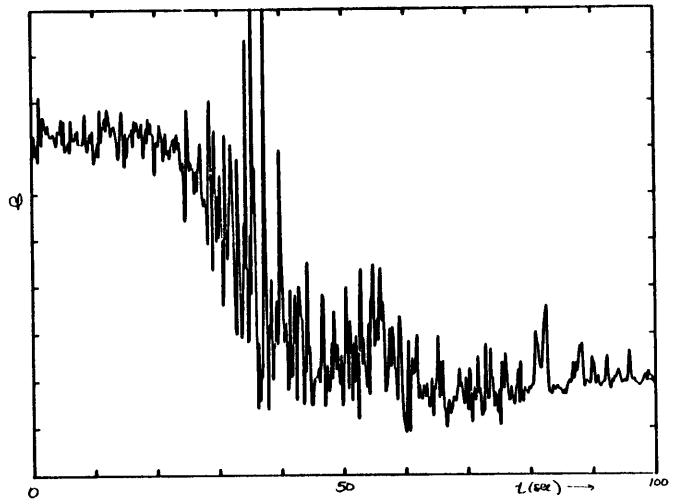

Figure 2-4,b. Color corrected Mt.Stromlo immersion light curve.
Start time = $14^h26^m40^s$ UT 15 June 1983

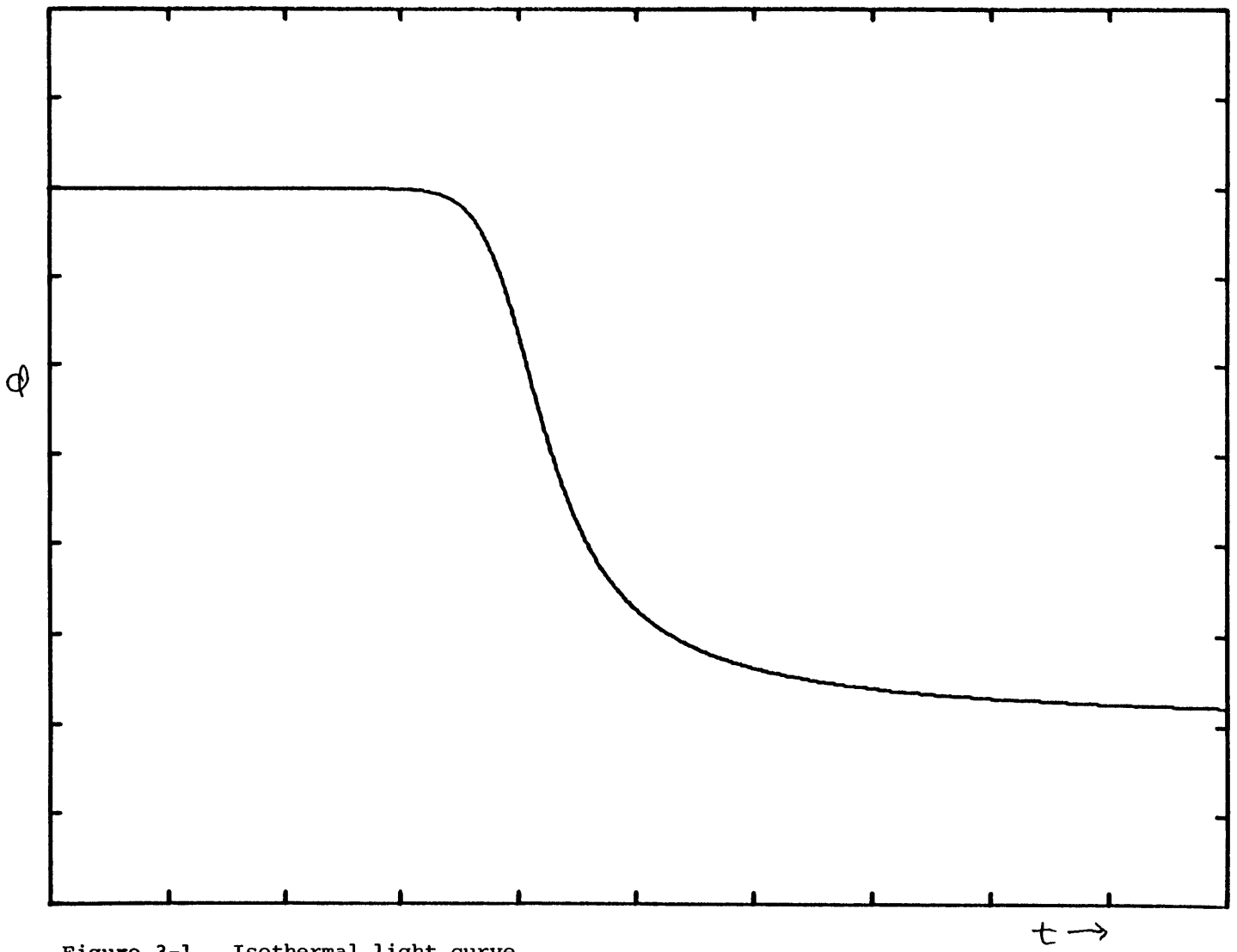

Figure 3-1. Isothermal light curve

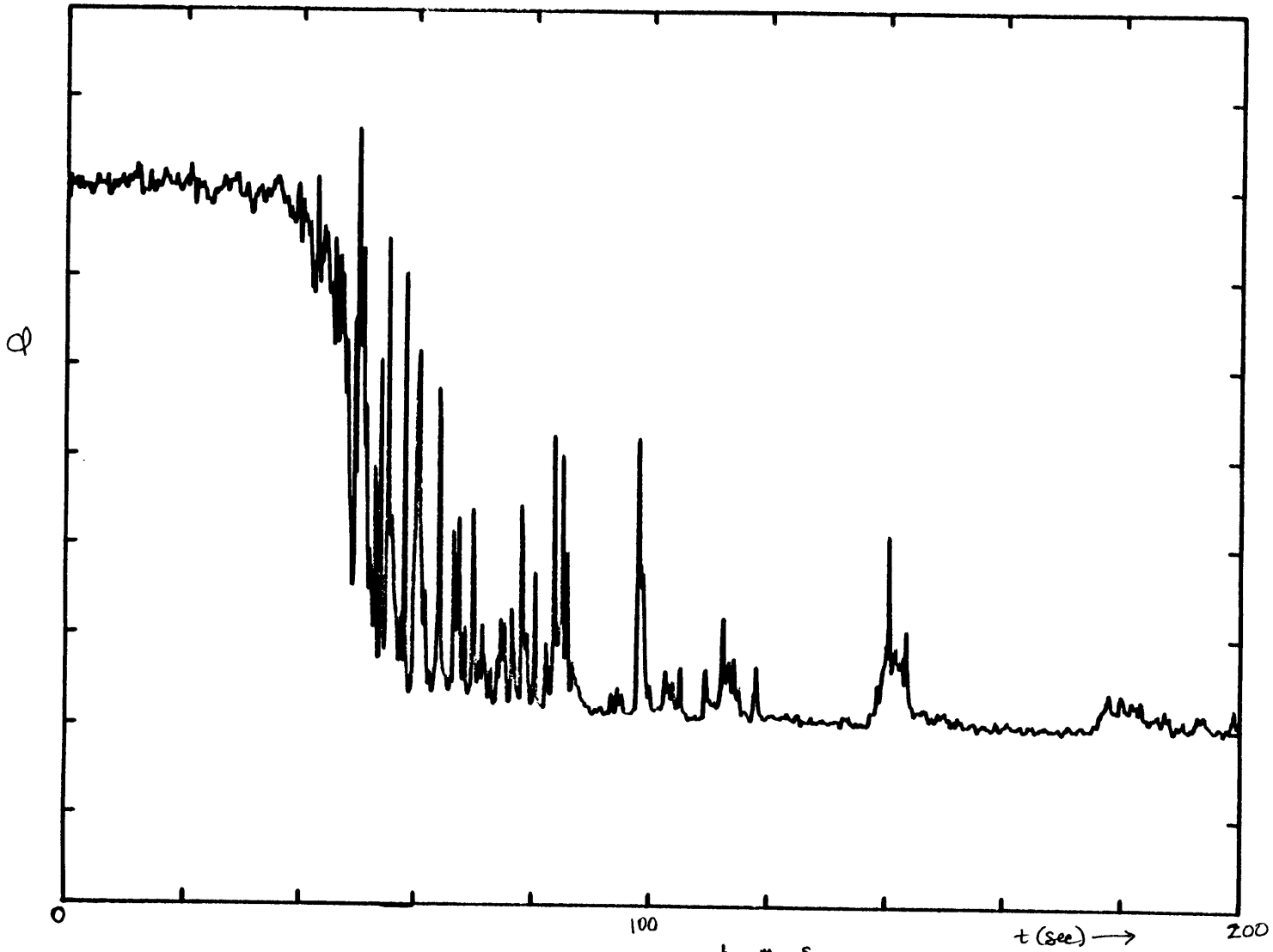

Figure 3-2, a. IRTF immersion curve, start time $14^h 23^m 00^s$ UT 15 June 1983

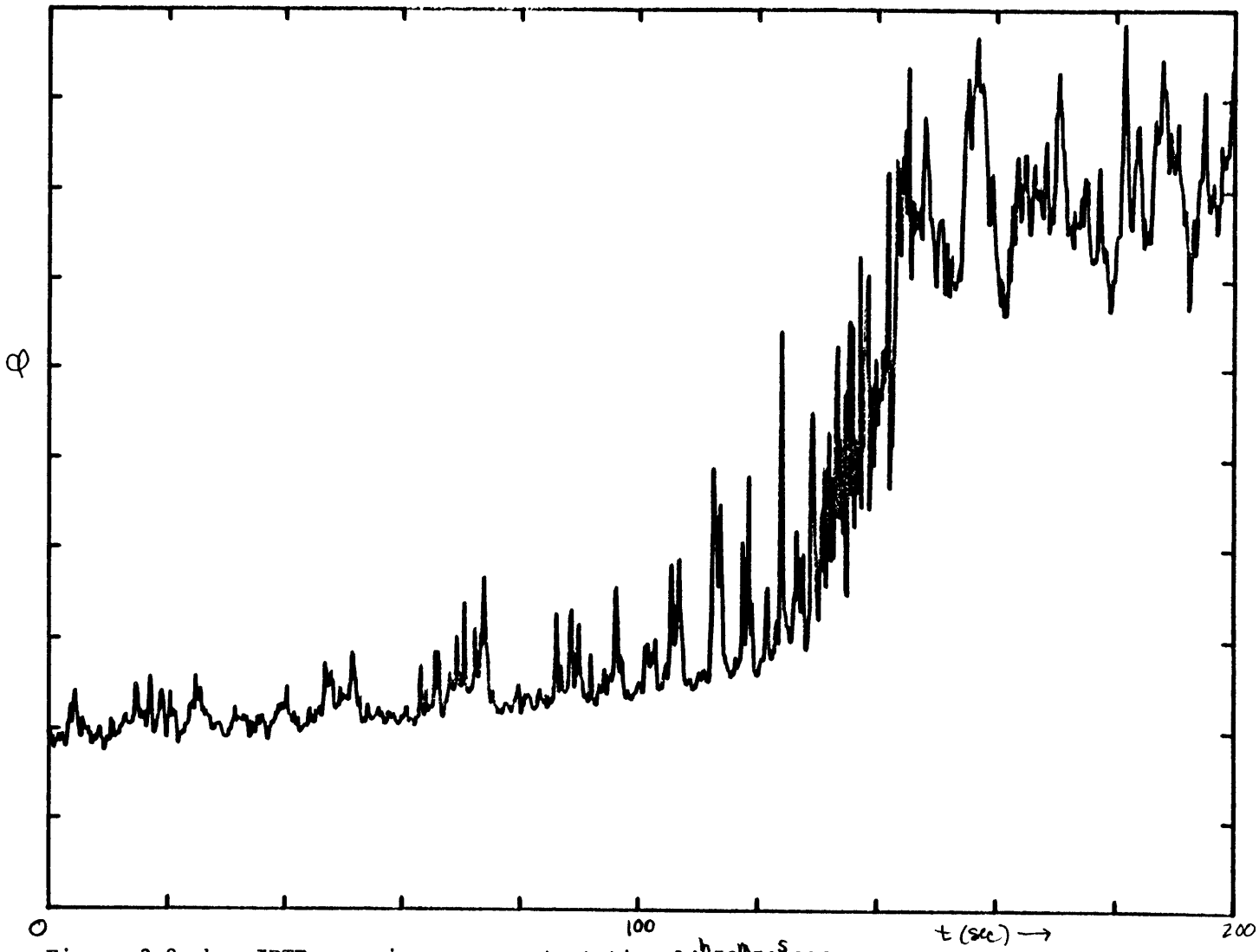

Figure 3-2, b. IRTF emersion curve, start time $14^h53^m59^s.996$ UT

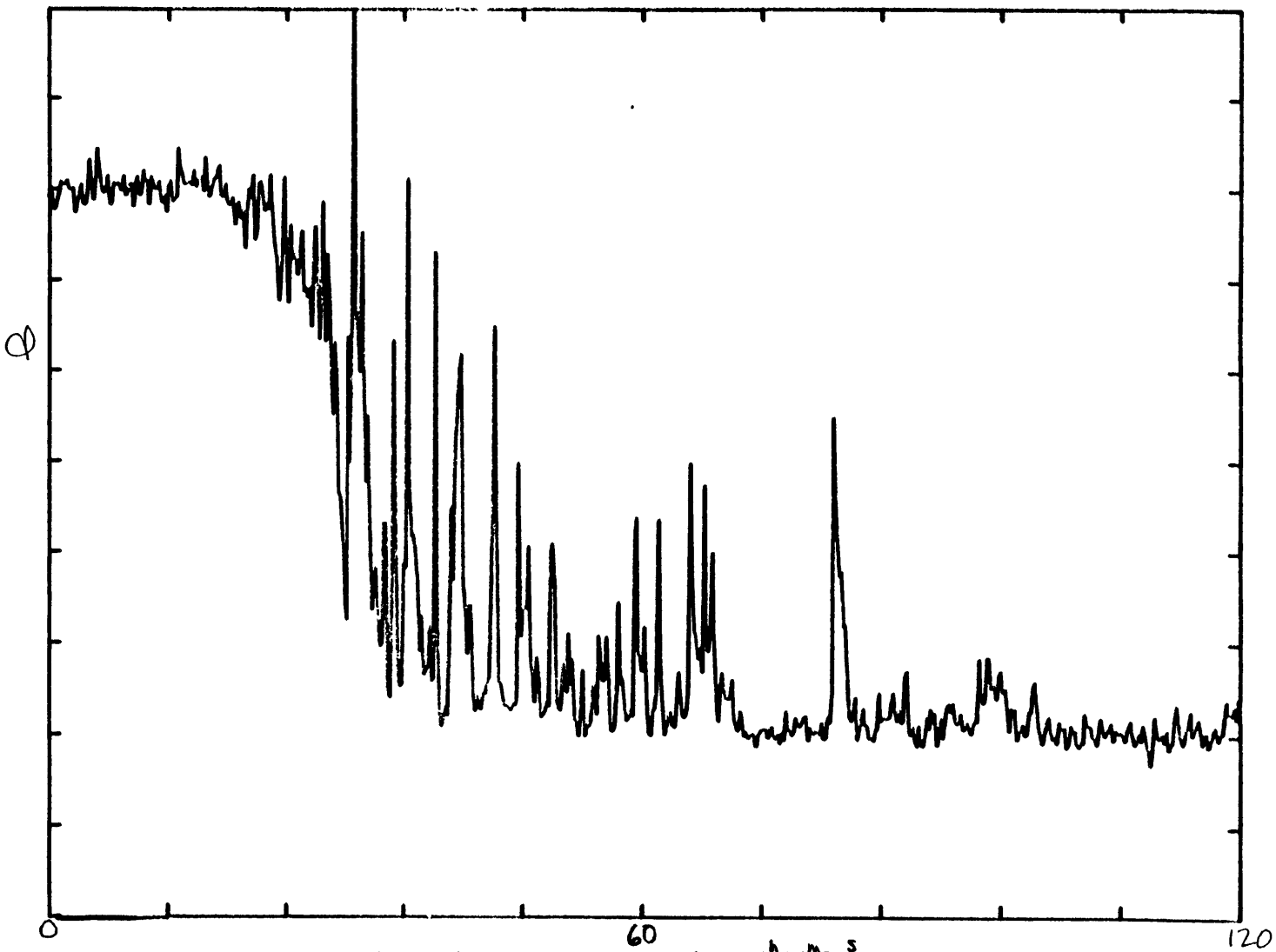

Figure 3-2, c. UH 2.2m immersion curve, start time $14^h24^m18^s.832$ UT

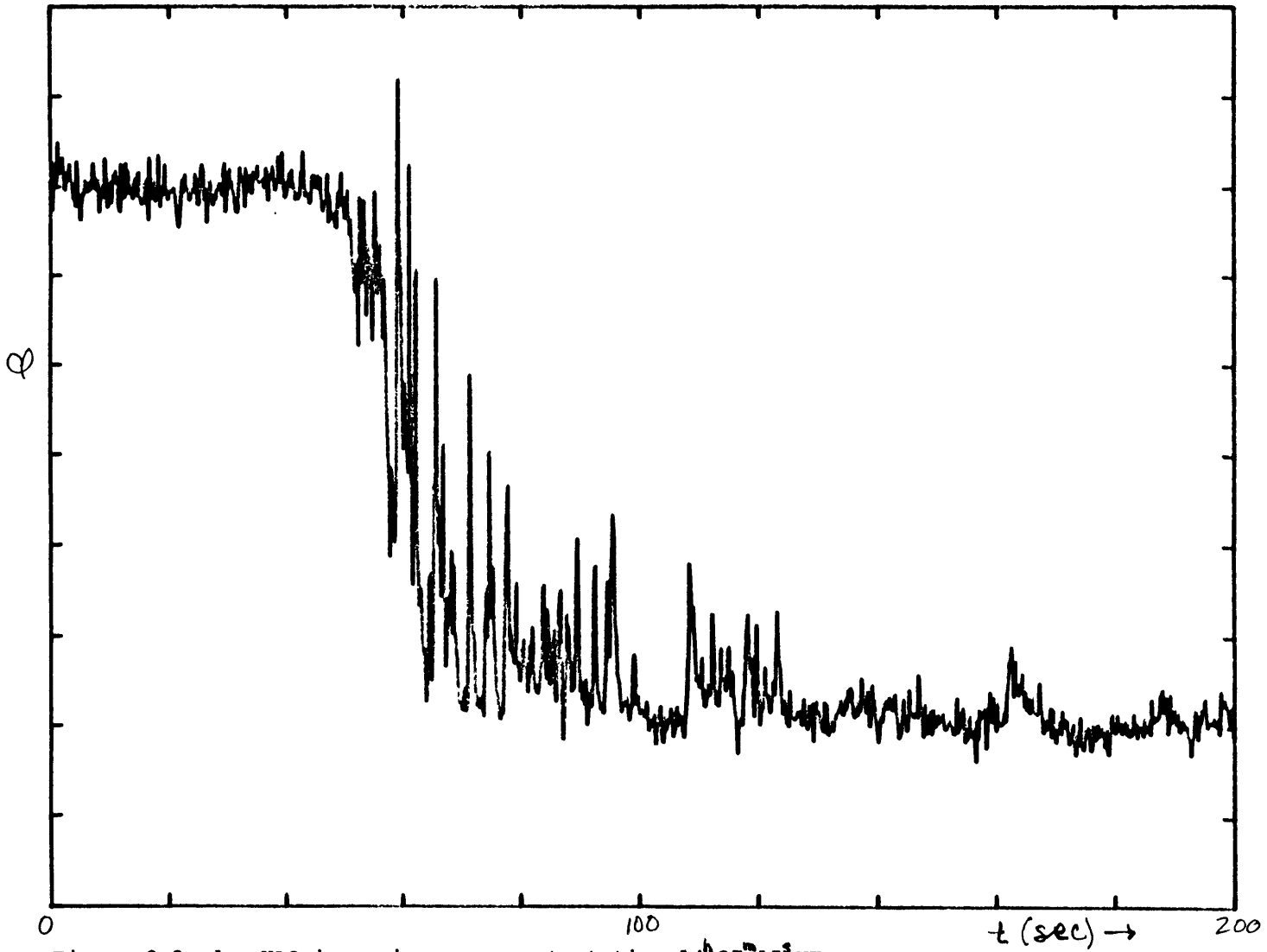

Figure 3-2, d. KAO immersion curve, start time $14^h 27^m 15^s$ UT

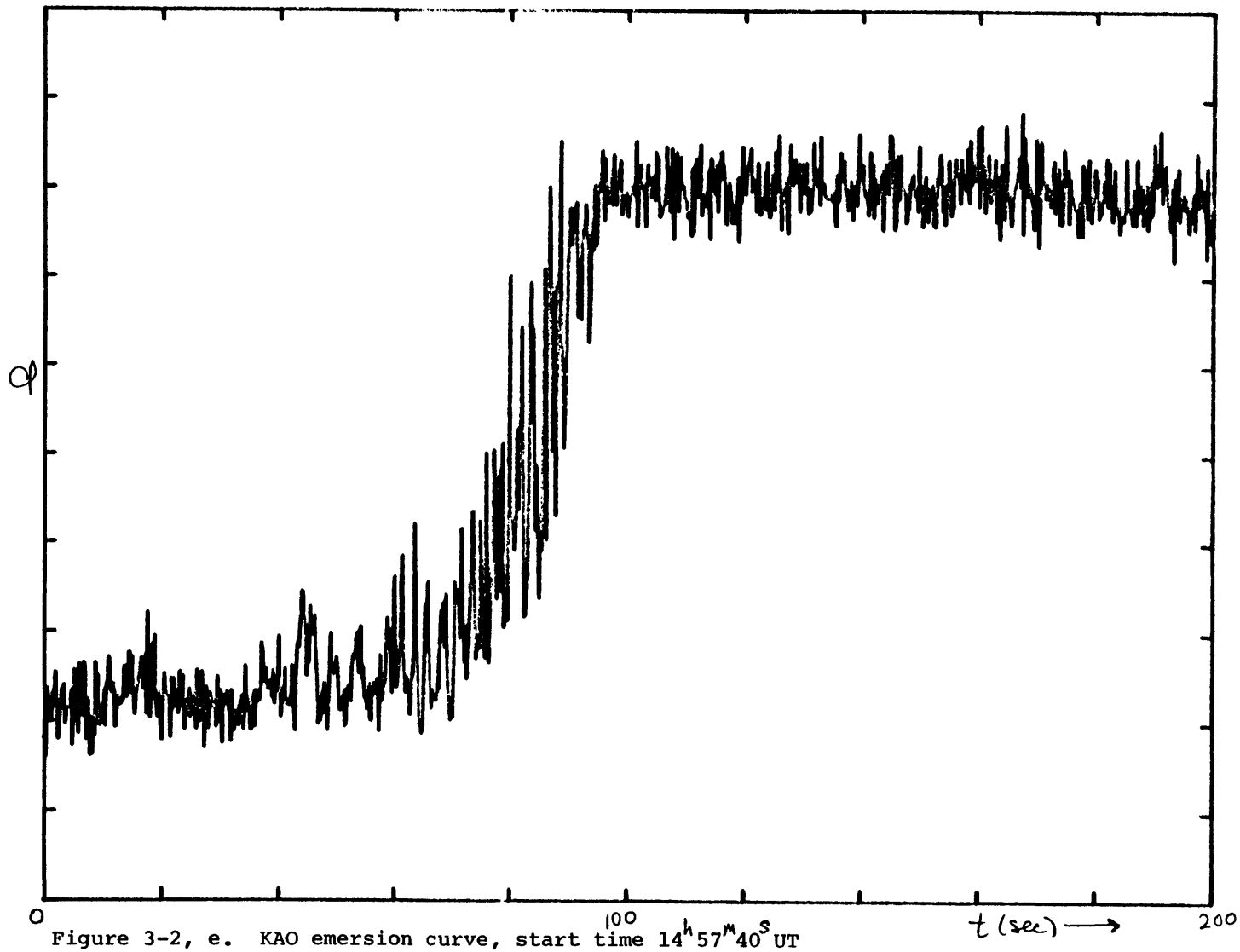

Figure 3-2, e. KAO emersion curve, start time $14^h57^m40^s$ UT

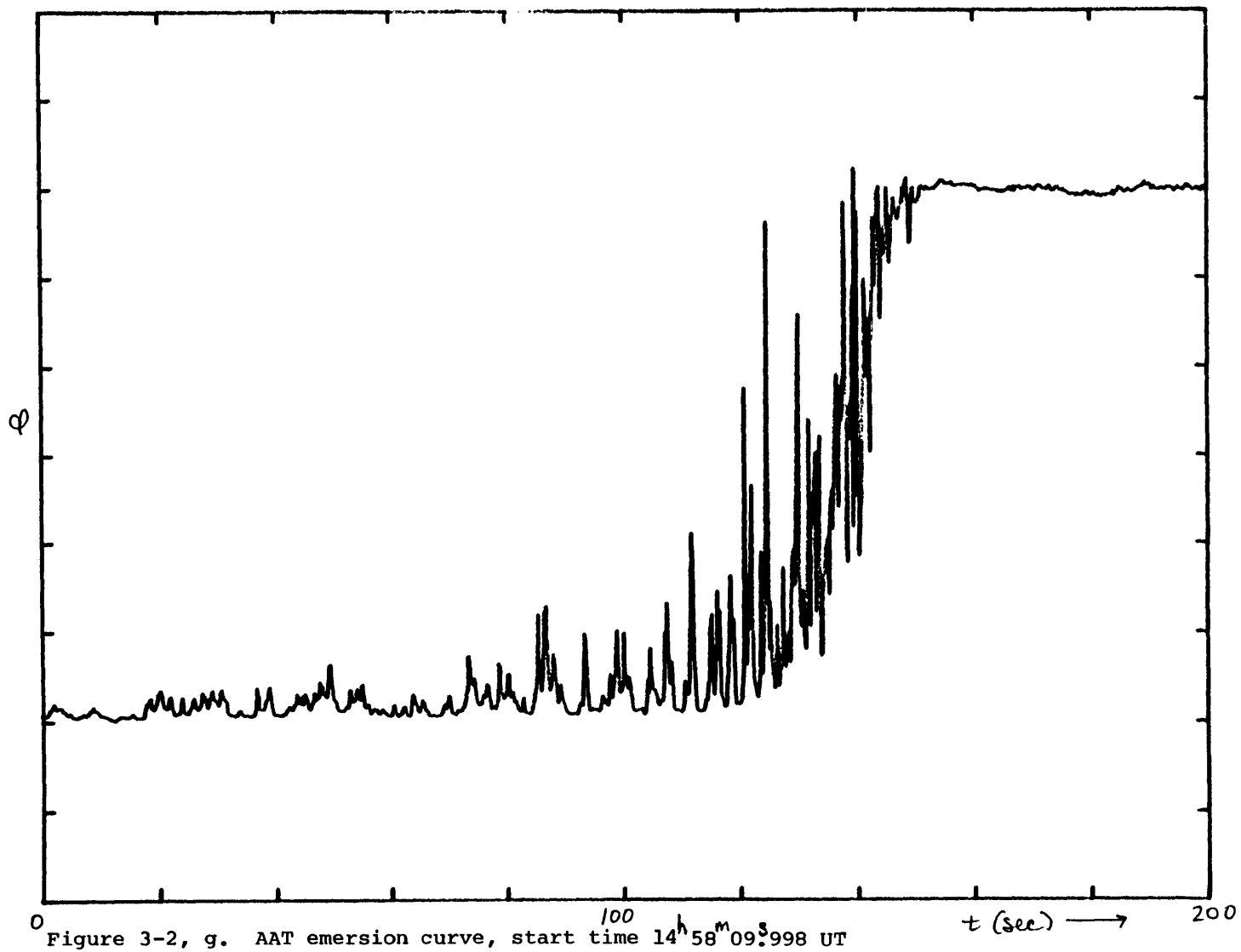

Figure 3-2, g. AAT emersion curve, start time $14^h58^m09^s.998$ UT

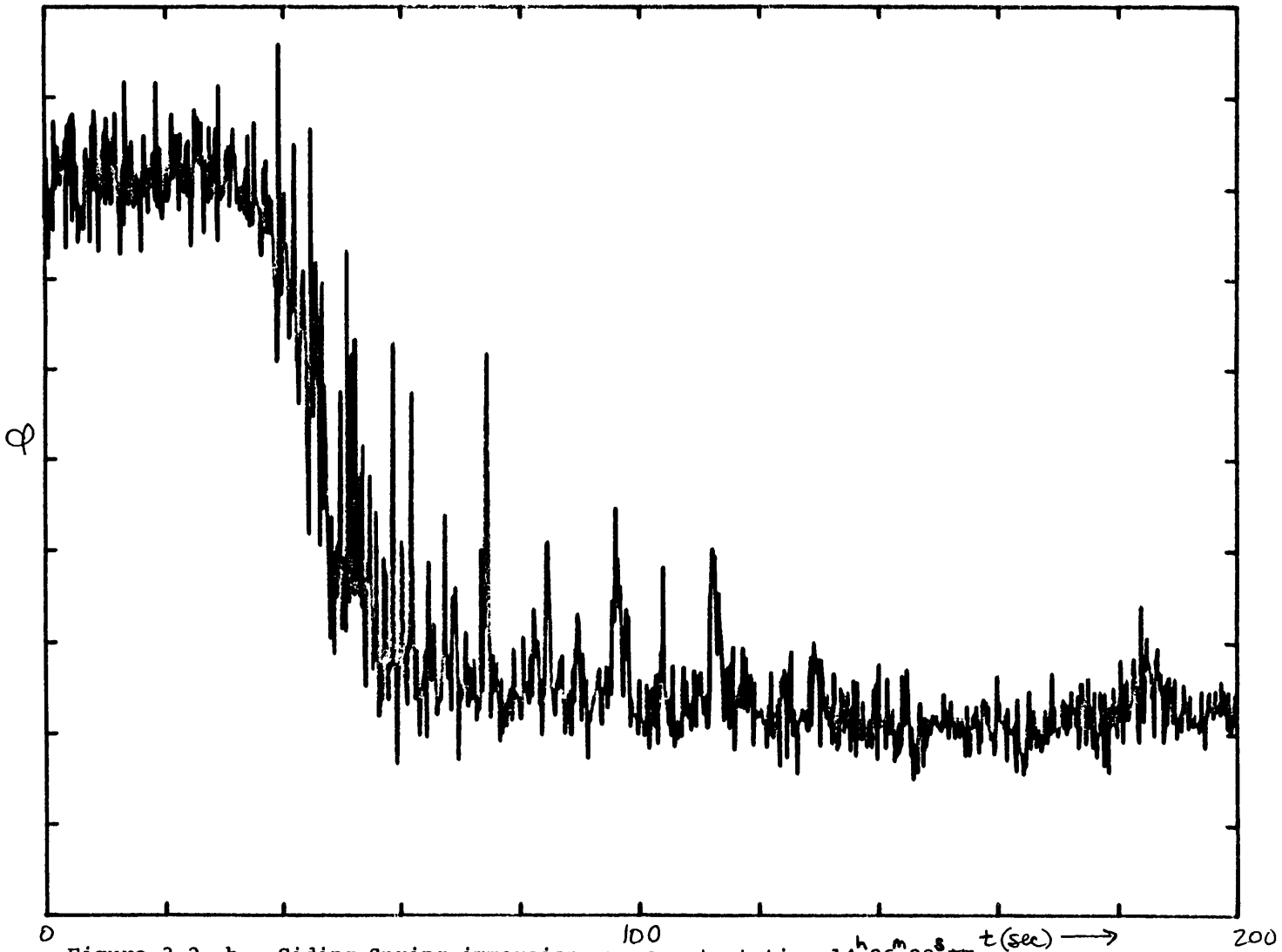

Figure 3-2, h. Siding Spring immersion curve, start time $14^h 26^m 20^s$ UT

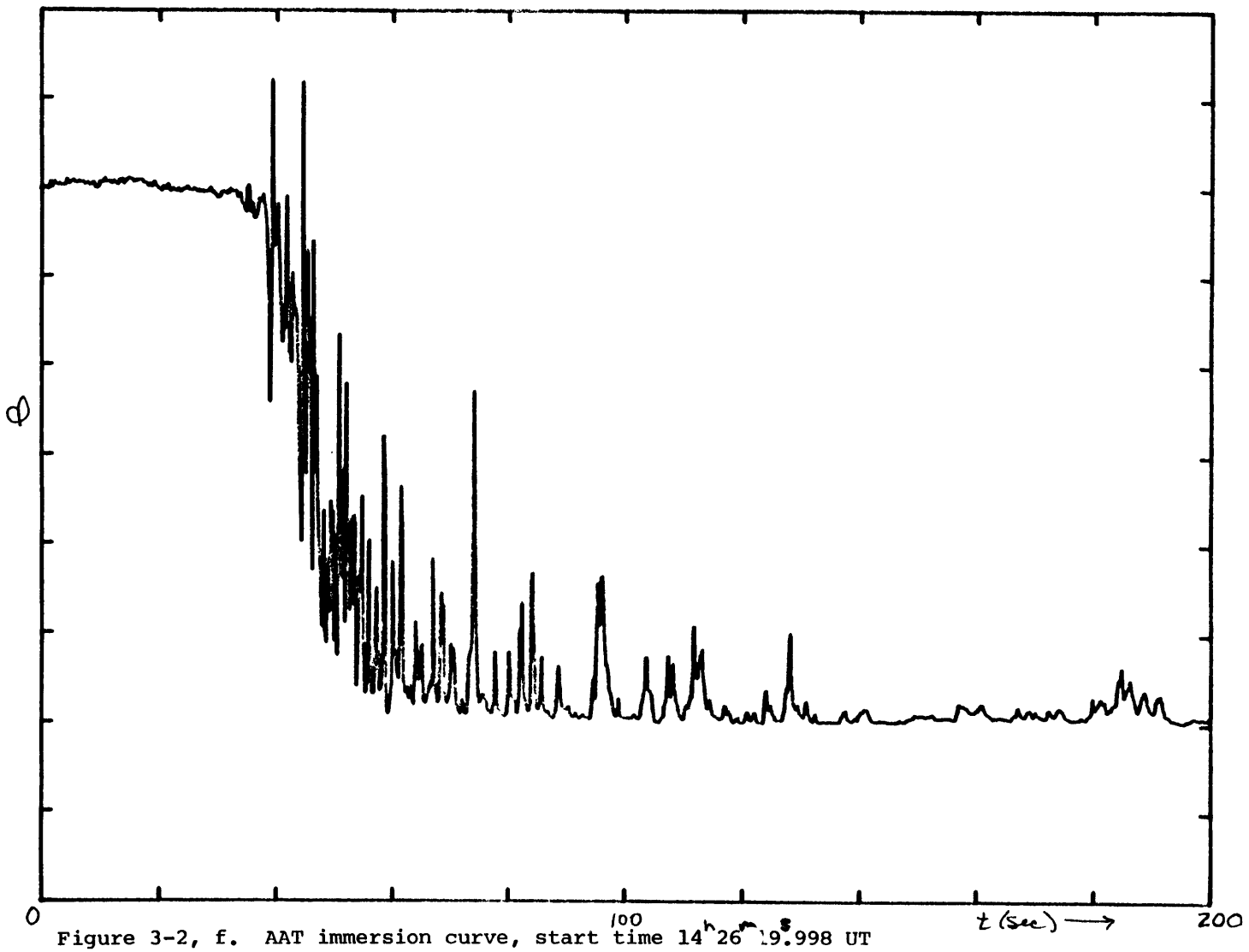

Figure 3-2, f. AAT immersion curve, start time 14^{h}26^{m}19.998 UT

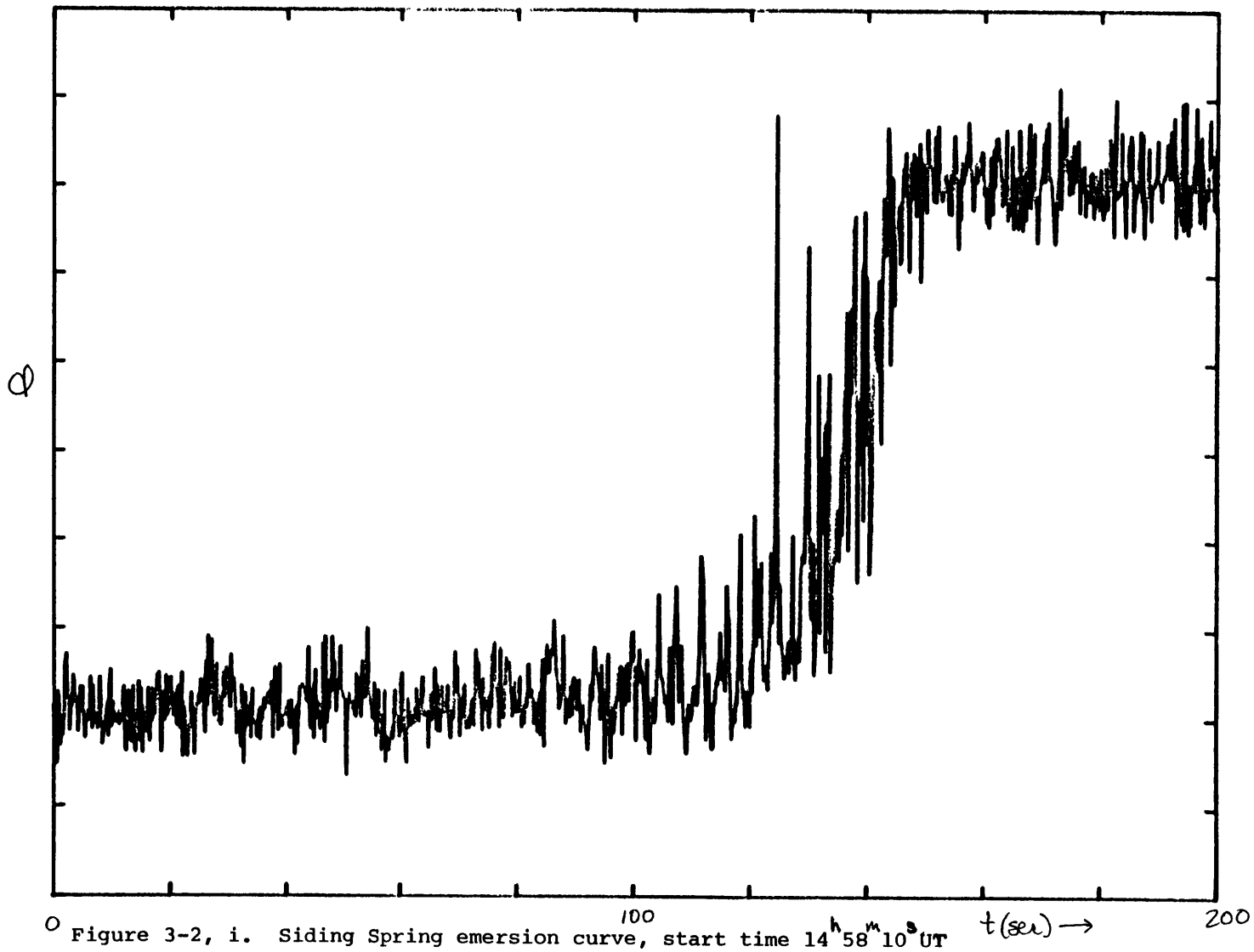

Figure 3-2, i. Siding Spring emersion curve, start time $14^h 58^m 10^s$ UT

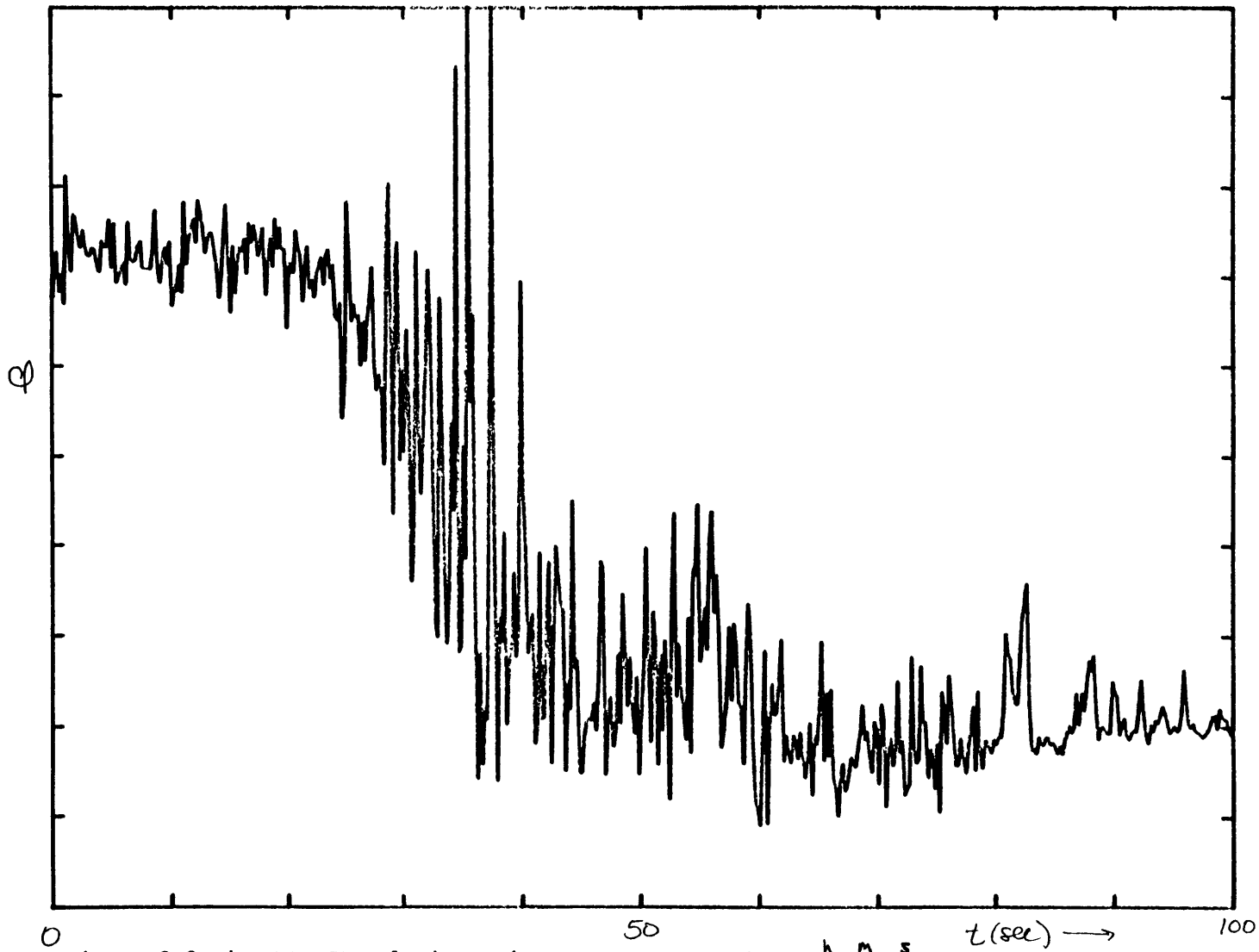

Figure 3-2, j. Mt. Stromlo immersion curve, start time $14^h26^m40^s$UT (1983)

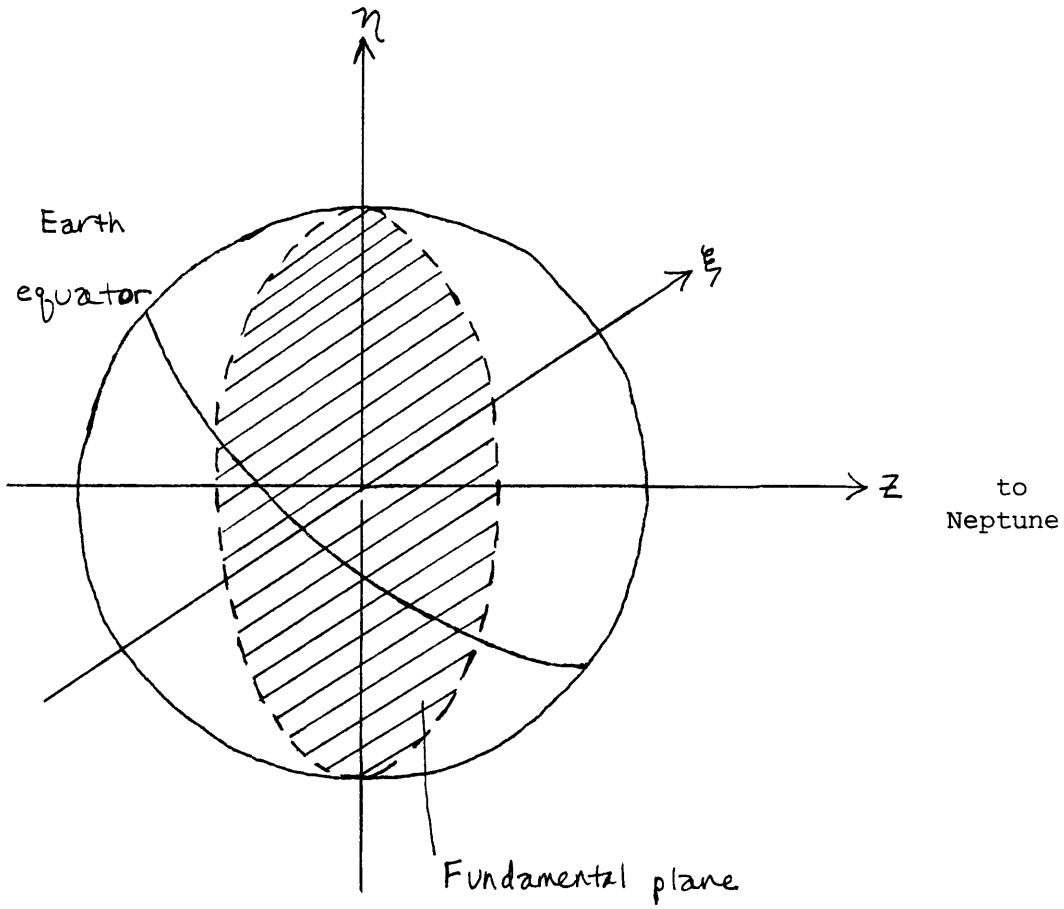

Figure 3-3. The fundamental plane (ξ = east, η = north).

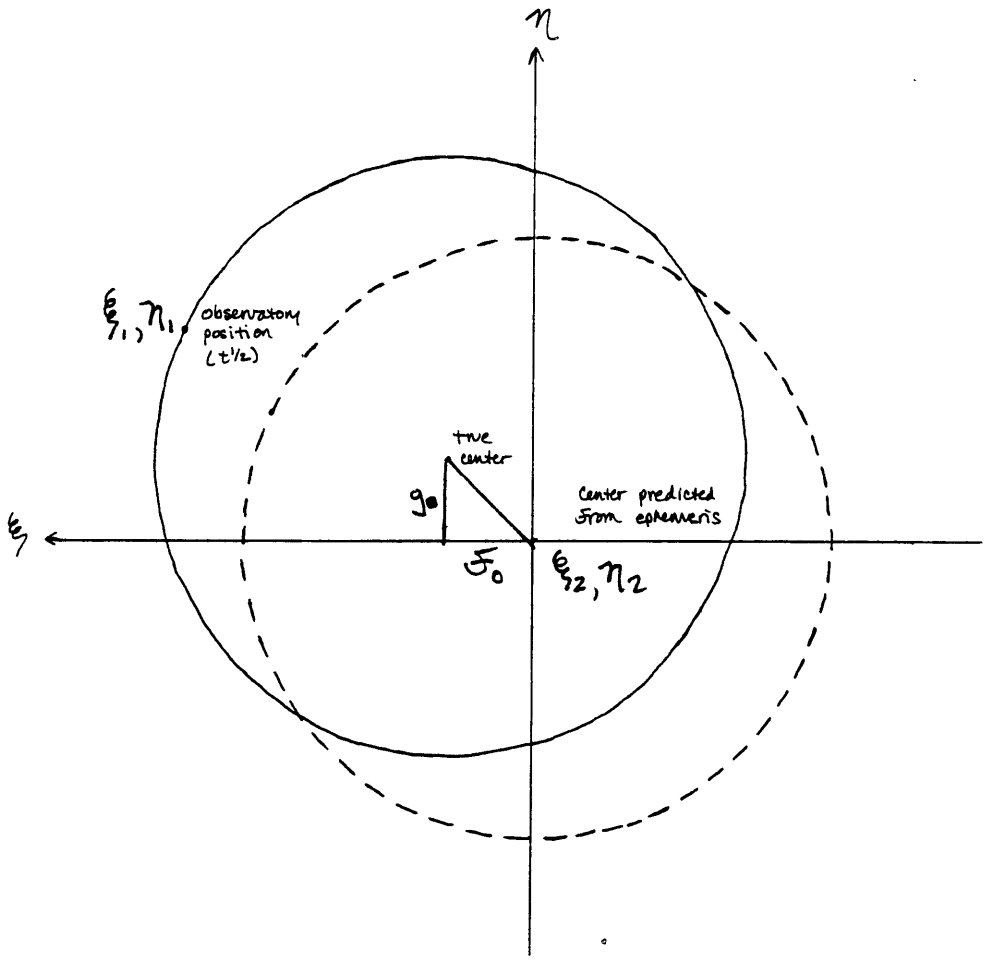

Figure 3-4. Neptune projected on to the fundamental plane.

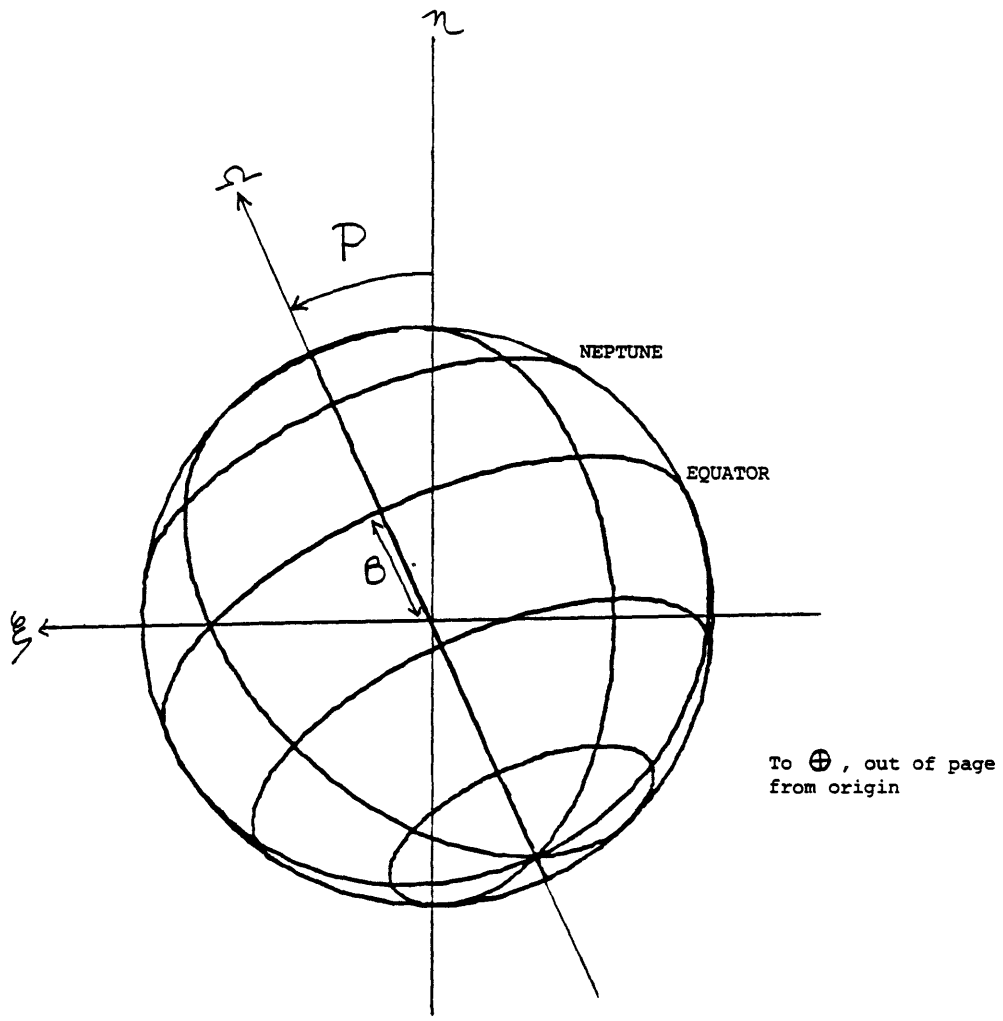

Figure 3-5. Position angle of the pole, P; Declination of Earth, B.

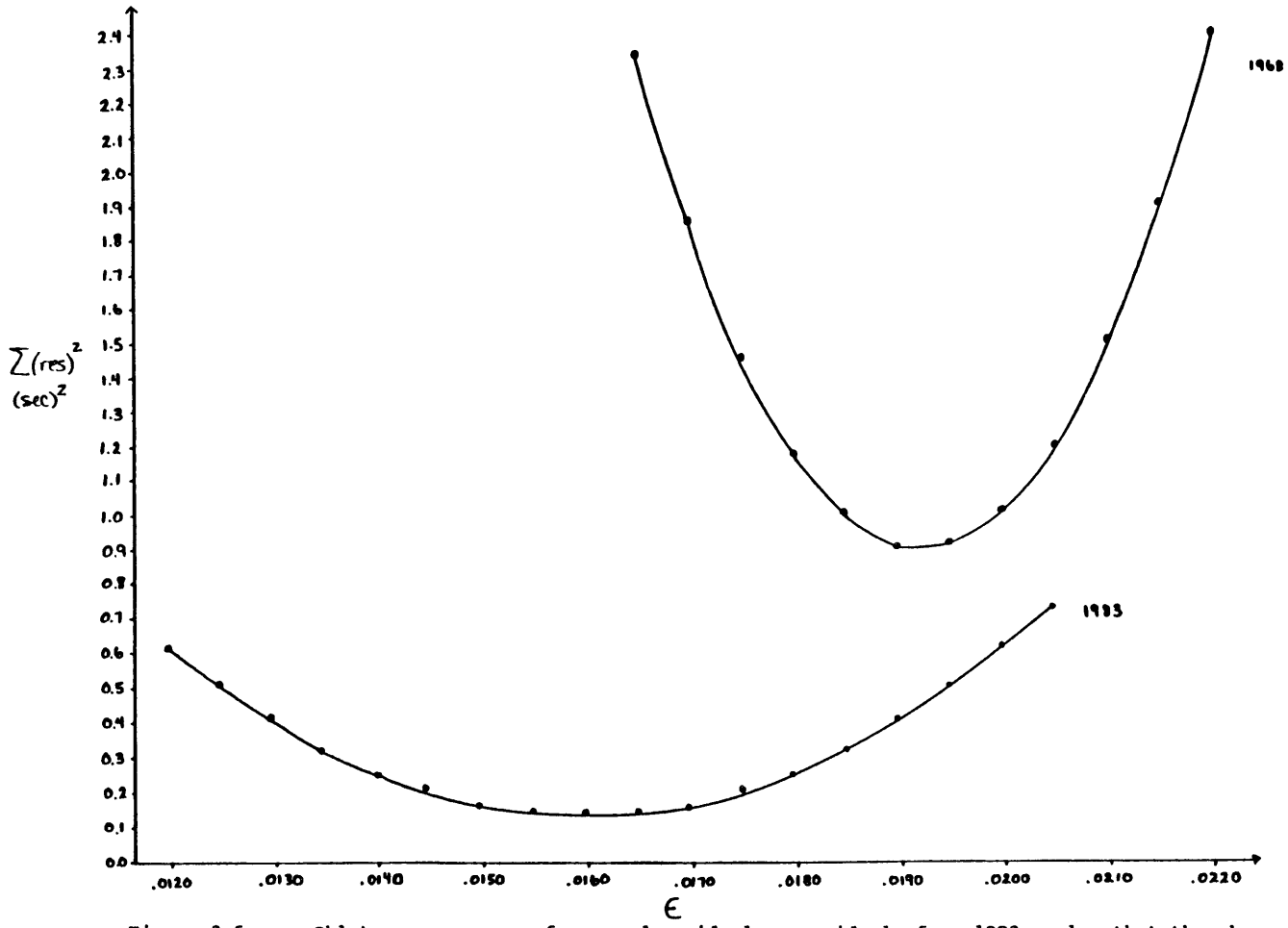

Figure 3-6, a. Oblateness vs. sum of squared residuals; residuals from 1983 so low that they have no leverage in joint fit.

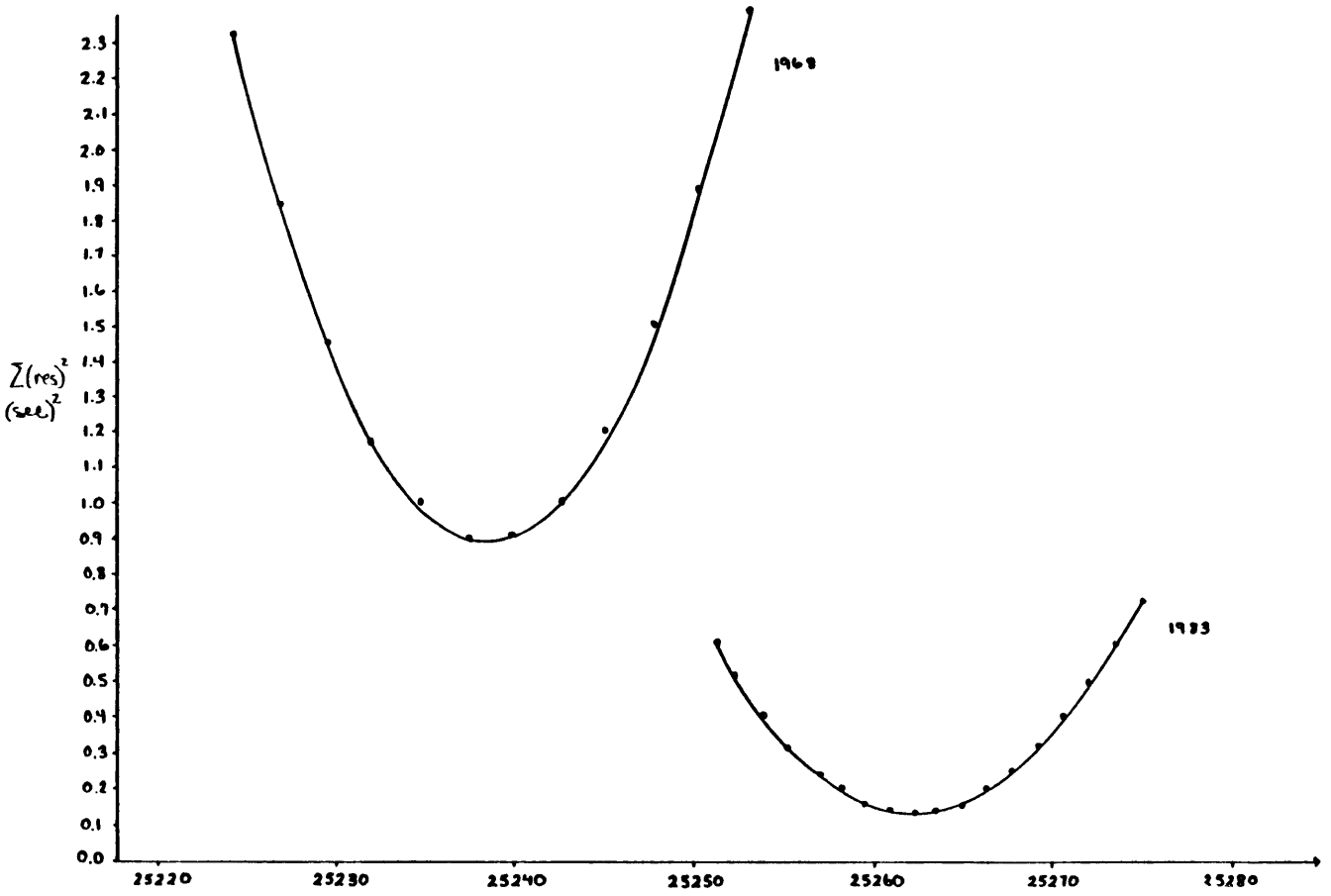

Figure 3-6, b. Sum of squared residuals vs. Radius

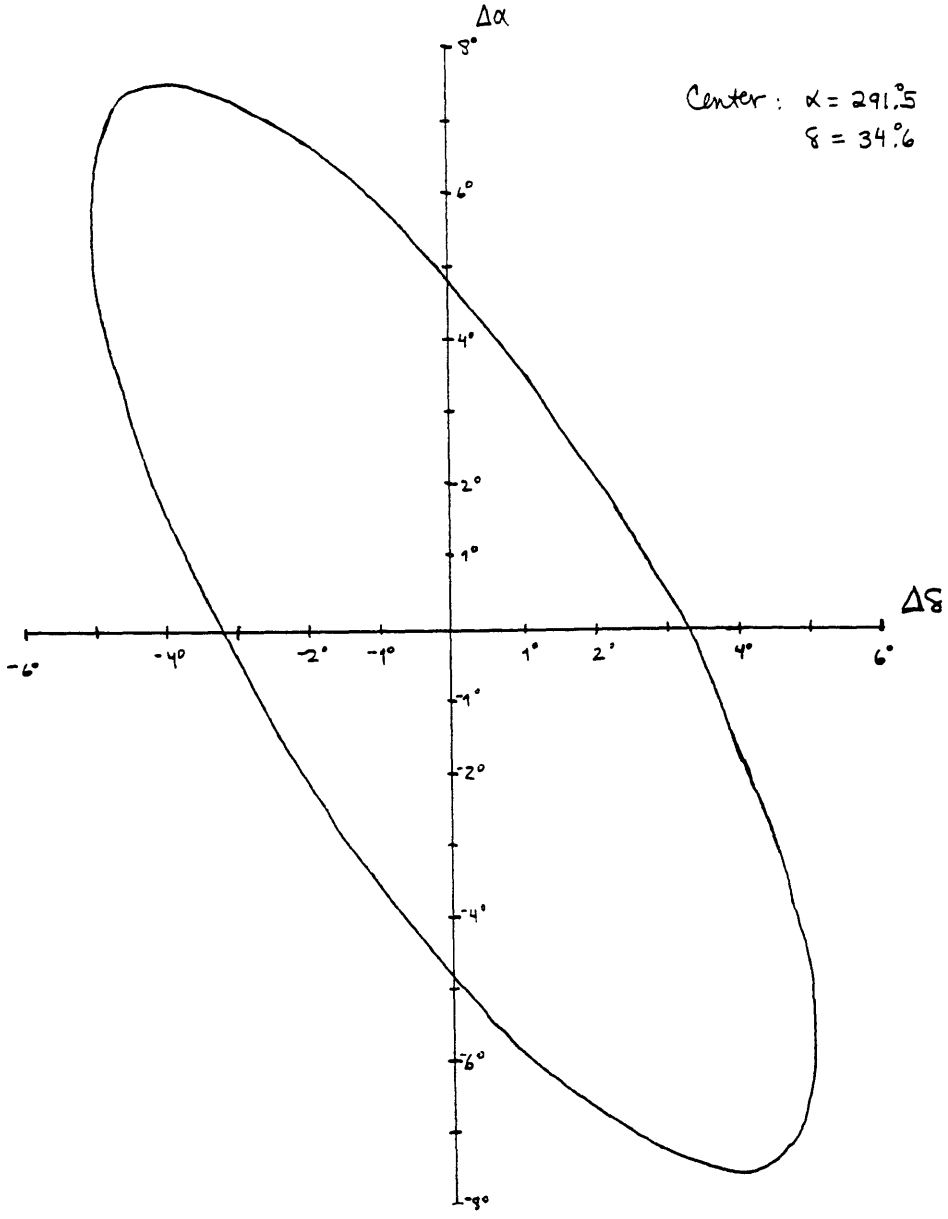

Figure 3-7. Error ellipse for pole position

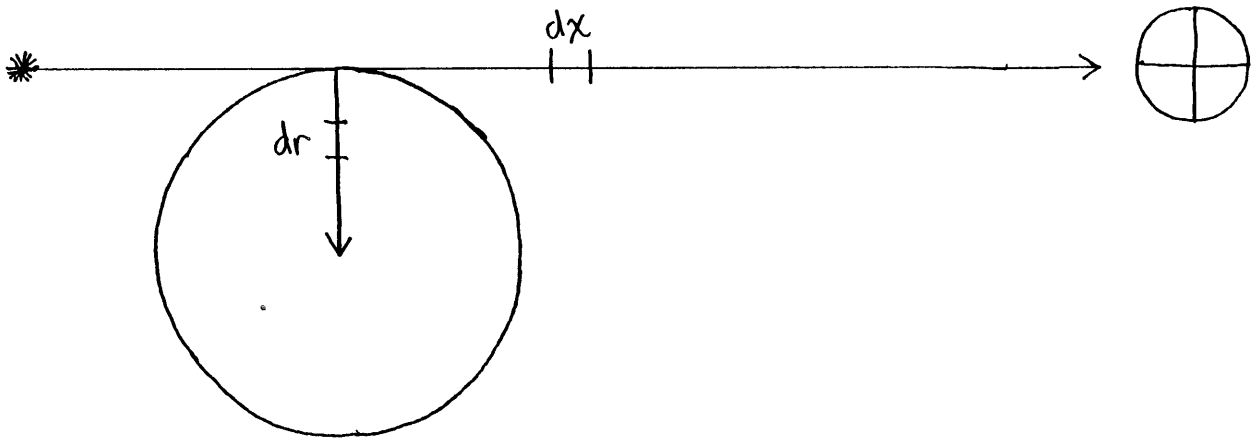

Figure 4-1. Geometry of inversion equation.

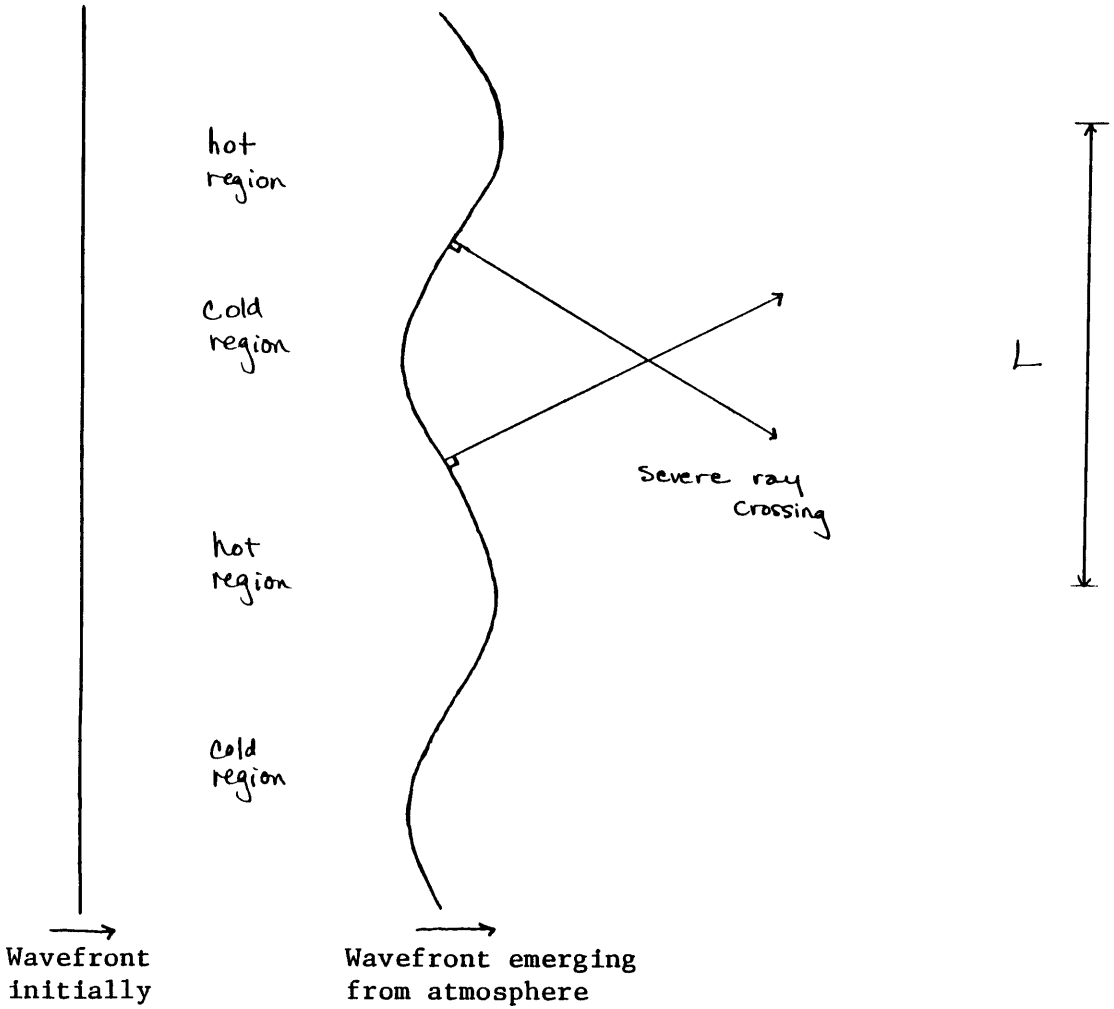

Figure 4-2. Ripples in wavefront caused by atmosphere leading to crossed rays.

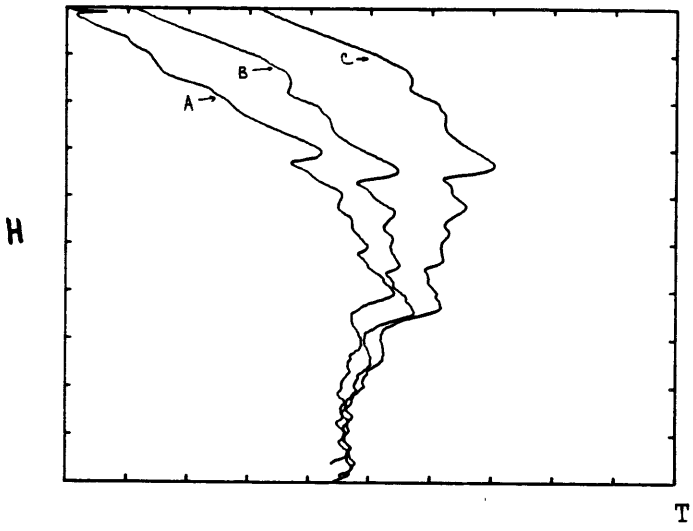

Figure 4-3,a. Temperature profile; T = 0 to 300° K; height spans 500 km. A profile started at 6.5 scale heights back in light curve; B profile started at 7.5 scale heights; C profile at 9 scale heights.

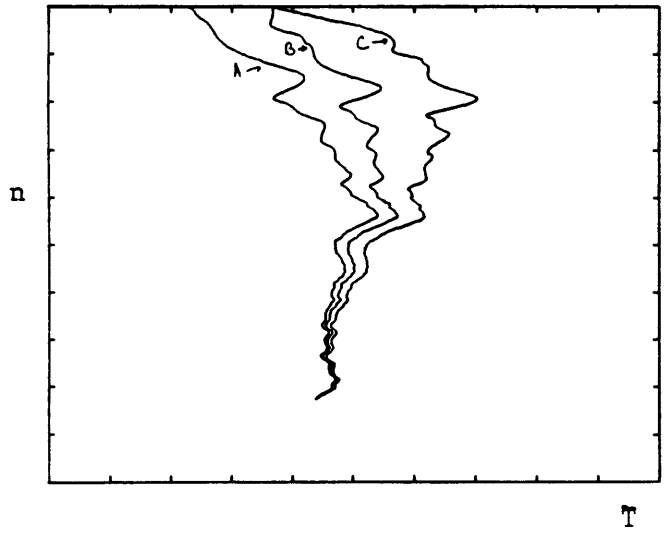

Figure 4-3,b. Number density profile; T = 0 to 300° K; number density spans 10^{12} to 10^{16} cm^{-3}.

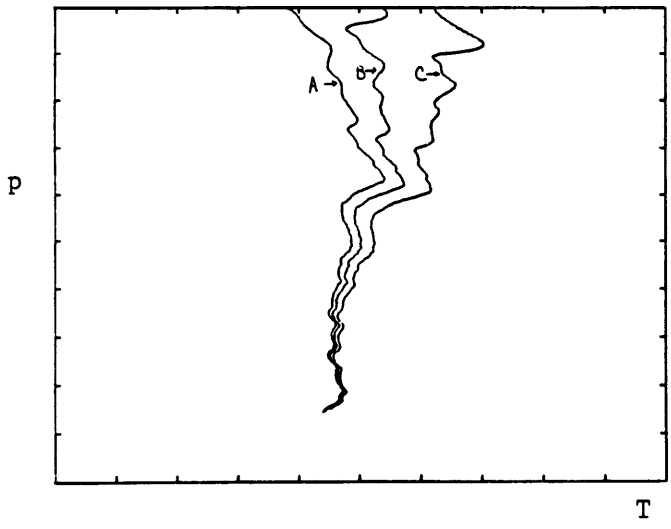

Figure 4-3,c. Pressure profile; T = 0 to 300°K; pressure spans 10^{-4} to 10^{-1}mbar.

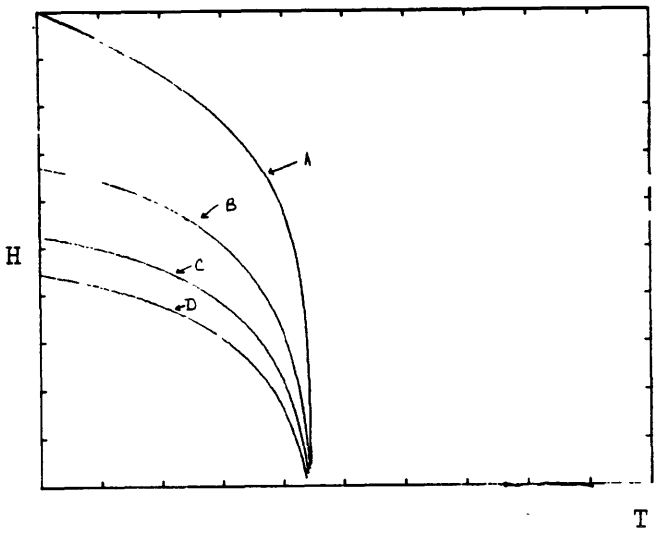

Figure 4-4,a. Temperature profile; T = 0 to 300° K; height spans 500 km. Isothermal profile, A; B profile has uncertainty in upper baseline of 1%; C has uncertainty of 2%; D has uncertainty of 3%.

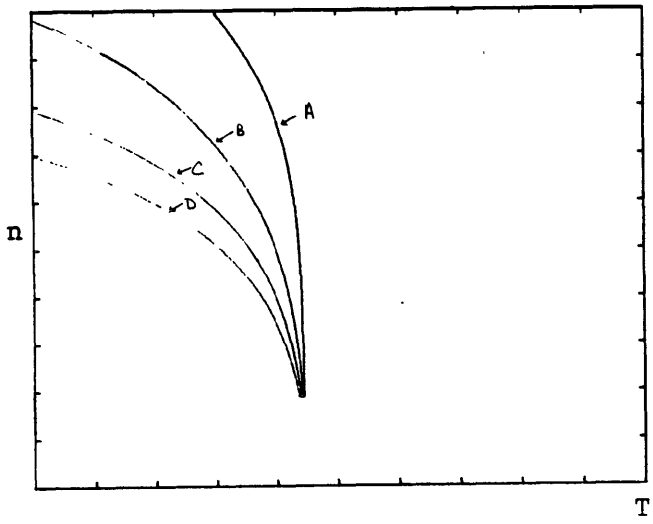

Figure 4-4,b. Number density profile; T = 0 to 300° K; number density scans 10^{12} to 10^{16} cm^{-3}.

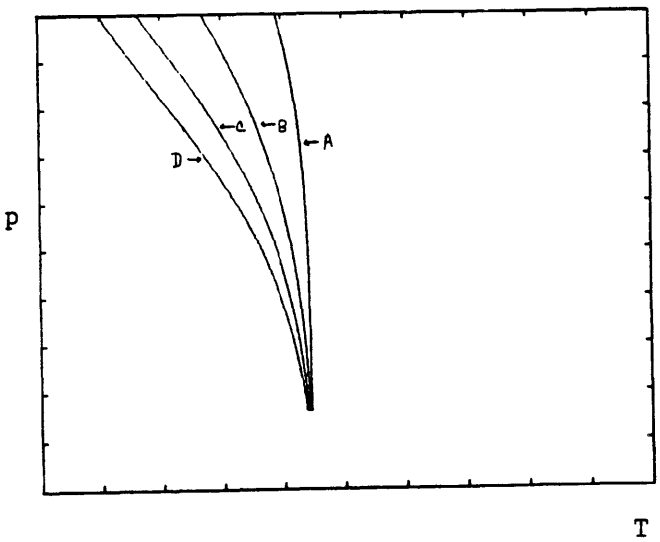

Figure 4-4,c. Pressure profile; T = 0 to 300° K; pressure spans 10^{-4} to 10^{-1} mbar.

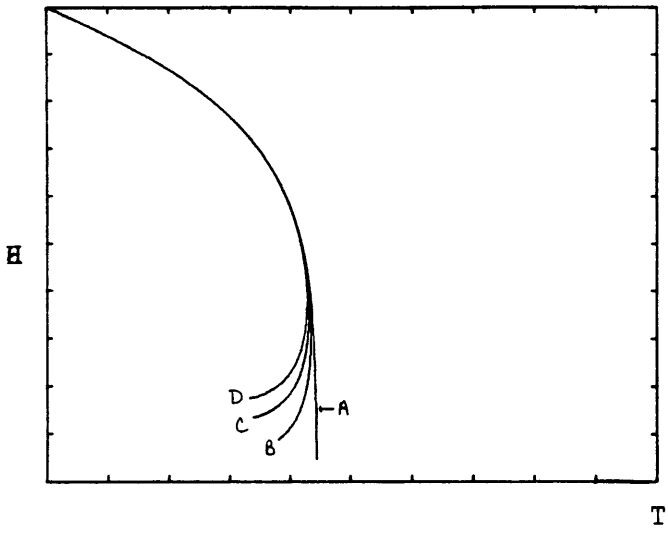

Figure 4-5,a. Temperature profile; T = 0 to 300°K. Isothermal profile, A; B profile has uncertainty in lower baseline of 1%; C profile has uncertainty of 2%; C profile has uncertainty of 3%.

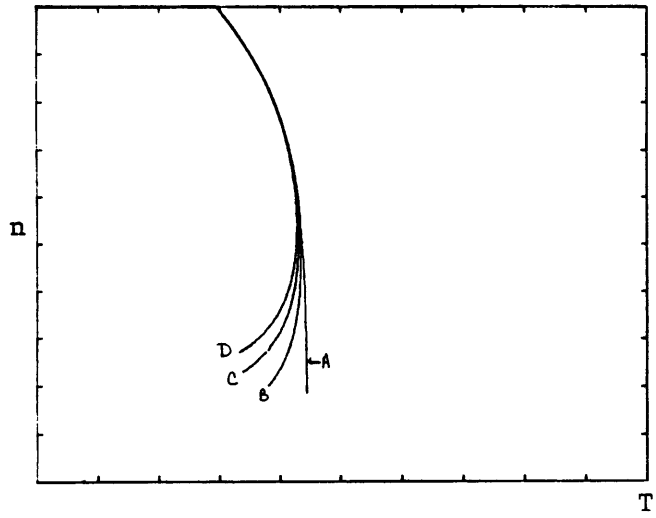

Figure 4-5,b. Number density profile; T = 0 to 300°K; number density spans 10^{12} to 10^{16} cm^{-3}.

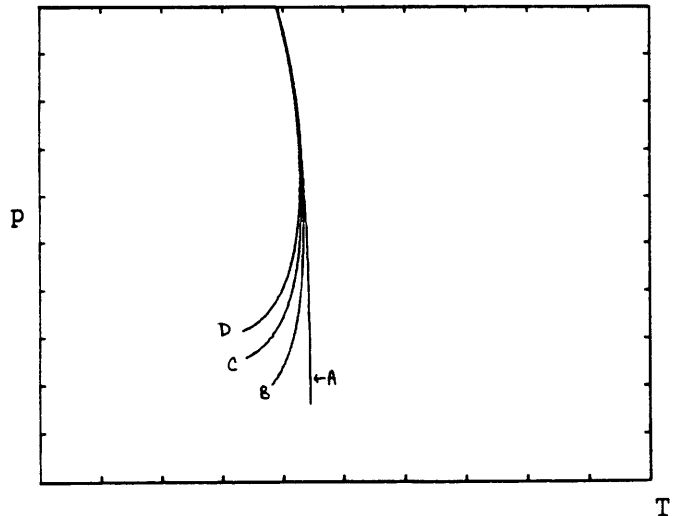

Figure 4-5,c. Pressure profile; T = 0 to 300°K; pressure spans 10^{-4} to 10^{-1} mbar.

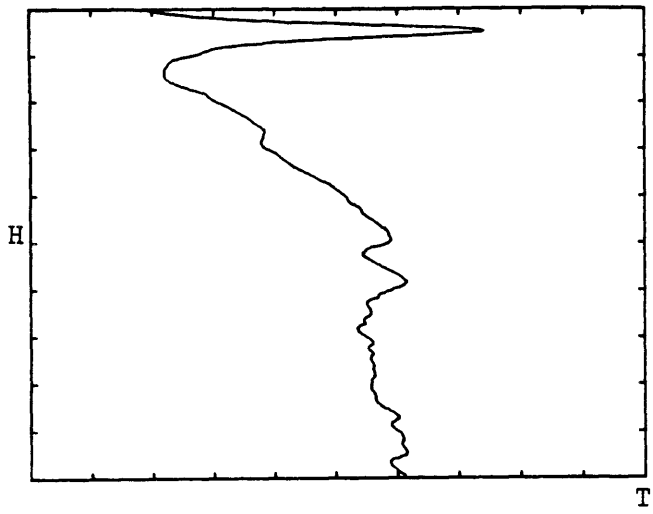

Figure 4-6,a Temperature profile; T = 0 to 300°K; Height spans 500 km; IRTF immersion

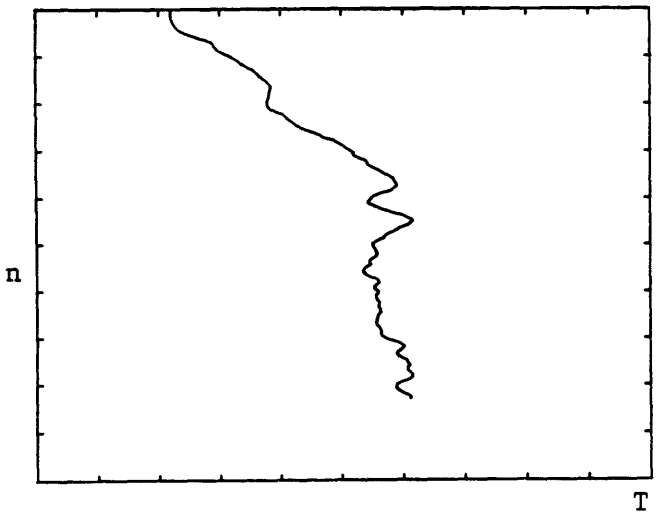

Figure 4-6,b. Number density profile; T = 0 to 300°K; number density spans 10^{12} to 10^{16} cm^{-3}.

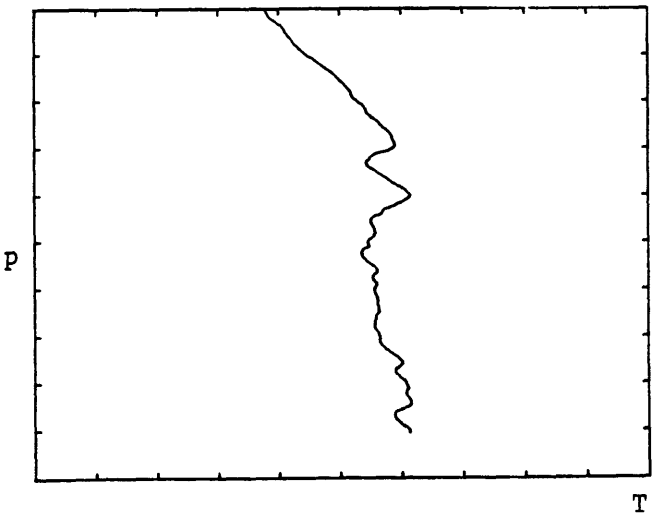

Figure 4-6,c. Pressure profile; T = 0 to 300°K; pressure spans 10^{-4} to 10^{-1} mbar.

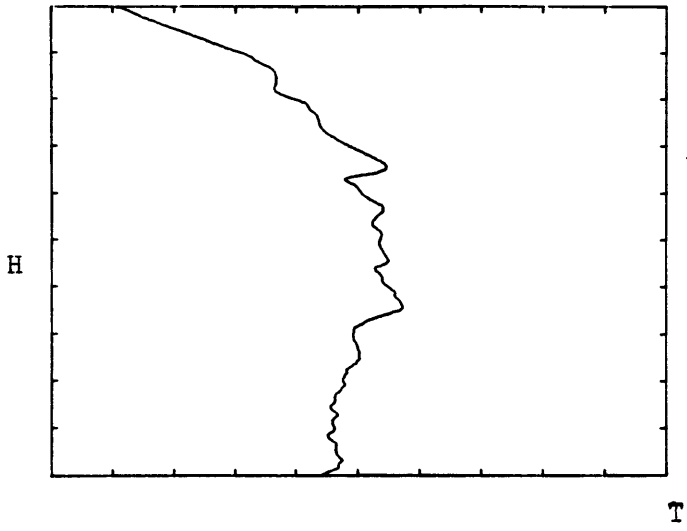

Figure 4-6,d. Temperature profile; T = 0 to 300°K; height spans 500 km; AAT immersion curve.

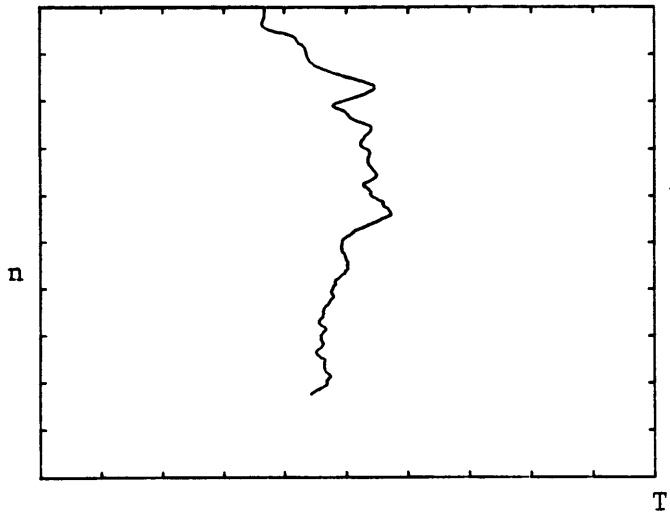

Figure 4-6,e. Number density profiles; T = 0 to 300°K; number density spans 10^{12} to 10^{16} cm^{-3}.

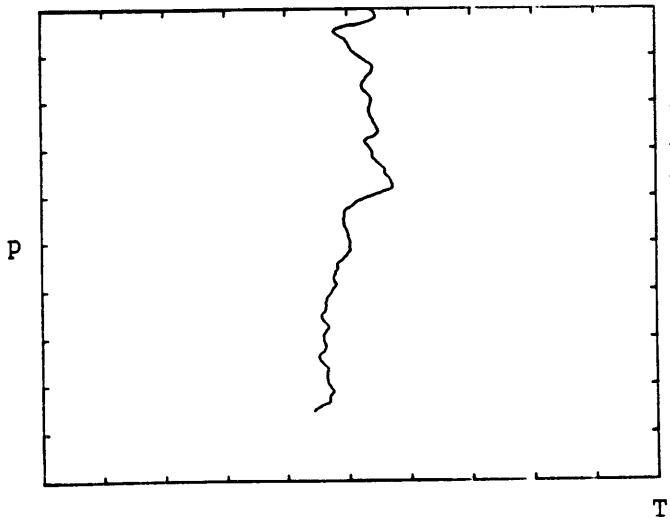

Figure 4-6,f. Pressure profile; T = 0 to 300°K; pressure spans 10^{-4} to 10^{-1}mbar.

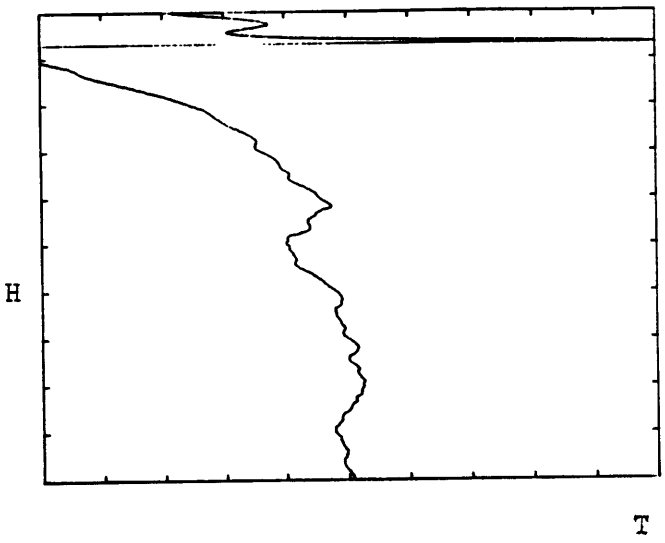

Figure 4-6,g. Temperature profile; T = 0 to 300° K; height spans 500 km. AAT emersion profile.

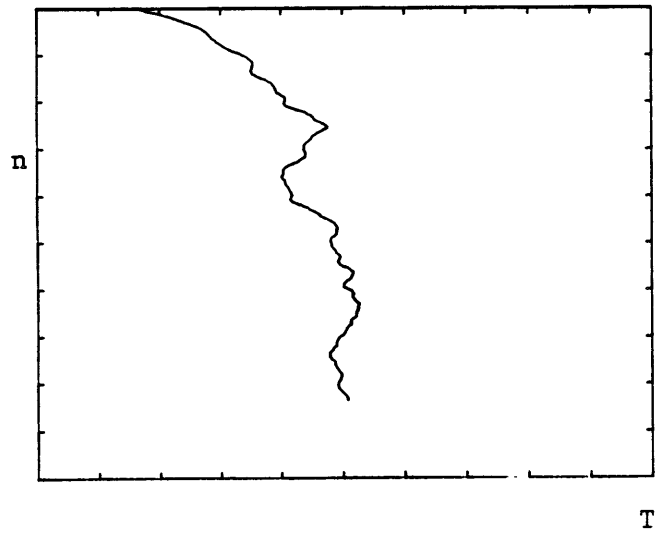

Figure 4-6,h. Number density profile; T = 0 to 300°K; number density spans 10^{12} to 10^{16} cm^{-3}.

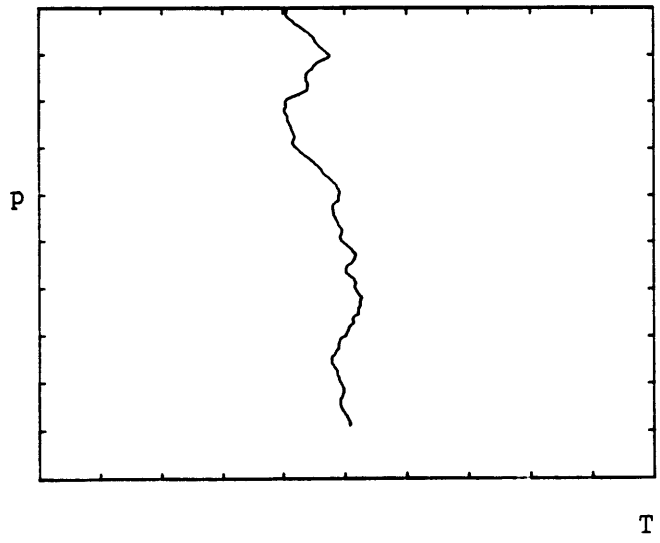

Figure 4-6,i. Pressure profile; T = 0 to 300°K; pressure spans 10^{-4} to 10^{-1} mbar.

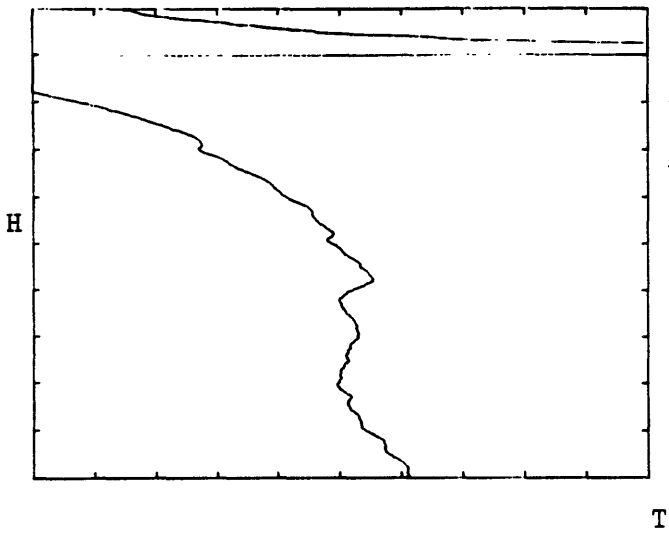

Figure 4-6,j. Temperature profile; T = 0 to 300°K; height spans 500 km; Sid. Spr. immersion.

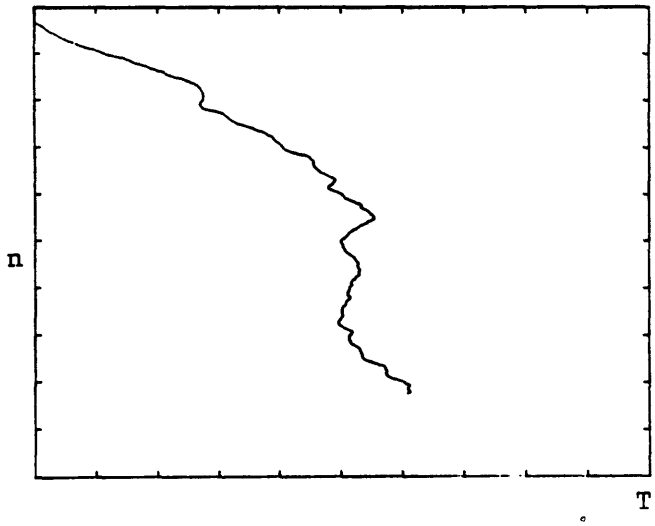

Figure 4-6,k. Number density profile; T = 0 to 300°K; number density spans 10^{12} to 10^{16} cm^{-3}.

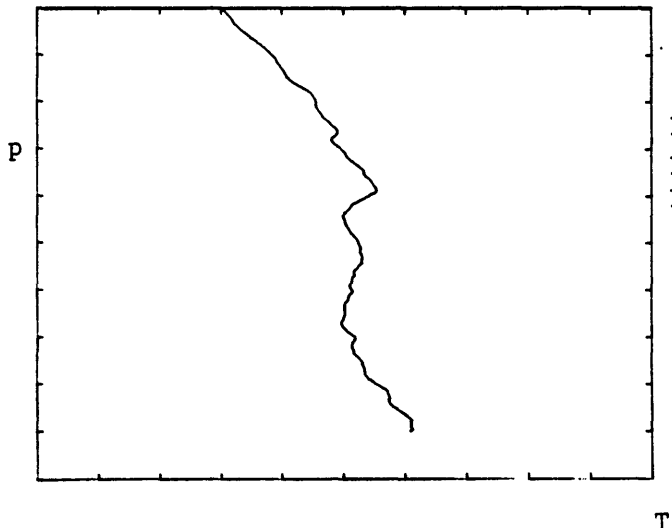

Figure 4-6,l. Pressure profile; T = 0 to 300°K; pressure spans 10^{-4} to 10^{-1} mbar.

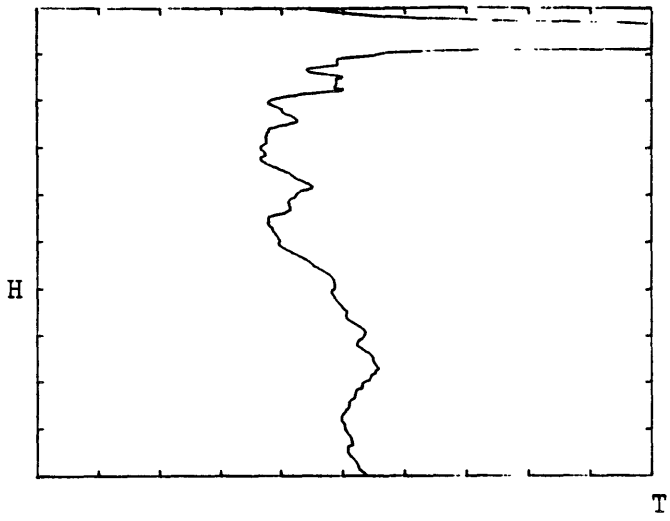

Figure 4-6,m. Temperature profile; T = 0 to 300 K; height spans 500 km; Sid. Spr. emersion.

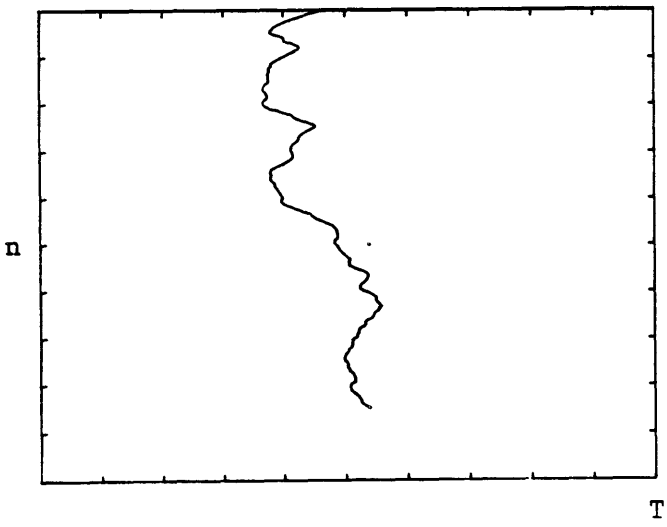

Figure 4-6,n. Number density profile; T = 0 to 300 K; number density spans 10^{12} to 10^{16} cm^{-3}.

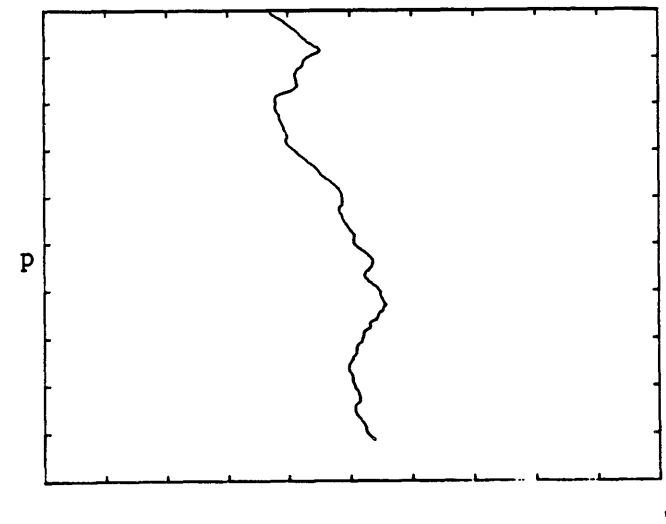

Figure 4-6,o. Pressure profile; T = 0 to 300 K; pressure spans 10^{-4} to 10^{-1} mbar.

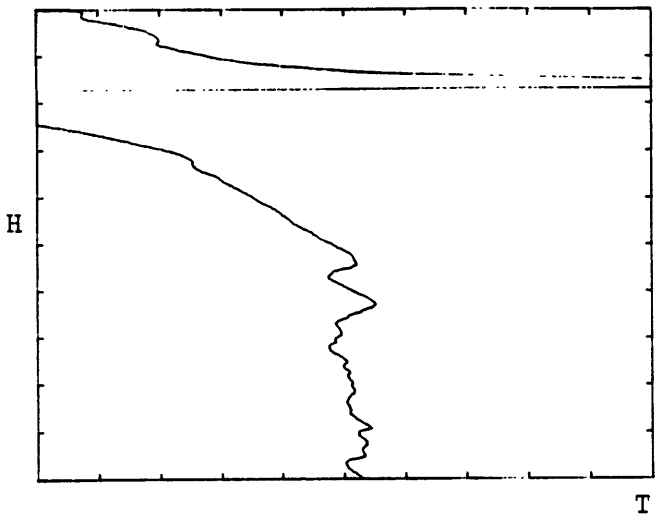

Figure 4-6,p. Temperature profile; T = 0 to 300° K; height spans 500 km. UH 2.2m immersion.

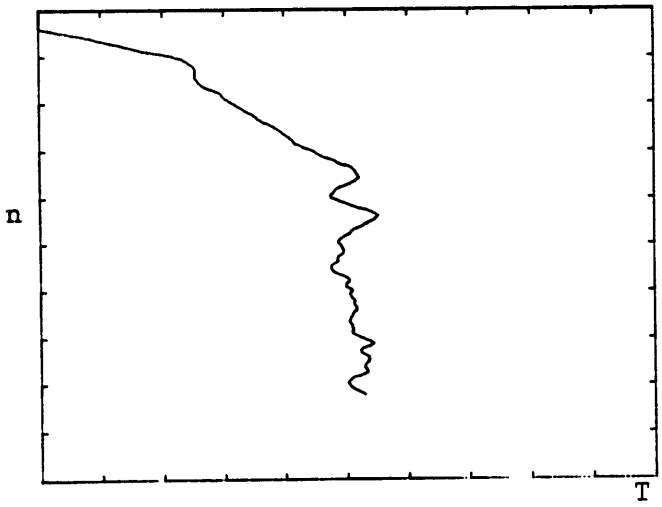

Figure 4-6,q. Number density profile; T = 0 to 300°K; number density spans 10^{12} to 10^{16} cm^{-3}.

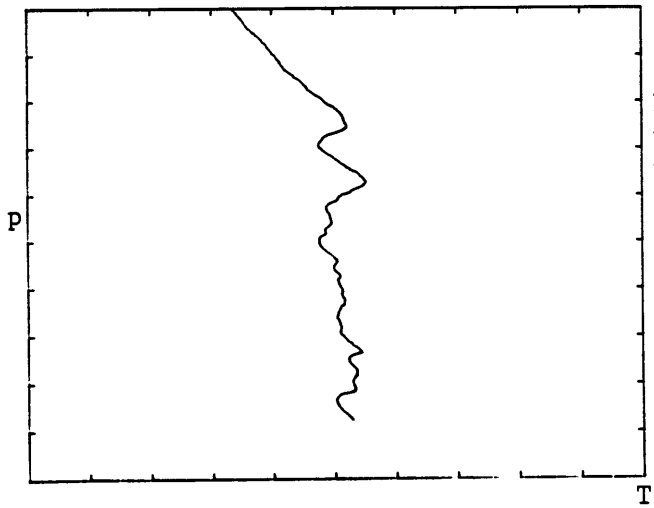

Figure 4-6,r. Pressure profile; T = 0 to 300°K; pressure spans 10^{-4} to 10^{-1} mbar.

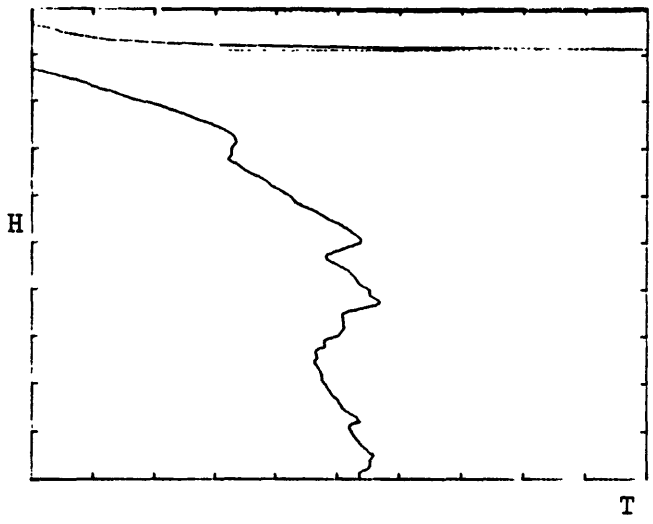

Figure 4-6,s. Temperature profile; T = 0 to 300°K; height span 500 km. KAO immersion.

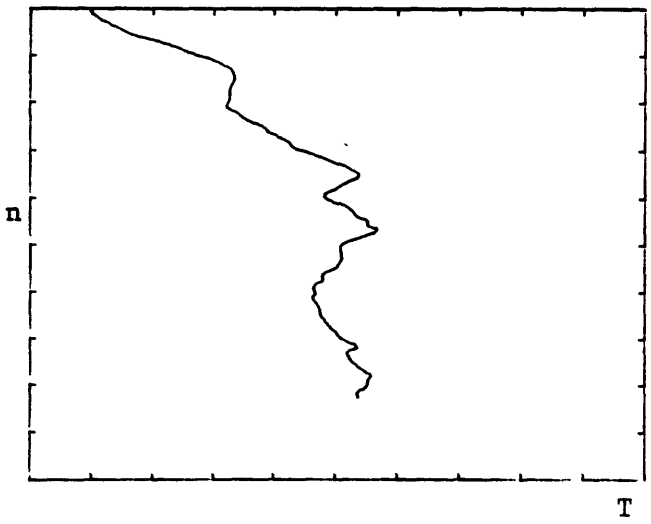

Figure 4-6,t. Number density profile; T = 0 to 300°K; number density spans from 10^{12} to 10^{16} cm^{-3}.

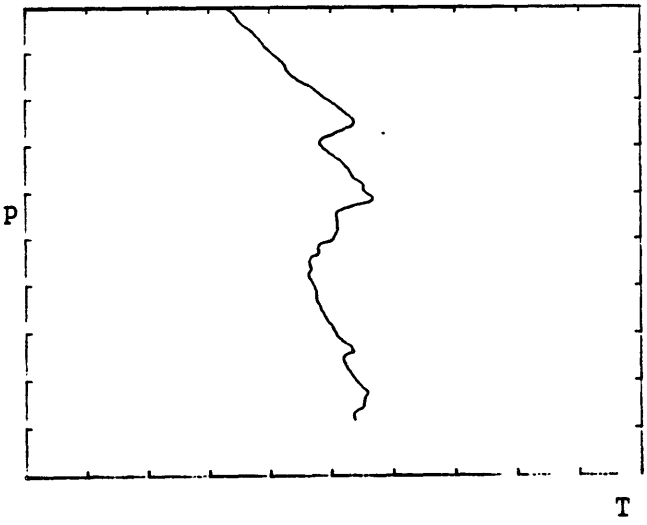

Figure 4-6,u. Pressure profile; T = 0 to 300°K; pressure spans from 10^{-4} to 10^{-1} mbar.

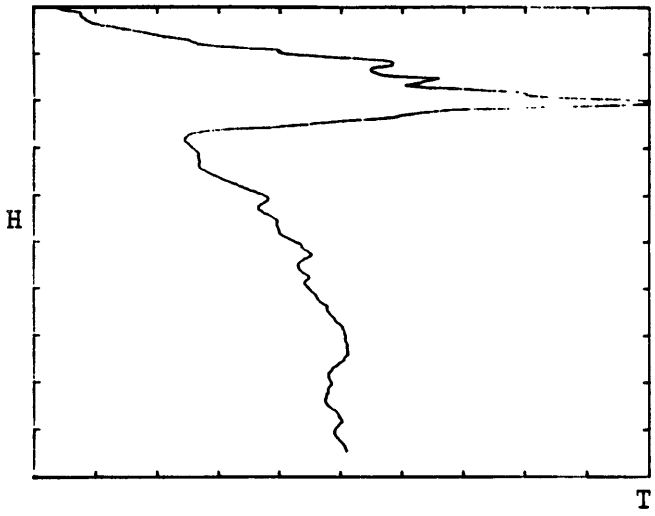

Figure 4-6,v.Temperature profile; T = 0 to 300°K; height spans 500 km; KAO emersion.

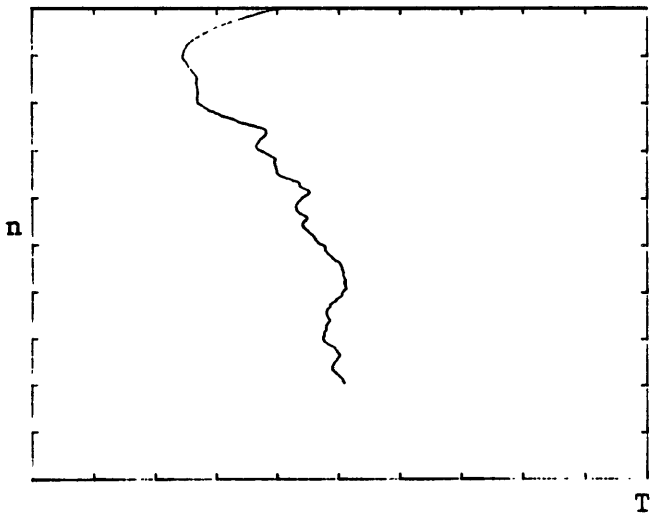

Figure 4-6,w. Number density profile; T = 0 to 300°K; number density spans from 10^{12} to 10^{16} cm^{-3}.

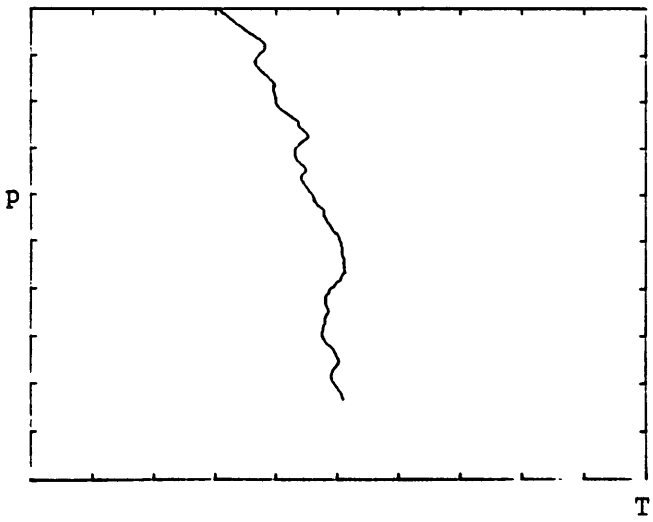

Figure 4-6,x. Pressure profile; T = 0 to 300°K; pressure spans 10^{-4} to 10^{-1} mbar.

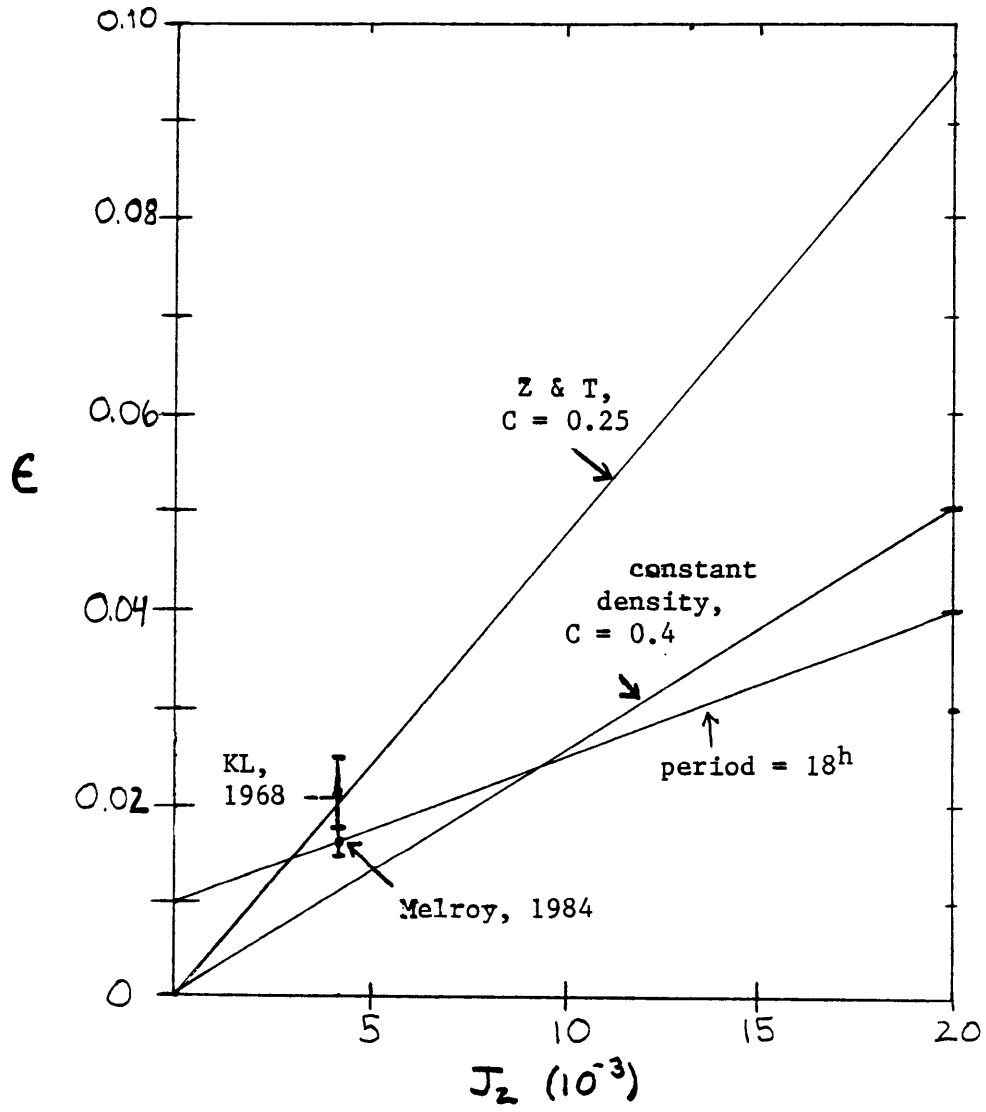

Figure 5-1. Relation between J_2, rotation rate, and oblateness.

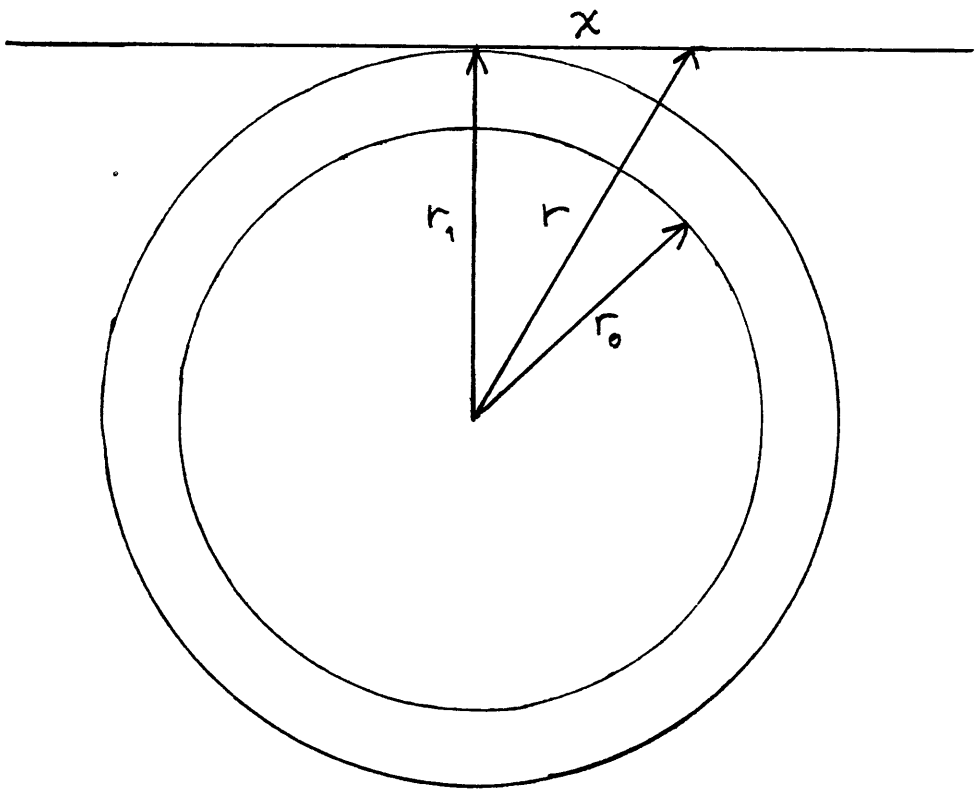

Figure A-1. Geometry of occultation for deriving an isothermal light curve.

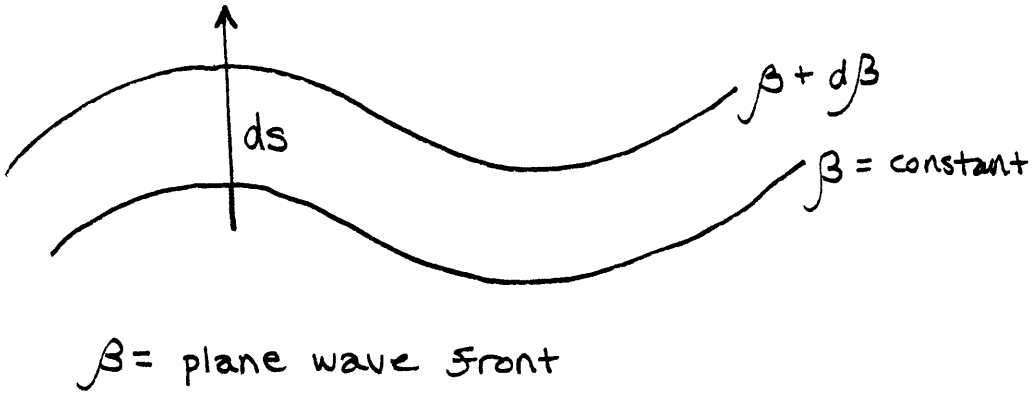

Figure C-1. Propagation of a plane wave front

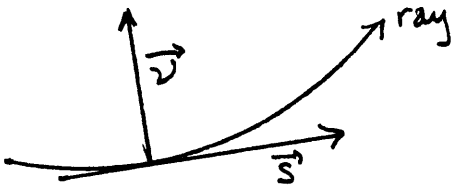

Figure C-2. Geometry of ray curvature.

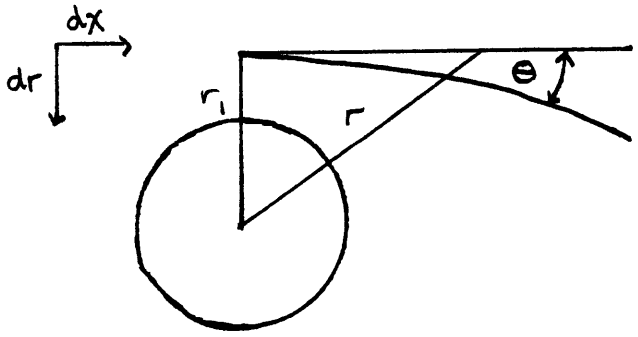

Figure C-3. Geometry of occultation.